Available online at www.sciencedirect.com

ScienceDirect

Nuclear Data Sheets

Nuclear Data Sheets 148 (2018) 254–292

www.elsevier.com/locate/nds

# IAEA CIELO Evaluation of Neutron-induced Reactions on $^{235}$U and $^{238}$U Targets

R. Capote,[1,*] A. Trkov,[1] M. Sin,[2] M. T. Pigni,[3] V. G. Pronyaev,[4] J. Balibrea,[5] D. Bernard,[6] D. Cano-Ott,[5] Y. Danon,[7] A. Daskalakis,[7] T. Goričanec,[8] M. W. Herman,[9] B. Kiedrowski,[10] S. Kopecky,[11] E. Mendoza,[5] D. Neudecker,[10] L. Leal,[12] G. Noguere,[6] P. Schillebeeckx,[11] I. Sirakov,[13] E. S. Soukhovitskii,[14] I. Stetcu,[10] and P. Talou[10]

[1] *NAPC–Nuclear Data Section, International Atomic Energy Agency, Vienna A-1400, Austria*
[2] *University of Bucharest, Faculty of Physics, Bucharest-Magurele, RO-077125, Romania*
[3] *Nuclear Data Criticality Safety, Oak Ridge National Laboratory, Oak Ridge, TN 37831, USA*
[4] *PI Atomstandart at SC Rosatom, Moscow, Russian Federation*
[5] *CIEMAT, Centro de Investigaciones Energéticas Medioambientales y Tecnólogicas, 28040 Madrid, Spain*
[6] *CEA, DEN, DER, SPRC, Cadarache, 13108 Saint-Paul-lez-Durance, France*
[7] *Gaerttner LINAC Center, Rensselaer Polytechnic Institute, Troy, NY 12180, USA*
[8] *Jožef Stefan Institute, 1000 Ljubljana, Slovenia*
[9] *National Nuclear Data Center, Brookhaven National Laboratory, Upton, NY 11973, USA*
[10] *Los Alamos National Laboratory, Los Alamos, NM 87544, USA*
[11] *EC-JRC, B-2440 Geel, Belgium*
[12] *IRSN/PSN-EXP/SNC/LNR, Institut de Radioprotection et de Sûreté Nucléaire, BP17, 92262 Fontenay aux Roses, CEDEX, France*
[13] *Institute for Nuclear Research and Nuclear Energy, BAS, BG-1784 Sofia, Bulgaria*
[14] *Nuclear Evaluation Laboratory, Joint Institute for Energy and Nuclear Research, Minsk, BY-220109, Belarus*

(Received 8 September 2017; revised received 10 November 2017; accepted 20 November 2017)

Evaluations of nuclear reaction data for the major uranium isotopes $^{238}$U and $^{235}$U were performed within the scope of the CIELO Project on the initiative of the OECD/NEA Data Bank under Working Party on Evaluation Co-operation (WPEC) Subgroup 40 coordinated by the IAEA Nuclear Data Section. Both the mean values and covariances are evaluated from $10^{-5}$ eV up to 30 MeV. The resonance parameters of $^{238}$U and $^{235}$U were re-evaluated with the addition of newly available data to the existing experimental database. The evaluations in the fast neutron range are based on nuclear model calculations with the code EMPIRE–3.2 Malta above the resonance range up to 30 MeV. $^{235}$U($n$,f), $^{238}$U($n$,f), and $^{238}$U($n$,$\gamma$) cross sections and $^{235}$U($n_{th}$,f) prompt fission neutron spectrum (PFNS) were evaluated within the Neutron Standards project and are representative of the experimental state-of-the-art measurements. The Standards cross sections were matched in model calculations as closely as possible to guarantee a good predictive power for cross sections of competing neutron scattering channels. $^{235}$U($n$,$\gamma$) cross section includes fluctuations observed in recent experiments. $^{235}$U($n$,f) PFNS for incident neutron energies from 500 keV to 20 MeV were measured at Los Alamos Chi-Nu facility and re-evaluated using all available experimental data. While respecting the measured differential data, several compensating errors in previous evaluations were identified and removed so that the performance in integral benchmarks was restored or improved. Covariance matrices for $^{235}$U and $^{238}$U cross sections, angular distributions, spectra and neutron multiplicities were evaluated using the GANDR system that combines experimental data with model uncertainties. Unrecognized systematic uncertainties were considered in the uncertainty quantification for fission and capture cross sections above the thermal range, and for neutron multiplicities. Evaluated files were extensively benchmarked to ensure good performance in reactor calculations and fusion-related systems. New comprehensive evaluations show excellent agreement with available differential data and integral performance better than current evaluated data libraries, and represent a step forward in a quest for better nuclear data for applications.

## CONTENTS



* Corresponding author: r.capotenoy@iaea.org

https://doi.org/10.1016/j.nds.2018.02.005
0090-3752/

## I. INTRODUCTION

The Nuclear Energy Agency of the OECD started a new international collaboration called CIELO (Collaborative International Evaluated Library Organisation) with the main goal to improve our understanding of neutron reactions on key isotopes that are important in nuclear applications [1–3]. A central role of this project is taken by $^{238}$U and $^{235}$U nuclei. $^{238}$U constitutes more than 90% of nuclear fuel in power reactors, being probably the most important isotope for neutron transport calculations in the active zone of a reactor, while $^{235}$U is the most important fissioning isotope in the same active zone.

While existing uranium evaluations (*e.g.*, ENDF/B-VII.1 [4], JEFF-3.2 [5], JENDL-4.0 [6], and CENDL-3.1 [7]) perform very well for many applications, several discrepancies have been highlighted between $^{235}$U integral and differential data (*e.g.*, for prompt fission neutron spectra of thermal $^{235}$U($n$,f) [8–10]), or between evaluated data from different libraries (*e.g.*, between $^{235}$U inelastic cross sections [11]).

In the case of $^{238}$U, the fission cross section is the Neutron Standard [12–14] and the capture cross section is a reference cross section evaluated within the Standards Project [12–14]. The total cross section is well known (within 2-3% above 1 MeV), so this essentially leaves the freedom to adjust only the ratio of the elastic and the inelastic cross sections and their angular distributions.

In view of the discrepancies observed with experimental data and the differences in the cross sections between existing libraries it is obvious that the good integral performance of the above-mentioned libraries was achieved by error compensation. The challenge of achieving consistency with measured differential data and at the same time retaining good performance in integral benchmarks could only be solved by a new and comprehensive evaluation of all neutron-induced reactions on $^{238}$U and $^{235}$U targets. This is the subject of the current contribution.

## II. EVALUATION METHODOLOGY

The methodology considers available differential (microscopic) data as the primary constraint, supplemented by a few selected simple integral benchmarks to provide guidance on preferences in the case of discrepant differential data, or to pin-down quantities for which no experimental information is available and are not constrained otherwise by the theoretical models. The aim is to constrain model parameters, which are then used to calculate final cross sections. The internal physical consistency of evaluated data is, therefore, preserved. No least-squares fitting of integral benchmarks is undertaken, as we do not aim at producing an adjusted library. It is also clear that evaluated uncertainties and covariances will lead to large uncertainties of integral parameters as expected for a general purpose evaluation.

An iterative procedure involving differential data calcu-

lated with the advanced reaction models was implemented in the evaluation system EMPIRE-3.2 [15, 16], and modelling of selected integral benchmarks such as the collection from the Handbook of Criticality Safety Benchmark Experiments [17] was followed to perform the present evaluation. Processing with the NJOY code system [18] was done to prepare the corresponding ACE libraries for use with the MCNP Monte Carlo transport code [19] in benchmark calculations.

Differences in integral benchmark performance of a few selected benchmarks depending on nuclear data were used as guidance to improve the reaction models and to fine-tune the reaction model parameters iteratively. Following this procedure, accurate model-based evaluations which reproduce both differential data and selected integral measurements have been obtained, which are used as a prior information in a subsequent Bayesian update. Efforts have been focused on calculating the optimal mean values for physical quantities of interest in neutron transport. Additional efforts to estimate uncertainties and correlations of the evaluated quantities are described below.

An evaluator is free to tune model parameters to make the calculated cross sections representative of differential experimental data as long as the changes remain well within the estimated model parameter uncertainties. Choosing parameters within these constraints that at the same time improve performance in integral benchmarks is a *pragmatic choice* by the evaluator in defining the prior cross sections to be used in a subsequent Bayesian update. The Bayesian update (GANDR [20]) defines evaluated nuclear data mean values and covariances. In authors' opinion such parameter tuning of the prior does not imply that the integral experimental data were "used" in the evaluation, since the tuning process does not affect the estimated prior nor the posterior nuclear data uncertainties. The tuning just changes the prior mean value well within assessed prior uncertainties. However, such statement may be controversial due to implicit correlations, which a rigorous Bayesian treatment of integral data would introduce.. Further investigation of such correlations is outside the scope of the present work.

The evaluation method used in this work belongs to the hybrid evaluation methods [21], and combines a prior produced using Monte Carlo (MC) techniques with a deterministic generalized least-squares fit that produces evaluated mean values and covariances.

By random sampling of the model parameters within their uncertainties assuming a normal distribution, the covariance matrix prior was obtained. Additional non-physical parameters that also feature uncertainties were also used if needed to describe a deviation of calculations from the experimental data, when the reaction model was not capable of describing such behaviour (*e.g.*, fluctuations around 1 MeV in $^{235}$U($n$,f) cross sections and fluctuations from 2 keV up to 200 keV in $^{235}$U($n$,$\gamma$) cross sections). The non-physical (scaling) parameters could be interpreted as a compensation of the model defects.

The MC calculated covariance prior was then fed to the GANDR system [20] which is the generalised least-squares code capable of adjusting the prior and constraining the covariances using the experimental data from the EXFOR database to produce the final evaluation. The same procedure was applied earlier in the evaluations of thorium, manganese, and tungsten as explained in Refs. [22, 23], where further details can be found.

## III. EVALUATION OF NEUTRON-INDUCED REACTIONS ON $^{235}$U TARGET

Two different energy ranges were considered, the resonance range covering both resolved (RRR) and unresolved (URR) resonances, and the fast neutron range. The RRR extends up to 2.25 keV, the URR goes from 2.25 keV up to 25 keV, and the fast range goes from there up to 30 MeV. A description of the evaluation and results in those energy ranges are given below.

### A. Resonance Range in $n+^{235}$U

The computer code system SAMMY [24] was used to analyze experimental data in the resolved resonance region (RRR) up to 2.25 keV using the multilevel multi channel $R$-matrix representation of the neutron cross sections defined according to the Reich-Moore (RM) approximation. Experimental conditions such as resolution function, finite size sample, nonuniform thickness, and nuclide abundances of sample, multiple scattering, self-shielding, normalization, background, and Doppler broadening were taken into account in performing the fitting analysis [25]. Due to the small average level spacings of the $^{235}$U nucleus, the entire resonance evaluation up to 2.25 keV includes a large number of $s$-wave resonances with spin and parity, $3^-$ and $4^-$, as displayed in Table I.

TABLE I. Neutron energy resonance range for the $^{235}$U evaluation and the number of fitted levels for the two channel spins related to $s$-wave neutrons.

| Nucleus ($I^\pi$) | $E_{\max}$ (keV) | Method | $J_{3-}$ | $J_{4-}$ |
|---|---|---|---|---|
| $^{235}$U ($7/2^-$) | 2.25 | Reich-Moore | 1433 | 1731 |

The upper energy limit $E_{\max} = 2.25\ keV$ of the current evaluation was kept as in the resolved resonance evaluation of the ENDF/B-VII.1 nuclear data library [4, 26], otherwise a re-evaluation of the unresolved resonance range below 2.25 keV would be needed.

Due to the limited resolution of the current measured data and the increasing number of missing levels, the most reasonable upper energy limit for determining rigorously the resonance parameters should be set at 500 eV. However, an extended energy range of the evaluation from 500 eV up to 2.25 keV can be justified by the improved description of the self-shielding effects obtained by reconstructing the cross sections directly from the resonance

parameters. In the neutron energy range between 100 eV up to 1 keV, the resonance parameters were constrained by the average fission cross-section integrals based on the results obtained within the Standards 2017 evaluation [14]. Additional evaluation work and new capture data will be needed to improve the evaluation of resolved/unresolved resonances from 500 eV up to 2.25 keV.

### 1. *Thermal Energy Region*

In the thermal energy range, the IAEA CIELO evaluation of n+$^{235}$U relies on the values of the fission and capture cross sections and neutron multiplicity $\bar{\nu}$ obtained within the standard evaluation of the Thermal Neutron Constants (TNCs) [14, 27]. The new evaluated set of TNCs is based on direct measurements in the neutron thermal energy range and features a reduction of the neutron thermal multiplicity $\bar{\nu}$ as well as an increase of the fission cross section at the thermal energy compared to previous evaluations.

A new evaluation of the PFNS [8–10] for thermal incident neutrons has determined a lower value (2.00 MeV) of the average fission-neutron energy than that reported in the existing evaluated nuclear data libraries (2.03 MeV). Simulations on a number of thermal-solution benchmarks has shown that the combined use of the new TNCs [14, 27] and a softer prompt fission neutron spectrum at the thermal energy yields $k_{\rm eff}$ values that are larger than measurements by a margin that increases as the above-thermal-leakage fraction (ATLF) increases. In view of these findings, the new evaluated values of the TNCs were used in our evaluation procedure to obtain the cross section values at thermal energy as reported in Table II, along with the values of other derived quantities such as $\alpha = \sigma_\gamma/\sigma_{\rm f}$ and $\eta = \nu \cdot (1+\alpha)^{-1}$ (where $\nu$ is the normalization factor related to the fission neutron multiplicity).

TABLE II. Thermal cross sections $\sigma_{\rm f}$, $\sigma_\gamma$, and $\sigma_{\rm el}$ in barns compared to the Neutron Standards 2017 [14] and CONRAD values [27]. Derived non-dimensional quantities like $\alpha$ and $\eta$ (computed for $\nu = 1$) are also reported.

| Quantity | IAEA CIELO[a] | Standards [14] | CONRAD [27] |
|---|---|---|---|
| $\sigma_{\rm f}$ | 586.7 | 587.3±1.4 | 586.4±1.5 |
| $\sigma_\gamma$ | 99.4 | 99.5±1.3 | 99.1±2.1 |
| $\sigma_{\rm el}$ | 14.11 | 14.09±0.22 | 14.05±0.22 |
| $\eta$[b] | 0.8550 | 0.8550 | 0.8550 |
| $\alpha$[b] | 0.1694 | 0.1694 | 0.1690 |

[a] T=0 K.

[b] Calculated from $\sigma_{\rm f}$ and $\sigma_\gamma$ for $\nu = 1$.

### 2. *Resolved Resonance Region (RRR)*

As in the thermal energy region, the evaluation methodology in the neutron resolved resonance range used the Bayesian method implemented in the *R*-matrix code SAMMY to fit available experimental data and ultimately to generate a set of resonance parameters with related covariance matrix. Table III presents an overview of the experimental data sets used in the fitting procedure, as well as some of their features, such as the energy range, sample thickness, and the type of data (*e.g.*, total cross section) and the corresponding normalization factor (*e.g.*, 1.0).

TABLE III. n+$^{235}$U experimental data overview in the resolved resonance region.

| Sample | First author Facility/Year | Energy range[a] Thickness(at/b) | Type Normalization |
|---|---|---|---|
| $^{235}$U(93%) | Spencer [28] ORNL/1985 | 0.3 eV–20 keV 0.001468 | Total 1.0 |
| $^{235}$U(99%) | n_TOF [29] CERN/2016 | 0.5–200 eV – | Fis./Cap. 0.98/1.01 |
| $^{235}$U(93%) | RPI [30] RPI/2016 | 0.01–40 eV 0.00054 | Fis./Cap. 0.99/1.01 |
| $^{235}$U(99%) | ORNL [31] ORNL/1966 | 0.4–65 eV – | Fis./Cap. 1.0/0.97 |
| $^{235}$U(99%) | Jandel [32] DANCE/2012 | 4 eV–0.8 MeV – | Capture 1.0 |
| $^{235}$U(99%) | Weigmann [33] Geel/1990 | 1.5 meV–0.15 eV – | $\eta$ 2.43 |
| $^{235}$U(99%) | Weigmann [33] Geel/1990 | 2 meV–0.5 eV – | $\eta$ 2.43 |
| $^{235}$U(93%) | Brooks [34] Harwell/1966 | 18 meV–0.5 eV – | $\eta$ 2.42 |
| $^{235}$U(99%) | Gwin [35] ORNL/1984 | 1.5 meV–100 eV – | Fission 1.0 |
| $^{235}$U(99%) | Gwin [36] ORNL/1984 | 4 meV–50 eV – | Fission 1.0 |
| $^{235}$U(%) | Weston [37] ORELA/1984 | 13 eV–20 keV – | Fission 1.0 |
| $^{235}$U(99%) | Perez [38] ORELA/1973 | 8 eV–200 eV – | Cap./Fis. 1.0/1.0 |
| $^{235}$U(99%) | Wagemans [39] Geel/1988 | 2 meV–20 eV – | Fission 0.98 |
| $^{235}$U(99%) | Schrack [40] RPI/1988 | 2 meV–20 eV – | Fission 1.0 |
| $^{235}$U(99%) | Harvey [41] ORELA/1988 | 4 eV–3.35 keV .032938 | Trans. 1.0 |
| $^{235}$U(99%) | Harvey [41] ORELA/1988 | 4 eV–3.35 keV .002343349 | Trans. 1.0 |
| $^{235}$U(99%) | Harvey [41] ORELA/1988 | 4 eV–3.35 keV .0005771334 | Trans. 1.0 |
| $^{235}$U(99%) | Harvey [41] ORELA/1988 | 4 eV–3.35 keV .00234335 | Trans. 1.0 |

[a] Measured energy range. Not fitted.

The starting resonance-parameter file was a modification of the ENDF/B-VII.1 evaluation fitted to reduce capture by 30% near 1 keV by Leal [42], using new experimental data by Jandel *et al.* [32] and Danon *et al.* [30] as suggested by Japanese researchers [43, 44].

For energies below 100 eV, particular emphasis was devoted to restore the ENDF/B-VII.1 benchmark performance for $^{235}$U solutions by combining changes to the prompt resonance $\bar{\nu}_p$ (as described in Sec. III A 4) and the resonance parameters. In achieving this, the present set of resonance parameters yields cross sections in reasonable agreement with a more comprehensive suite of experimental data than the one included in the previous resonance evaluations. In this respect, the set of $\eta$

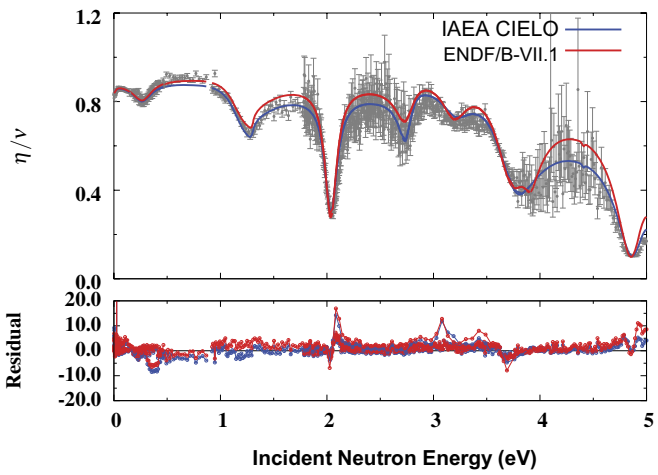


FIG. 1. (Color online) n+$^{235}$U $\eta$ measurements of Brooks [34], Wartena and Weigmann [33] compared to ENDF/B-VII.1 [4] and IAEA CIELO evaluations.

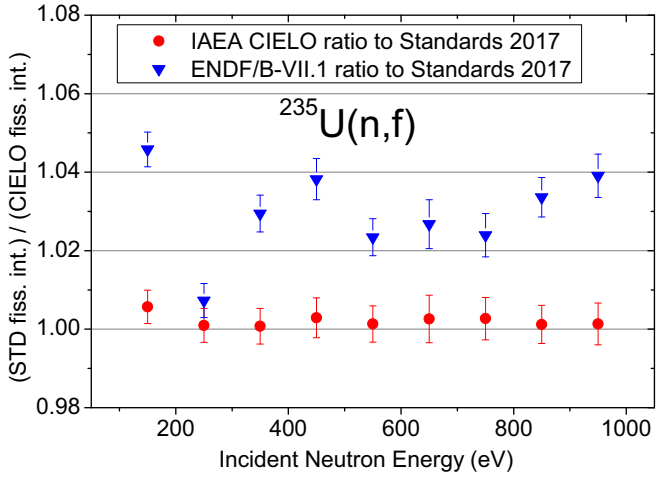


FIG. 2. (Color online) Ratio of n+$^{235}$U average fission cross sections (in 100 eV bins) of ENDF/B-VII.1 [4] and IAEA CIELO values to the Standards 2017 evaluation [14].

measurements performed by Brooks [34] in the mid-1960s at the Atomic Energy Research Establishment (Harwell) were analyzed and included in the fit for incident neutron energies up to 20 eV. Fig. 1 displays multiple measurements of Brooks [34] in the incident neutron energy range up to 5 eV and also measured data of Wartena and Weigmann [33] in the low-energy range up to 0.5 eV. All measurements are normalized to the reported $\nu$ value. The comparison of ENDF/B-VII.1 (in red) and IAEA CIELO (in blue) $\eta$ values is also shown. Although there are large uncertainties above 2 eV, the (lower) $\eta$ values for IAEA CIELO are in better agreement with the experimental data than ENDF/B-VII.1 values. This was achieved by increasing the capture cross sections mostly in the valleys of the resonances while keeping their peak values unchanged. The resonance at $E_{\rm n}$=2 eV is a clear example. The decreased neutron production suggested by Brooks' data also seems consistent with the use of a softer PFNS in order to compensate the increased criticality. Note that high-leakage solution benchmarks feature a neutron spectra slightly harder than well-thermalized systems, therefore, an increase of capture in the region of the first resonances as shown in Fig. 1 preferentially reduces criticality of high-leakage benchmarks with minor impact on well-thermalized systems. This type of information is an example of how the integral experiments have been used in this evaluation to select from different choices of resonance parameters,

In addition to new experimental data sets, the values of the resonance parameters were constrained by cross section integrals, namely, the fission integral in the incident energy range between 7.8–11 eV,

$$I_{\rm f} = \int_{E=7.8\ {\rm eV}}^{E=11\ {\rm eV}} \sigma_{\rm f}(E)dE = 247.5\ {\rm b{\cdot}eV}\,. \qquad (1)$$

The normalization of TOF fission experiments to the integral from 7.8 to 11 eV was recommended by Wagemans and Deruytter [45] in the mid-1980s with a value of 246.1 b·eV. The integral was evaluated to 246.4±1.2 b·eV in the Standards 2006 evaluation [12, 13] in an excellent agreement with Wagemans recommendation. Unfortunately, the recommendation was disregarded in the resonance evaluation in the ENDF/B-VII libraries. The Standards 2017 recommended the value of 247.5 ± 3.0 b·eV which is also in good agreement with the Standards 2006 evaluation.

For incident neutron energies above 100 eV up to 1 keV, a significant constraint on the resonance parameter evaluation was applied by matching the average fission cross section values of the Standards 2017 evaluation [14] as shown in Fig. 2. Average differences of about 3% in the ENDF/B-VII.1 fission cross sections were reduced to less than 1% in the IAEA CIELO resonance evaluation. In doing this, due to the correlation between the ($n$,f) and ($n$,$\gamma$) reaction channel, the resonance parameters were also constrained by keeping constant the ratio between $\sigma_\gamma$ and $\sigma_{\rm f}$ average cross sections, *i.e.*, keeping the average value of $\alpha$, comparable to the ENDF/B-VII.1 evaluation.

### 3. *Unresolved Resonance Region (URR)*

The evaluation in the URR from 2.25 keV up to 25 keV was adopted from ENDF/B-VII.1. The average fission cross section was adjusted to reproduce the low-resolution fission cross sections derived within the Standards project [14]. However, the existing URR evaluation does not reproduce fluctuations observed in high-resolution TOF experiments which are consistent among themselves. Additional evaluation work and new high-resolution capture data will be needed to improve the evaluated fission and capture cross sections in the energy region up to about 50 keV. A good URR evaluation may allow restricting the RRR up to 500 eV to mitigate problems related to the missing higher angular momentum levels.

#### 4. *Fission Neutron Multiplicities and Spectra in $^{235}$U(n,f) Resonance Region*

The quantity $\bar{\nu}_p$ represents the average value of the prompt neutron emission multiplicity distribution, $P_\nu$, and correlates each fission event occurring in a nucleus with the emission of prompt neutrons. In the past, high-resolution measurements of the average number of prompt neutrons, $\bar{\nu}_p$, depending on the incident neutron energy were performed for the most important fissile materials. An example of these measured data for neutrons incident on $^{235}$U target is given in Fig. 3. Here, several data sets from different authors [46–49] are plotted normalized to the $\bar{\nu}_p(E_{\rm th})$ at the thermal energy $E_{\rm th}$=0.0253 eV.

One could describe these measured data by fluctuations that can be roughly correlated with the energy of compound nucleus resonances. Moreover, it is theoretically possible to expect other processes involved in decreasing the number of emitted neutrons; among these, the influence of the $(n,\gamma f)$ process for which a $\gamma$-ray is emitted prior to the fission event. Here, the excitation energy available for the fission reaction channel is diminished leading to a lower neutron multiplicity. As displayed in Fig. 3, in the JEFF-2.2 nuclear data library (solid cyan line), these fluctuations were included in the evaluated data; however, they have been neglected in all other modern libraries.

Fluctuations tend to reduce the average neutron multiplicity for HEU critical solutions having an average energy above 1 eV, therefore, such fluctuations may compensate for the observed increase in criticality of high-leakage assemblies. However, experimental $\bar{\nu}_p$ data are not consistent, therefore, no least-squares evaluation was done. The current evaluated shape of $\bar{\nu}_p(E)$ follows Reed data taken from the EXFOR entry `10427003` [46] up to the maximum energy available of 26.4 eV. A good agreement with Howe data (EXFOR 12870002 [47]) is also demonstrated in Fig. 3 in this energy region. The data were normalized to the prompt thermal value of 2.414 which agrees within uncertainties with the Thermal Neutron Constant value ($\bar{\nu}_{tot}$ = 2.425±0.01) [14]. Simon [49] and Frehaut [50] data shapes (after normalization to thermal nubar) are identical; but show large uncertainties. These data sets are not shown below 30 eV in Fig. 3 to avoid cluttering, but Simon data [49] were used in the evaluation to fill the gap between 30 eV and 75 eV. The energy grid used for nubar tabulation was modified slightly by shifting the energies at 1.135 eV to 1.5 eV and 2.370 eV to 2.25 eV without changing the $\bar{\nu}_p$ values, thus narrowing the dip at 1 eV in order to slightly increase the reactivity of thermal systems. In addition, the dip at 2.04 eV was made shallower by 0.02, which is within the experimental uncertainty.

In summary, the current evaluation in the IAEA CIELO nuclear data library restored the fluctuations of the average number of prompt neutrons as displayed by the solid red line. Further details about the file assembly can be found in Sec. V. To better understand the energy-dependent behaviour of the prompt neutrons and to disentangle the underlying physical processes that are responsible for their fluctuations, high-resolution TOF $\bar{\nu}_p$ measurements in the incident neutron energy range up to 100 eV would be needed, and measurements up to 20 keV are highly desirable. There are no $\bar{\nu}_p$ measurements available from 100 eV up to 20 keV of incident neutron energy.

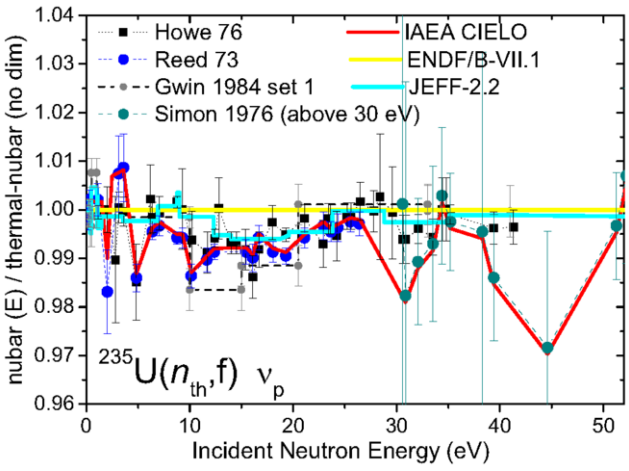


FIG. 3. (Color online) $\bar{\nu}_p(E)$ relative to $\bar{\nu}_p(E_{\rm th})$ calculated at the thermal energy (0.0253 eV) for n+$^{235}$U reactions. Several experimental data sets are compared to ENDF/B-VII.1 (=JENDL-4=JEFF-3.3) and IAEA CIELO evaluations.

The $^{235}$U prompt fission neutron spectrum induced by thermal neutrons was evaluated for Standards 2017 based purely on experimental data using the GMA generalised least-squares code below 10 MeV of outgoing neutron energy combined with the measured spectrum-averaged cross section of $^{90}$Zr(n,2n) reaction to pin down the PFNS above 10 MeV. Further details are given in Sec. III B 3 and Refs. [8–10].

### B. Fast Neutron Range in $n+^{235}$U

Neutron-induced reactions on $^{235}$U have been calculated following the reaction modelling reviewed in Ref. [51]. A preliminary version of the evaluation of $n+^{235}$U reaction in the fast neutron range was published in Ref. [52].

We have used the optical and direct reaction models, pre-equilibrium exciton model, and a full featured Hauser-Feshbach statistical model to calculate the observables for neutron-induced reactions on $^{235}$U and $^{238}$U. The initial model parameter values were those from the Reference Input Parameter Library (RIPL) [53].

The ECIS06 code [54], integrated in the EMPIRE-3.2 code system, was employed to calculate the total, direct elastic and inelastic cross sections as well as the transmission coefficients for the incident neutron channel, using dispersive coupled-channel optical model potentials (*e.g.*, see Ref. [55]). Dispersive integrals were calculated analytically [56–58]. These optical models are isospin-dependent and approximately Lane consistent [59, 60] as shown in Ref. [61].

It has been shown [56] that the Rigid-rotor structure is an excellent approximation for odd-mass actinides. As a consequence, the rigid-rotor optical model optical model potential of Capote *et al.* [62, 63] (RIPL 2408 [53]) was used for neutron-induced reactions on $^{235}$U target. As recommended in Refs. [56, 64], 7 levels of the ground-state rotational band were coupled. When compared with available "optical" experimental data, an excellent agreement was achieved, including total and elastic cross sections and angular distributions.

We employed DWBA calculations on un-coupled discrete levels and pseudo-levels in the continuum to estimate the "collective" direct cross sections. The collective levels used were the same used in $^{238}$U calculations described in Sec. IV C that includes those given by Young *et al.* [65]. Calculated cross sections from these collective states were spread in the continuum using a Gaussian resolution function with $\sigma$=120 keV. These calculations were combined with a compound nucleus contribution to determine the inelastic scattering cross sections and the corresponding angular distributions on low-lying discrete states as well as the elastic cross section and corresponding angular distribution.

An advanced implementation of the Hauser-Feshbach theory [66] is behind the statistical model calculations used in the EMPIRE system, which includes an an exact angular momentum and parity coupling. Discrete level schemes retrieved from RIPL [53] are considered up to a pre-established cut-off energy, and level densities are used above. The correlation between incident and exit channels in elastic scattering (*i.e.*, the width fluctuation correction), was accounted for using the model proposed by Hofmann, Richert, Tepel and Weidenmüller (HRTW) [67]. The importance of considering the influence of direct reactions on calculated neutron inelastic scattering for well-deformed nuclei was recently highlighted [68, 69]. This effect increases the neutron inelastic scattering cross section on coupled levels and decreases the elastic cross section, accordingly [68]. The effect is important to increase the inelastic scattering cross section of even-even targets at incident neutron energies of 100-300 keV. This effect, however, is weaker for odd targets, due to a higher excited-levels density, and it was not employed in the current calculations for $^{235}$U.

The level densities, for both equilibrium deformation and saddle points, are described with the Enhanced Generalized Superfluid Model (EGSM) [15, 16, 53] with parameters appropriate for each deformation. The order of symmetry of the nuclear shape at saddles was incorporated by multiplying the level density with specific enhancement factors as given in Refs. [70, 71].

The full $\gamma$-cascade in the compound and residual nuclei included both continuum and discrete transitions, with a maximum multipolarity equal to 2. Gamma-ray transmission coefficients were obtained from $\gamma$-ray strength functions computed using the Modified Lorentzian model (MLO1 closed form) as detailed in Ref. [53], renormalized to $2\pi\Gamma_\gamma/D_0$ determined from experimentally deduced values of $\Gamma_\gamma$ and $D_0$ [53].

The module PCROSS in EMPIRE was used to calculate pre-equilibrium emission, incorporating a one-component exciton model with gamma, nucleon and cluster emissions [72].

Theoretical fission barriers have been used to calculate neutron-induced fission cross sections, nevertheless, an accurate prediction of fission cross sections remains elusive [73–76]. Empirical triple-humped fission barriers with shallow tertiary humps were employed for the compound nucleus $^{236}$U and lighter uranium isotopes responsible for the multiple fission chances [51, 77], as suggested by theoretical barrier studies [78]. The fission coefficients have been calculated with a formalism based on the extension of the optical model for fission [77, 79], which describes the direct and indirect transmission across the multi-humped fission barriers.

### 1. *Calculated Cross Sections*

Fig. 4 shows all major calculated cross sections, excluding total and elastic. Neutron capture is negligible above 2 MeV, the inelastic cross section is larger than fission's from 300 keV up to 5 MeV, and multiple neutron emission is much lower than fission. We have considered emission of up to four neutrons, one proton and one alpha particle.

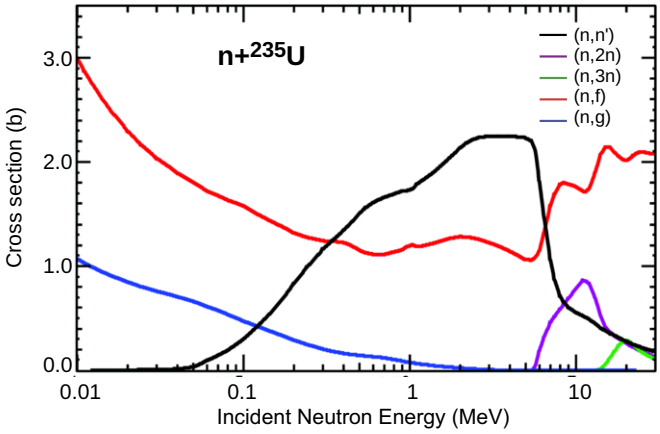


FIG. 4. (Color online) EMPIRE calculated cross sections for major neutron-induced reactions on $^{235}$U used in IAEA CIELO evaluation. Calculated fission cross section was replaced by the Neutron Standard cross section in the evaluated file.

We will now review some of relevant reaction channels. The calculated $^{235}$U($n$,f) cross section is within 3% of the IAEA library Standard cross section [12, 13] as shown in Fig. 5. Such agreement allows for a proper calculation of competing neutron emission channels - ($n$,$n$'), ($n$,2$n$), ($n$,3$n$) - and neutron capture. The calculated $^{235}$U($n$,f) cross section was replaced by the Neutron Standard $^{235}$U($n$,f) cross section [12, 13] in the IAEA CIELO $^{235}$U evaluated file.

EMPIRE calculations of $^{235}$U($n$,$n'$) cross sections adopted as the IAEA CIELO evaluation are compared

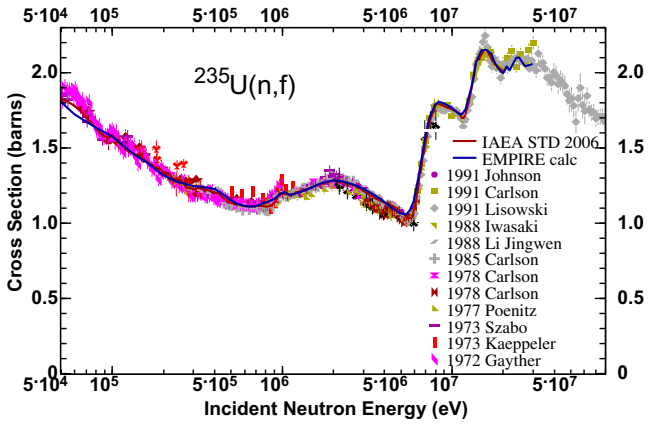


FIG. 5. (Color online) EMPIRE calculated $^{235}$U($n$,f) cross section in the fast neutron range compared with Neutron Standards 2006 [12, 13] and selected experimental data [80–90] retrieved from EXFOR [91].

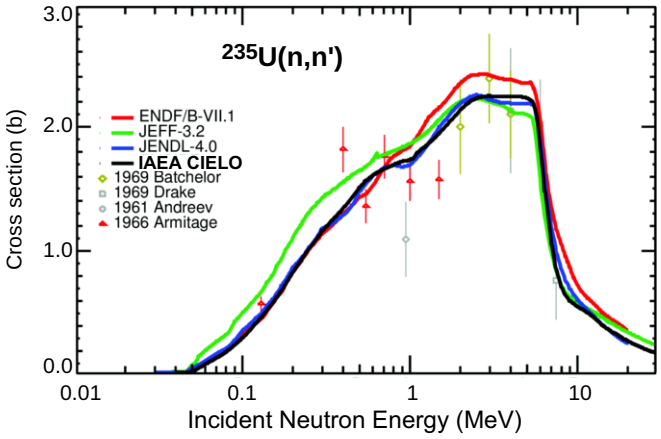


FIG. 6. (Color online) Evaluated total inelastic cross sections [4–6] for $^{235}$U target compared to current evaluation and experimental data [92–95] retrieved from EXFOR [91].

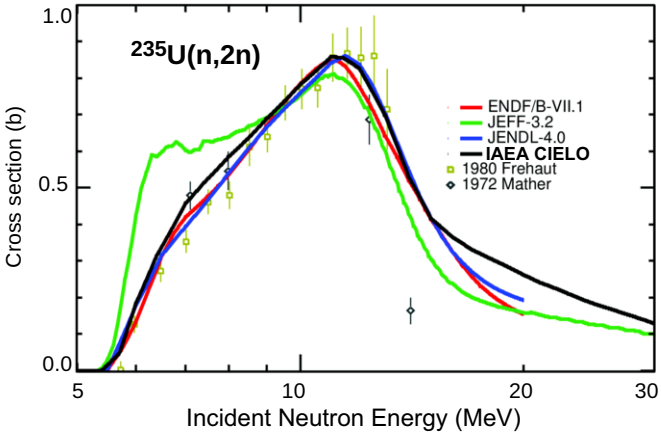


FIG. 7. (Color online) Evaluated cross sections [4–6] for $^{235}$U($n$,2$n$) compared to current IAEA CIELO evaluation and experimental data [96, 97] retrieved from EXFOR [91].

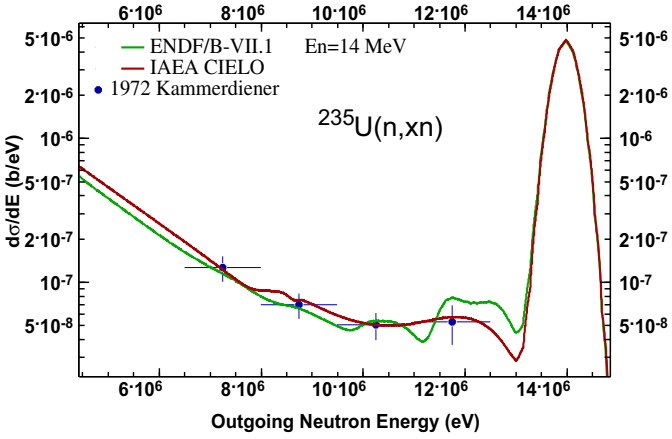


FIG. 8. (Color online) Evaluated neutron emission spectra on $^{235}$U target at 14 MeV incident neutron energy vs Kammerdiener experimental data [98].

with selected evaluations [4–6] in Fig. 6. Important differences among evaluations from 100 keV up to 2 MeV can be seen [11]. The JEFF-3.2 evaluation [5] is consistently larger than all other evaluated data from the threshold up to around 1 MeV. The ENDF/B-VII.1 evaluation [4] is slightly higher than current calculations at the maximum, while JENDL-4.0 evaluation [6] is in very good agreement with the current IAEA CIELO evaluation in the whole energy range.

The ($n$,2$n$) reaction is the main competition for fission above neutron incident energies of 7–8 MeV; Fig. 7 shows a comparison between EMPIRE calculations and selected evaluations. Calculations were adopted as the IAEA CIELO evaluation. Pre-equilibrium emission plays an important role in multiple neutron emission calculations, and the high energy (HE) tail seen in ($n$,2$n$) evaluations originates in the contribution of non-compound reactions (either from the direct inelastic scattering to discrete levels or continuum, or from pre-equilibrium emission). The HE tail in the ($n$,2$n$) current evaluation above 15 MeV is higher than in other evaluations because of additional contributions from inelastic scattering to states in the continuum. The IAEA CIELO evaluation agrees much better with the ENDF/B-VII.1 and JENDL-4 evaluations up to 15 MeV, and experimental data are well accounted for by the current calculations.

The assumed collective levels in the continuum also lead to an improved description of Kammerdiener's experimental data [98] on neutron emission spectra at 14 MeV as shown in Fig. 8, as well as to an improved Monte Carlo simulations of the time-of-flight spectra in pulsed-sphere experiments performed at Lawrence Livermore National Laboratory (LLNL) for the $^{235}$U target [99, 100] (see also Sec. VII C).

Calculated neutron capture cross sections using the statistical model agrees well on average with existing evaluations at energies from 10 keV up to 1 MeV as shown in Ref. [51]. However, recent experimental data for $^{235}$U($n$,$\gamma$) reaction have been published by Jandel *et al.* [32] showing fluctuations from 2 keV up to 200 keV. Neutron capture cross sections were modified using the tuning-factor feature of EMPIRE to follow Jandel fluctuations as shown in Fig. 9(a), since the statistical model alone cannot describe those fluctuations. With this procedure the internal

consistency of the cross sections was preserved.

Additionally, unique AMS $^{235}$U($n$,$\gamma$) measurements have been published by Wallner *et al.* [101], using well-defined neutron spectra relative to well-known neutron capture cross section of gold and $^{238}$U targets, with average incident neutron energies equal to 25 and 426 keV, respectively. Additional reduction of capture was needed to agree with Wallner's data; the relatively large reduction around 25-35 keV is confirmed by Kononov *et al.* [80], Vertebniy *et al.* [102] and Corvi [103] datasets, which were recalculated from measured $\alpha$ ratio using the $^{235}$U($n$,f) standards cross sections [12, 13]. There is some discrepancy in data near 35 keV; the lower data were preferred in the IAEA CIELO evaluation similar to what was done in the ENDF/B-VII.1 evaluation.

Finally, some reduction of the capture cross section from 300 to 500 keV following Wallner measurement [101] was made as shown in Fig. 9(b) compared to the ENDF/B-VII.1 evaluation. In that energy region, the measured spectrum-averaged cross section by Wallner is in agreement within uncertainties with the Jandel [32], Weston [104], De Saussure [105], and Hopkins [106] data, which were recalculated from measured $\alpha$ ratio using $^{235}$U($n$,f) standards cross sections [12, 13].

The agreement of several experimental datasets with Wallner data [101] at both 25 keV and 426 keV supports the choices made in the current evaluation. It should be noted that changes made in capture and fission cross sections in the evaluated file are well within uncertainties of the measured total cross sections. No modification of the elastic cross section was made in the evaluated file. Therefore, small differences are reflected in the summed total cross section.

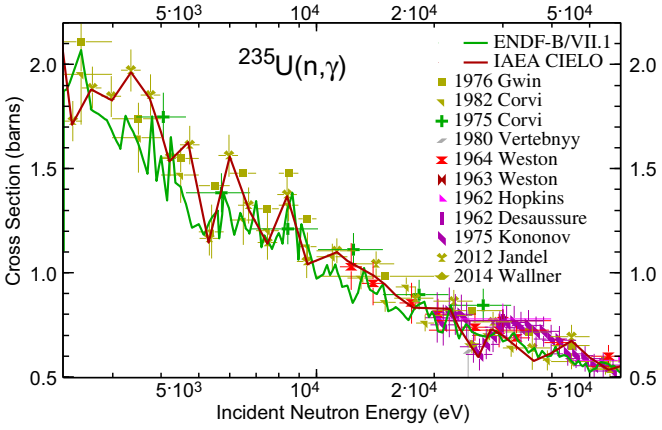


(a) Above the resolved resonance range up to 100 keV.

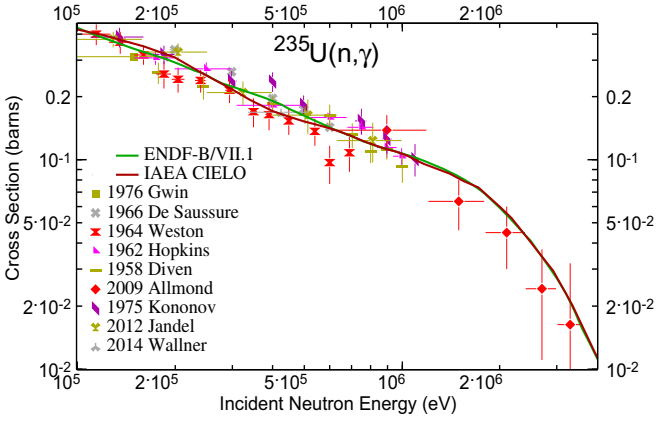


(b) Fast neutron range above 100 keV.

FIG. 9. (Color online) Evaluated $^{235}$U($n$,$\gamma$) cross section compared to experimental data retrieved from Refs. [32, 80, 101–113].

### 2. *Fission Neutron Multiplicities in $^{235}$U(n,f) Fast Neutron Range*

The prompt fission neutron multiplicities above the resonance range were adopted from the ENDF/B-VII.1 library, with the following adjustments. In the energy range 30-70 keV $\bar{\nu}_p$ was reduced following the JENDL-4 evaluation as shown in Fig. 10. Some difference is observed between evaluated dependence and the JENDL-4 evaluation from 1 to 3 MeV. Additionally, the revised interpretation of Standards 2017 [14] as of July 2017 caused an increase in the fission cross section in the unresolved resonance range, which was compensated by a decrease in $\bar{\nu}_p$, starting at 100 eV, reaching the minimum value at 20 keV. A point was added at 30 MeV (approximately extrapolating Frehaut data) for continuity. The number of delayed neutrons per fission $\bar{\nu}_d$ and the corresponding spectra are taken from the ENDF/B-VII.1 library. Delayed neutron uncertainties were taken from Keepin [114] as tabulated by Tuttle [115].

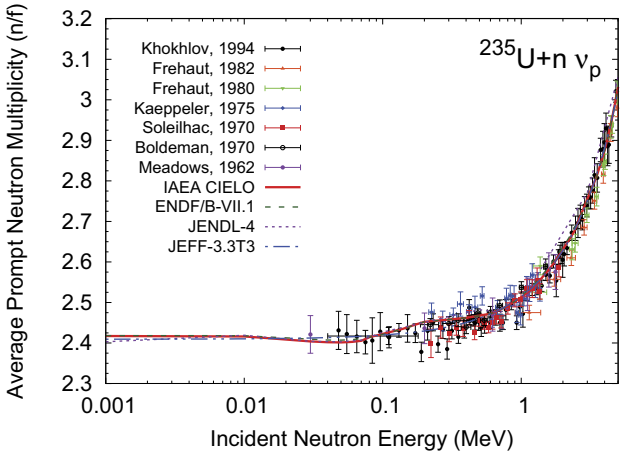


FIG. 10. (Color online) Neutron multiplicity $\bar{\nu}_p(E)$ for $^{235}$U($n$,f) reaction for incident neutron energies from 1 keV up to 5 MeV. Several experimental data sets taken from EXFOR [91] are compared to ENDF/B-VII.1, JENDL-4, JEFF-3.3, and IAEA CIELO evaluations.

### 3. *Prompt Fission Neutron Spectrum in $^{235}$U(n,f) Fast Neutron Range*

The $^{235}$U prompt fission neutron spectrum (PFNS) was studied in detail as part of the "Coordinated Research Project on Prompt Fission Neutron Spectra of Actinides" [10], CIELO [1–3] and the Standards project [14]. As part of these projects, $^{235}$U experimental PFNS, their uncertainties, the PFNS evaluation methodology and models describing PFNS were revisited in great detail in order to give a more reliable estimate of the $^{235}$U PFNS, thus contributing to the reduction of compensating errors in the assembled evaluation. Complementary to the thermal-neutron induced PFNS from the Standards 2017, a model based evaluation [116] that did not consider the experimental data by the Chi-Nu collaboration [117] was adopted for incident neutron energies $E_n$ =0.5–5 MeV; a very similar evaluation, differing only by including the Chi-Nu data, was incorporated for $E_n$ =6–20 MeV.

All three partial PFNS evaluations were obtained via the generalized least-squares algorithm. However, the input for these evaluations differs. Only experimental data at $E_n$=thermal, namely those of Refs. [118–125], were used for the evaluation of PFNS in Standards 2017 [8–10], while the experimental data shown in Table IV were used for IAEA CIELO evaluation by Neudecker *et al.*. Note that Neudecker evaluation included the data measured at the thermal point [118–122] to help fixing the energy-independent model parameters. The experimental covariances of the latter evaluation were estimated in detail following an approach recommended in Sec. III.M of Ref. [10] and included covariances between different experimental data sets. Uncertainty sources were added to these covariances to account for possible biases in the measurements of Refs. [120–122, 126, 127, 130] uncovered in Refs. [132, 133]. This experimental uncertainty estimate and the evaluation itself were undertaken independently from the Standards evaluation [8–10] at $E_n$=thermal. Still, both evaluations agree very well with each other and experimental data up to outgoing neutron energies of $E$ = 8 MeV as shown in the upper part of Fig. 11. Consequently, the mean energies differ only little: the mean energy of the evaluation of Standards 2017 [10] is 2.000 MeV and the one of Ref. [116] is 1.995 MeV in perfect agreement within the estimated 10 keV uncertainty [8–10][1]. The evaluation of Ref. [10] is higher at $E > 8$ because the spectrum averaged cross section (SACS) of $^{90}$Zr(n,2n) was used to fit the high-energy PFNS tail, where available differential experimental data were considered discrepant. The use of SACS of $^{90}$Zr(n,2n) allowed to reduce the estimated uncertainty to around 7% in the high energy tail of the spectrum from 9 up to 14 MeV. Only differential experimental PFNS were used in the evaluation of Ref. [116] leading to much larger uncertainties at 14 MeV outgoing neutron energy and above.

TABLE IV. The experimental data sets used for evaluating the $^{235}$U PFNS for incident neutron energies $E_n$=0.0253 eV–20 MeV are listed with their EXFOR number, first author, outgoing energy range ($E$) and the range of estimated uncertainties $\delta$.

| $E_n$ (MeV) | EXFOR # | First Author | $E$ (MeV) | $\delta$ (%) |
|---|---|---|---|---|
| thermal | 41597002 | Vorobyev [118] | 0.2–10.9 | 1.9–27.9 |
| thermal | 31692006 | Kornilov [119] | 0.7–11.8 | 2.1–36.3 |
| thermal | 40871007 | Nefedov [120] | 0.1–1.9 | 4.2–36.5 |
| thermal | 40871012 | Nefedov [121] | 1.0–7.8 | 2.7–9.1 |
| thermal | 40872007 | Starostov [122] | 4.1–12.1 | 2.8–52.0 |
| 0.4 | 20385003 | Islam [126] | 0.6–6.9 | 8.7–54.8 |
| 0.53 | 20175003 | Johansson [127] | 0.6–14.5 | 3.6–31.6 |
| 1.5 | – | Lestone [128, 129] | 1.5–9.5 | 2.5–66.8 |
| 1.5 | 20394008 | Knitter [130] | 1.8–7.0 | 16.4–124.6 |
| 2.9 | 41110009 | Boikov [131] | 0.2–11.9 | 2.9–35.2 |
| 0.5–1.0 | – | Chi-Nu [117] | 0.1–2.1 | 9.3–11.8 |
| 1.0–1.5 | | | 0.1–2.1 | 9.2–42.0 |
| 1.0–1.5 | | | 0.01–2.1 | 9.2–164.3 |
| 1.5–2.0 | | | 0.01–2.1 | 9.1–51.9 |
| 2.0–3.0 | | | 0.01–2.1 | 9.1–98.0 |
| 3.0–4.0 | | | 0.01–2.1 | 9.2–65.2 |
| 4.0–5.0 | | | 0.01–2.1 | 9.3–126.6 |
| 5.0–5.5 | | | 0.01–2.1 | 9.7–157.8 |
| 5.5–6.0 | | | 0.01–2.1 | 9.6–127.2 |
| 6.0–7.0 | | | 0.01–2.1 | 9.2–360.8 |
| 7.0–8.0 | | | 0.01–2.1 | 9.2–42.2 |
| 8.0–9.0 | | | 0.01–2.1 | 9.3–128.0 |
| 9.0–10.0 | | | 0.01–2.1 | 9.3–70.7 |
| 10.0–11.0 | | | 0.01–2.1 | 9.4–143.5 |
| 11.0–11.5 | | | 0.01–2.1 | 9.6–177.7 |
| 11.5–12.0 | | | 0.01–2.1 | 9.8–129.4 |
| 12.0–13.0 | | | 0.01–2.1 | 9.4–204.6 |
| 13.0–14.0 | | | 0.01–2.1 | 9.4–233.5 |
| 14.0–15.0 | | | 0.01–2.1 | 9.4–56.5 |
| 15.0–17.5 | | | 0.01–2.1 | 9.2–65.9 |
| 17.5–20.0 | | | 0.01–2.1 | 9.2–112.4 |

The evaluations of Refs. [8–10] and Ref. [116] differ also in the model used for the prior. A basis function consisting of a linear combination of a Maxwellian and a Watt function was used for the evaluation at $E_n$=thermal only for scaling the experimental data and to extrapolate to energy ranges without experimental data. In contrast to that, the prior mean values and covariances underlying the Neudecker evaluation were calculated with an extended Los Alamos model (LAM) [116, 136, 137] and the exciton model implemented in the code CoH-3.3.1-Titania [138]. A physics-motivated model is needed for evaluating the $^{235}$U PFNS at $E_n$ ≥1.5 MeV as the few experimental data sets used in the evaluations (see Table IV) cover only part of the outgoing energy range needed for a complete PFNS evaluation. For instance, the data provided by the Chi-Nu collaboration [117] are the only ones considered for $E_n$ ≥3 MeV. These data cover an outgoing energy range of $E$=0.01–2.1 MeV, while evaluated PFNS are usually given for $E$=10 eV–30 MeV.

The simple basis function well-suited for the evaluation at $E_n$ =thermal cannot be used for extrapolating to higher $E_n$, *e.g.*, for evaluations at $E_n$ =14 MeV, because it cannot describe the structures in the PFNS around $(E_n - V_{fis})$ MeV of outgoing neutron energy stemming from the pre-equilibrium component, being $V_{fis}$ the fission barrier of the corresponding fissioning nucleus. These

[1] The uncertainty of the average energy derived from the GMA fit was 5 keV [10]. The uncertainty was increased to 10 keV to consider unrecognized shape uncertainties [14] by scaling the whole PFNS covariance matrix by a factor of 4.8.

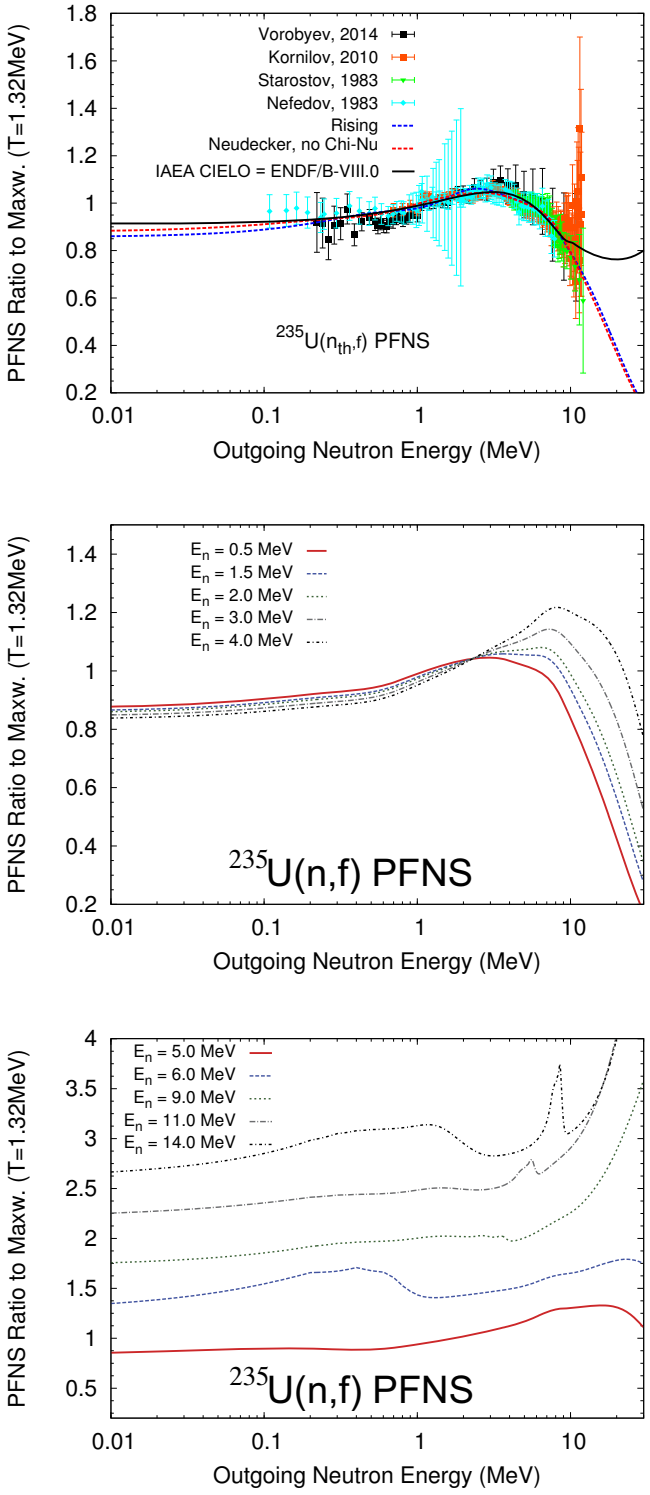


FIG. 11. (Color online) IAEA CIELO evaluated $^{235}$U($n$,f) PFNS spectra are shown for $E_n$ =thermal–14 MeV in ratio to a Maxwellian with temperature $T$=1.32 MeV. At $E_n$ =thermal, the IAEA CIELO evaluation is compared to experimental data [118–122], the evaluation by Rising *et al.* [134, 135], and the evaluation [116] using the Los Alamos Model without considering Chi-Nu data [117]. The latter evaluation was adopted by IAEA CIELO for $E_n$ =0.5–5 MeV. The evaluated data in the bottom panel are shifted vertically for better visibility.

structures are modeled via the exciton model in the evaluation of Ref. [116]. The structures are visible in the bottom panel of Fig. 11 for incident neutron energies starting at 11 MeV as pre-equilibrium contribution to the inelastic spectra becomes significant at those energies. On the other hand, the contribution of very soft fission neutrons (outgoing neutron energies lower than 1 MeV) from $^{235}$U fissioning compound nucleus (due to the $^{235}$U(n,n'f) reaction) is clearly seen at $E_n$ =6 MeV as soon as the second fission chance is open.

Prior covariances for model values of the same and between different $E_n$ were calculated via the extended LAM and varying model parameters as described in detail in Ref. [116]. These prior cross-correlations lead to a consistent behaviour of PFNS across the different $E_n$: the spectra become harder with increasing $E_n$ in the middle part of Fig. 11 and the structures stemming from pre-equilibrium neutron emission move to higher values of $E$ with increasing $E_n$. The good agreement of the independent evaluations at the thermal energy and the consistent modelling of the PFNS should thus lead to an improved evaluation compared to ENDF/B-VII.1 across different incident neutron energies $E_n$.

### C. Gamma Multiplicities and Spectra in $n+^{235}$U

The $\gamma$-ray multiplicities and spectra for individual reactions are obtained from model calculations combined with newer experimental data. The largest contribution to gamma-emission in $^{235}$U target comes from the fission reaction, evaluated by I. Stetcu, P. Talou and M.B. Chadwick, based on experimental data and prompt fission emission modelling [139]. A general description of the evaluation procedure is available in the accompanying paper [139]. An example of the total gamma-emission spectrum induced by 14 MeV neutrons is shown in Fig. 12.

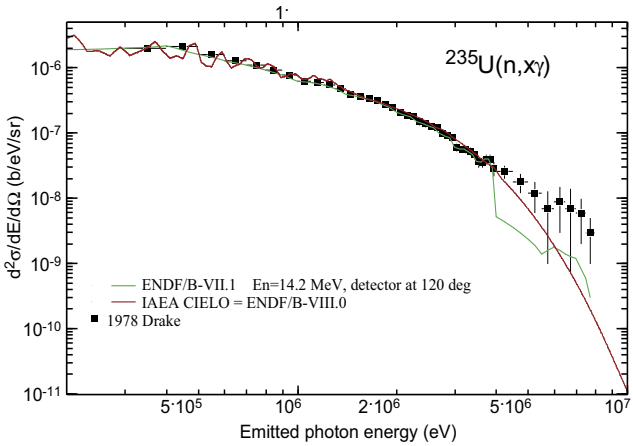


FIG. 12. (Color online) Total $\gamma$-ray emission spectrum at 120 degrees induced by 14 MeV neutrons incident on $^{235}$U compared with data by Drake *et al.* [140].

Note the unusual shape of the spectrum from the ENDF/B-VII.1 library in the energy range 4–6 MeV: the

evaluation followed incorrectly interpreted $\gamma$-ray emission spectrum data by Drake *et al.* [140]. The data in EXFOR were consistent with the published values and were declared as average spectrum integrals. At 4 MeV the energy interval increases from 0.1 MeV to 0.5 MeV, but in the reported average integrals the constant width of 0.1 MeV was used for all points, as can be seen from the figure in the original publication. This was the root cause for the incorrect interpretation of the data in the past, where the wider bin width was assumed above 4 MeV to reconstruct the average spectra from the integrals. Note that the EXFOR entry was recently corrected after discussing it with Drake.

## IV. EVALUATION OF NEUTRON-INDUCED REACTIONS ON $^{238}$U TARGET

Two different energy ranges were considered, the resonance range covering both resolved (RRR) and unresolved (URR) resonances, and the fast neutron range. The RRR extends up to 20 keV, the URR goes from 20 keV up to 150 keV, and the fast range goes from there up to 30 MeV. Description of the evaluation and results in those energy ranges are given below.

### A. Thermal and Resolved Resonance Range

The status of the evaluated data files for neutron interactions on $^{238}$U in the resonance region is discussed in detail by Kopecky *et al.* [141]. This work reveals that in the Resolved Resonance Region the basis of the present evaluated data files is the work of Derrien *et al.* [142]. Results of recent capture cross section measurements reported by Kim *et al.* [143] indicate that the description of the total cross section using the resonance parameters of Derrien *et al.* [142] in the low energy region can be improved. Therefore, the IAEA CIELO file in the RRR was constructed by replacing parameters proposed by Derrien *et al.* [142] for energies below 1200 eV by the ones obtained by Kim *et al.* [143]. The latter were obtained from the least-squares fit to the experimental capture yields derived by Kim *et al.* [143] and the transmission data of Olsen *et al.* [144, 145]. The fission widths were adjusted to reproduce the fission areas of Difilippo *et al.* [146]. For the induced fission reaction a background cross section increasing from 1 keV to the upper RRR boundary of 20 keV was added to conform to the average fission cross section in the unresolved resonance region (URR) at this boundary.

The capture experiments of Kim *et al.* [143] were carried out at the 12.5 and 60 m measurement station of the time-of-flight facility GELINA. The total energy detection principle in combination with the pulse height weighting technique was applied using $C_6D_6$ liquid scintillators as prompt $\gamma$-ray detectors. The data were normalised to the isolated and saturated $^{238}$U resonance at 6.67 eV. Special procedures were applied to reduce bias effects due to the weighting function, normalization, dead time and background corrections, and corrections related to the sample properties. The total uncertainty due to the weighting function, normalization, neutron flux and sample characteristics is $\sim$ 1.5%. The transmission data of Olsen *et al.* [144, 145] resulted from time-of-flight experiments at a 42 m and 150 m station of ORELA using 7 samples of different areal density (from 0.0002 at/b to 0.175 at/b).

TABLE V. $^{238}$U total, elastic and capture cross sections at the neutron thermal energy and resonance integrals (RI) between 0.5 eV and 100 keV calculated from the resonance parameter file recommended in this work.

| Reaction | Cross section (barn) | RI (barn) |
|---|---|---|
| $(n, tot)$ | 11.924 | 593.20 |
| $(n, n)$ | 9.240 | 318.35 |
| $(n, \gamma)$ | 2.684 | 274.63 |

For the analysis in the RRR the resonance shape analysis code REFIT [147], which is based on the Reich-Moore [148] approximation of the $R$-matrix formalism [149], was used. This code also accounts for various experimental effects such as Doppler broadening, neutron self-shielding, multiple interaction events and the response function of the TOF-spectrometer [150]. Both transmission and capture data were analysed without applying any additional background or normalisation correction [150]. The free gas model with an effective temperature of 295 K was used to account for the Doppler effect. The initial resonance parameters, including parity spin and effective scattering radius R' = 9.48 fm, were taken from Derrien *et al.* [142].

To fit the transmission data of Olsen *et al.* [144, 145], without applying a normalization factor, the contribution of the two bound states at -7 eV and -33 eV were adjusted maintaining the thermal capture cross section of (2.683 $\pm$ 0.012) b recommended by Trkov *et al.* [151]. The result of this adjustment is shown in Fig. 13.

After the adjustment the elastic scattering cross section at the thermal energy was reduced by about 0.5% compared to the one in ENDF/B-VII.1. The corresponding coherent scattering length $b_c = 8.57\ fm$ is in agreement with $b_c = (8.63 \pm 0.04)\ fm$ determined by Koester *et al.* [152]. The average total, elastic and capture cross section at the thermal energy are listed in Table V. Kos *et al.* [153] demonstrated that the adjustment of the bound states has no substantial impact on the interpretation of integral benchmark experiments that are sensitive to the cross section data in the thermal energy region, such as the LMT-006 integral criticality benchmark experiment, included in the ICSBEP Handbook [154].

### B. Unresolved Resonance Region in $n$+$^{238}$U

Most of the data libraries refer to the work of Fröhner [155, 156] for the cross sections in the Unresolved Resonance Region (URR). Nevertheless, Kopecky *et al.* [141] observed differences of more than 5% between the capture

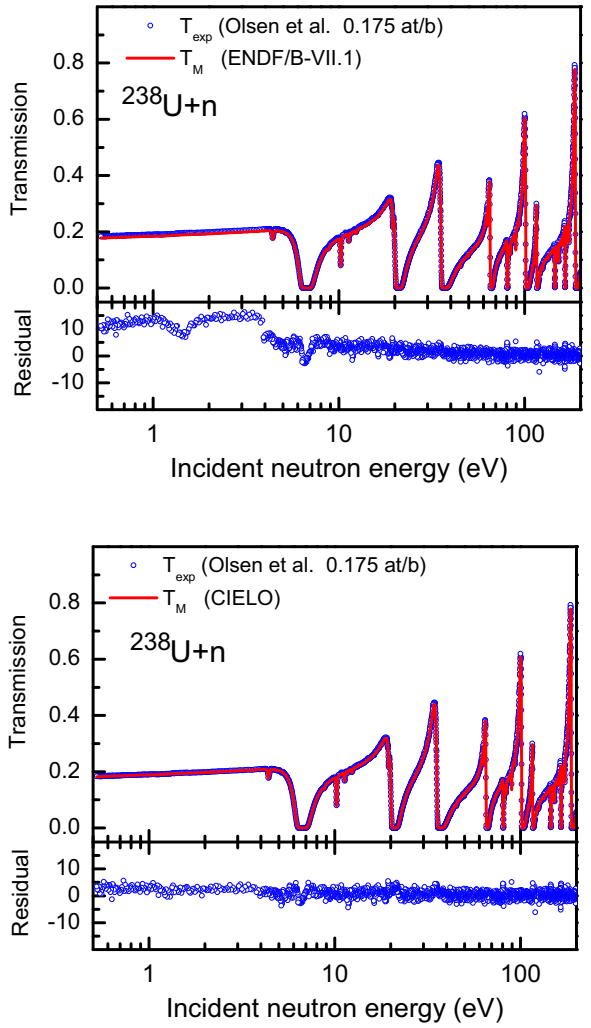


FIG. 13. (Color online) Comparison of the experimental $T_{exp}$ and theoretical transmission $T_M$. The experimental data result from measurements at ORELA with a thick $^{238}$U sample (areal number density of 0.175 at/b). The theoretical transmission results from calculations with REFIT using the ENDF/B-VII.1 resonance parameters (top) and the IAEA CIELO file with the parameters of the bound states at -7 eV and -33 eV adjusted (bottom). The residuals are calculated considering only the uncorrelated uncertainties due to counting statistics.

cross sections recommended in the main data libraries, *i.e.*, ENDF/B-VII.1, JEFF-3.2 and JENDL-4. Therefore, a new evaluation of both the infinitely dilute cross sections and average resonance parameters was performed in the URR. The evaluation is based on the least-squares adjustment to experimental total and capture cross section data reported in the literature. A more detailed discussion on this evaluation is given in Ref. [157]. The generalised least-squares code GMA developed by Poenitz [158], which is available at the IAEA [159], was used to determine an average total $\overline{\sigma}_{tot}$ and capture $\overline{\sigma}_{\gamma}$ cross section for neutron energies between 5 keV and 150 keV. In the analysis the total cross section data of Refs. [160–165] were included. The data of Derrien *et al.* [165] result from the analysis of the high resolution transmission measurements of Harvey *et al.* [166] at the 200 m station of ORELA. The experimental capture cross section data used in the Standards 2006 evaluation [12, 13] were complemented with the capture data of Refs. [143, 167–169].

The results of the GMA analysis are shown in Figs. 14 and 15. Note that GMA cross sections for capture were fitted in the whole energy range above the thermal point; fitted results above 1 keV are shown in Fig. 15. They are compared with the experimental data used in the analysis and the cross sections recommended in the JEF-2.2 library. The latter are based on the analysis of Moxon *et al.* [170] in the RRR and the work of Fröhner [155, 156] in the URR. The average capture cross section $\overline{\sigma}_{\gamma}$ obtained by Carlson *et al.* [13] is also shown in Fig. 15. The GMA results are in much better agreement with the experimental data below 10 keV than Carlson *et al.* [13]; moreover, the uncertainty of the average capture cross section is reduced by about 25%.

As already noted by Sirakov *et al.* [157], differences with the evaluation of Carlson *et al.* [13] are predominantly due to the GELINA data of Kim *et al.* [143]. The uncertainty of their data is substantially smaller compared to the ones of Ullmann *et al.* [167], Mingrone *et al.* [168] and Wright *et al.* [169]. Moreover, there is a large deviation of these new data sets from the Standards evaluated data above 80 keV, even if declared uncertainties are large. Authors of those publications should check missing corrections as their data look very inconsistent with our current knowledge. Note that the $\overline{\sigma}_{tot}$ and $\overline{\sigma}_{\gamma}$ cross sections resulting from the present GMA analysis are in very good agreement with those derived from the JEF-2.2 library in the whole energy range up to 150 keV.

The average total and capture cross sections resulting from the GMA analysis were parameterized in terms of average resonance parameters maintaining full consistency with results of optical model calculations using a dispersive coupled channel potential. The average partial cross sections have been expressed in terms of transmission coefficients by applying the Hauser-Feshbach statistical reaction theory including width-fluctuations. The generalized ENDF-6 model together with the standard boundary conditions has been used (see Sirakov *et al.* [171]).

The coupled-channel OPTMAN code [172, 173] incorporated into the EMPIRE system [15, 16] was used for the optical model calculations. The direct reaction contribution to the inelastic scattering was calculated by using the Dispersive Coupled-Channel Optical Model (DCCOM) potential of Quesada *et al.* [56, 174]. The hard-sphere potential scattering radius R' = 9.483 fm at zero energy, which was adjusted on the results of the GMA average total cross section, is fully consistent with the effective scattering radius used for the analysis in the RRR. The cross sections calculated from the average parameters are compared with the results of the GMA analysis in Figs. 14 and 15.

The average total and capture cross section resulting from the GMA analysis were adopted in File 3 with the LSSF=1 option as infinitely dilute total and capture cross sections, respectively. The inelastic neutron scattering

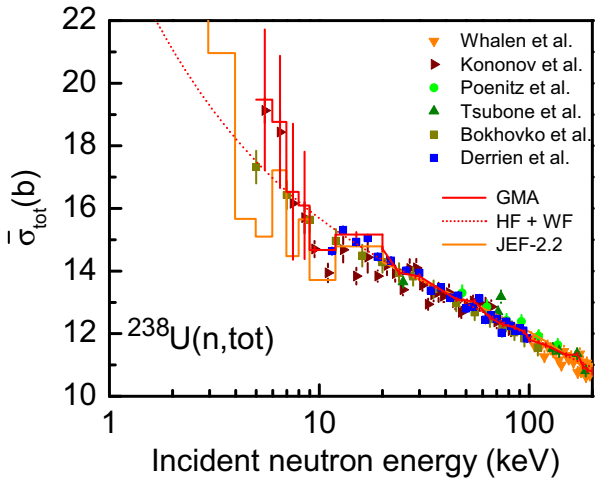


FIG. 14. (Color online) Average total cross section $\overline{\sigma}_{tot}$ for neutron interactions on $^{238}$U as a function of neutron energy. The experimental data of Whalen *et al.* [160], Kononov *et al.* [161], Poenitz *et al.* [162, 163], Tsubone *et al.* [164] and Derrien *et al.* [165] are compared with the results of a GMA analysis of these data and a description of the GMA data by average resonance parameters. The cross section of JEF-2.2, which is based on the Fröhner evaluation [155, 156], is also shown.

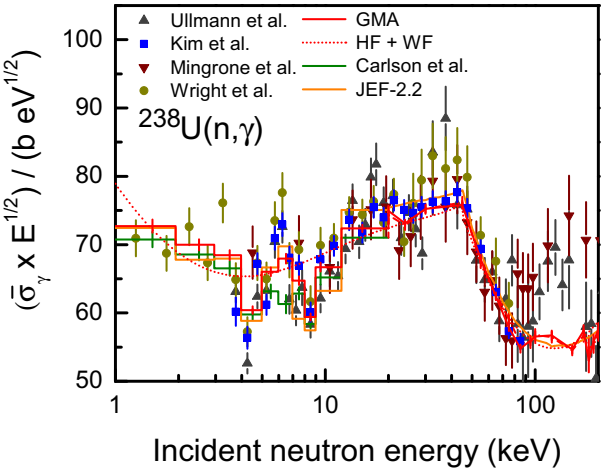


FIG. 15. (Color online) Average capture cross section $\overline{\sigma}_{\gamma}$ for $^{238}$U(n,$\gamma$) as a function of neutron energy. The experimental data of Ullmann *et al.* [167], Kim *et al.* [143], Mingrone *et al.* [168] and Wright *et al.* [169] are compared with the results of a GMA analysis of these data combined with the data used by Carlson *et al.* [13] and a description of the GMA data by average resonance parameters. The cross sections recommended by Carlson *et al.* [13] and the one of JEF-2.2, which is based on the Fröhner evaluation [155, 156], are also shown.

cross section data of Capote *et al.* [69, 175, 176], which include compound-direct interference effects, were also adopted for the present evaluation by modifying the calculated infinitely dilute inelastic cross section.

At lower energies extending into the unresolved and the resolved resonance region the information on the sub-threshold fission resonance data is poor. The shape of the cross sections in ENDF/B-VII.1 is un-physical. Background was added so that after resolution-broadening the fission cross section matches the low-resolution experimental data (some difference remain fom 2 to 5 keV), particularly those of Slovacek [177], as shown in Fig. 16. This estimation is very close to the fission cross section in JEFF-3.2, but shows a more reasonable trend at the URR boundaries. The boundary between RRR and URR was kept at 20 keV. It should be noted that no substantial difference was found in the interpretation of integral benchmark experiments by reducing the upper level of the RRR to 10 keV, which shows the consistency between RRR and URR cross sections. More details on the effect of the upper boundary for the RRR can be found in Ref. [141].

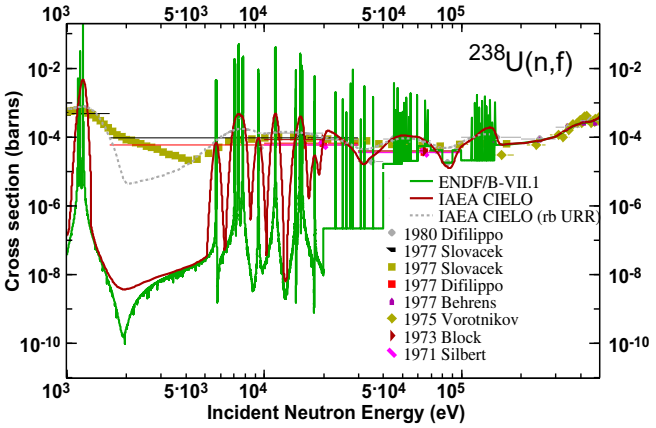


FIG. 16. (Color online) $^{238}$U(n,f) cross sections from ENDF/B-VII.1 and ENDF/B-VIII.0 evaluations are compared with the resolution-broadened ENDF/B-VIII.0 evaluation (dashed), the low-resolution data of Slovacek *et al.*[177], and other data taken from EXFOR [91].

To construct the covariance matrix of the cross sections in both the RRR and URR a covariance matrix of the resonance parameters is combined with one fully correlated uncertainty cross section component. The covariance matrix of the resonance parameters is derived by propagating mainly the uncorrelated uncertainties due to counting statistics. For the elastic cross section a correlated component due to a correction with an uncertainty of 0.05 b is propagated, reflecting the uncertainty on the scattering radius. For the capture cross section an additional uncertainty of 1.5% due to a normalisation correction factor is propagated. By this approach these correlated components can be included over the full energy range from the thermal energy region up to the continuum.

### C. Fast Neutron Range in $n+^{238}$U

The fast energy range of neutron scattering on $^{238}$U is of particular interest to many nuclear applications. Given the large uncertainty and scarcity of the available experimental inelastic scattering data on $^{238}$U (especially of the total inelastic), nuclear reaction modelling plays a central role in the evaluation of neutron scattering cross sections [11]. Therefore, improvement and benchmarks of the modelling are crucial for better prediction of the unknown inelastic scattering cross sections.

Neutron-induced reactions on $^{238}$U have been calculated following the reaction modelling reviewed in previous Sec. III B. A detailed description of different aspects of the reaction modelling have been published in Refs. [51, 69, 175, 176].

Significant advances have been made in the formulation and parametrization of coupled-channel optical model potentials based on dispersion relations capable of describing existing total cross section measurements within quoted experimental uncertainties in the whole energy range of interest (see Refs. [53, 55] and references therein). A new rotational-vibrational dispersive optical model potential has been derived that couples the low-lying collective bands of vibrational character observed in $^{238}$U nucleus while preserving the good quality of description of other observables [56, 174]. Special attention is paid to the coupling of almost all excited levels below 1 MeV of the excitation energy, because neutron scattering on these low-lying levels plays a significant role in the energy region from 0.5 to 1 MeV of maximum interest for fast reactor systems. The coupled-channel OPTMAN code [172, 173] was used for the optical model calculations.

Additionally, we followed the empirical approach proposed by Young *et al.* [65], who postulated the existence of a series of collective $2^+$ and $3^-$ states (see Table VI in Ref. [65]) at excitation energies in the continuum ($E_x$ =1–4 MeV) with dynamical deformations fitted to reproduce measured emission spectra at 14 MeV on $^{238}$U target, in particular Kammerdiener measurements using thin targets [98]. Cross sections and angular distributions from these collective states were also calculated by DWBA, and their strength was spread in the continuum using a Gaussian resolution function with $\sigma$=70 keV.

Double-humped fission barrier model was employed for $^{238}$U target [51, 69, 175, 176]. The fission coefficients have been calculated with a formalism based on the extension of the optical model for fission [77, 79], which describes the direct and indirect transmission across the multi-humped fission barriers.

### 1. *Calculated Cross Sections*

All major calculated cross sections are shown in Fig. 17(top). Neutron capture is practically negligible above 3 MeV, inelastic cross section is much larger than fission and capture from 60 keV up to 5 MeV, and (n,2n) cross section is larger than fission from 8–12 MeV. This explains the importance of inelastic scattering to properly describe neutron-induced reactions on $^{238}$U target. Inelastic scattering is the dominant reaction channel in the region of interest for reactor applications, which corresponds to the maximum of $^{235}$U($n$,f) PFNS from 1–2 MeV. Emission of up to 4 neutrons, 1 proton and 1 $\alpha$ were considered. Let review calculated cross sections.

The effect of target deformation on the calculated compound inelastic scattering cross sections is demonstrated in Fig. 17(bottom) and was studied in Refs. [69, 175]. As

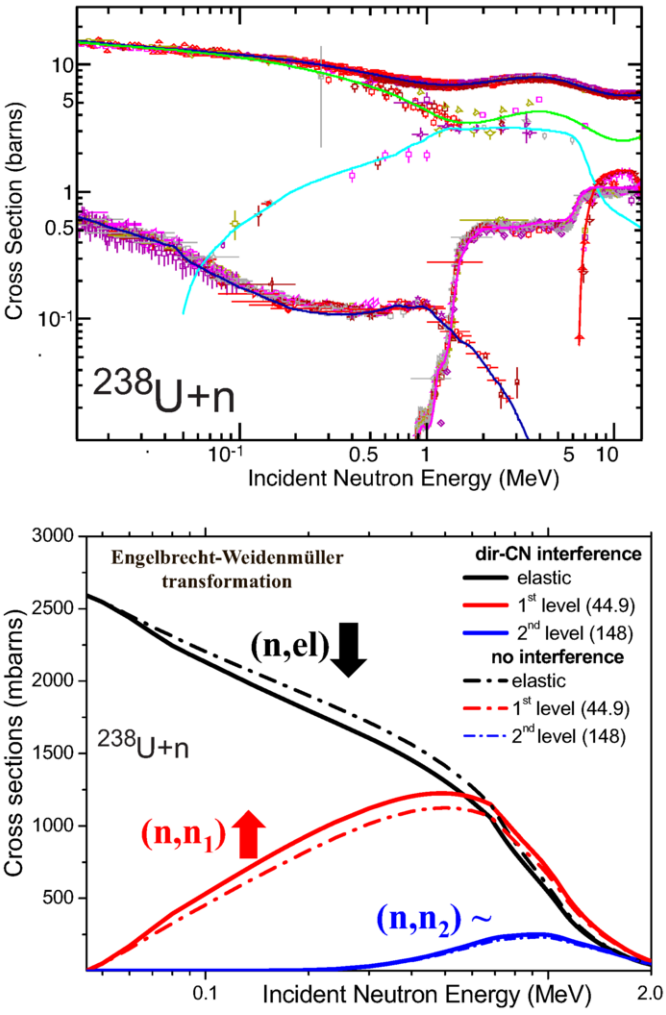


FIG. 17. (Color online) Neutron-induced reaction cross sections on $^{238}$U (top) and effect of the Engelbrecht-Weidenmüller transformation [179] on elastic and inelastic scattering on the first two excited levels of $^{238}$U (bottom). Experimental data in the top panel have been taken from EXFOR [91].

discussed by Moldauer [178], the interference between the neutron scattering on the ground state (elastic channel) and the scattering on the first inelastic level causes an enhancement of the fluctuating compound-nucleus (CN) cross sections in the presence of direct reactions [68]. The strongest interference effect is expected when only two channels contribute, as it is precisely the case for neutron incident energies below 300 keV (see Fig. 17(bottom)). CN calculations that consider interference effects were carried out by using the Engelbrecht-Weidenmüller transformation [179] as implemented within the ECIS code [54]. The interference effect results in a net increase of the CN inelastic scattering cross section on the first excited level at 45 keV compensated by a reduction in the elastic channel (due to the reduction in the CN elastic cross section) as shown in Fig. 17(bottom). This effect goes in the opposite direction to the width fluctuation correction.

A comparison of evaluated total inelastic cross section with experimental data is shown in Fig. 18. The effect of

deformation on calculated CN inelastic scattering results in the observed cross section increase compared with the JEFF-3.2 [5] and JENDL-4 [6] evaluations below 500 keV. However, these calculations are still lower than ENDF/B-VII.1 evaluation [4] in the same energy region.

Current calculations produce the highest inelastic cross sections from 700 keV up to approximately 1 MeV, as a direct result of the strong coupling between all low-lying collective levels extending up to an excitation energy of 1 MeV (see Fig. 18). The agreement of calculated (n,n') cross sections with experimental data is very reasonable considering inconsistencies between measured datasets.

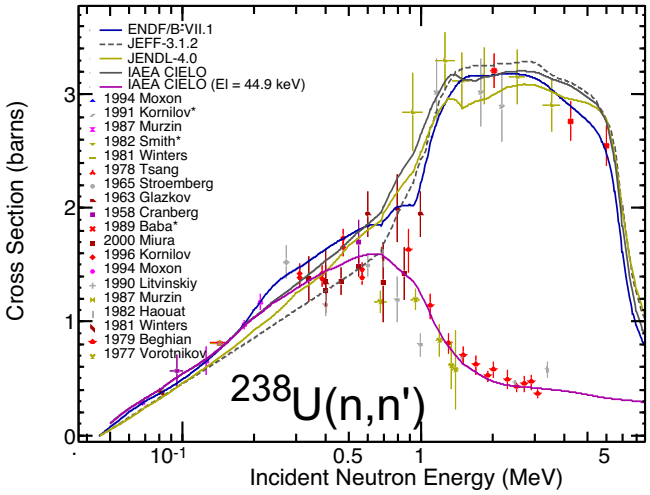


FIG. 18. (Color online) Calculated total and partial inelastic $^{238}$U(n,n') cross sections on 45 keV level compared with experimental and evaluated data files. Experimental data have been taken from EXFOR [91].

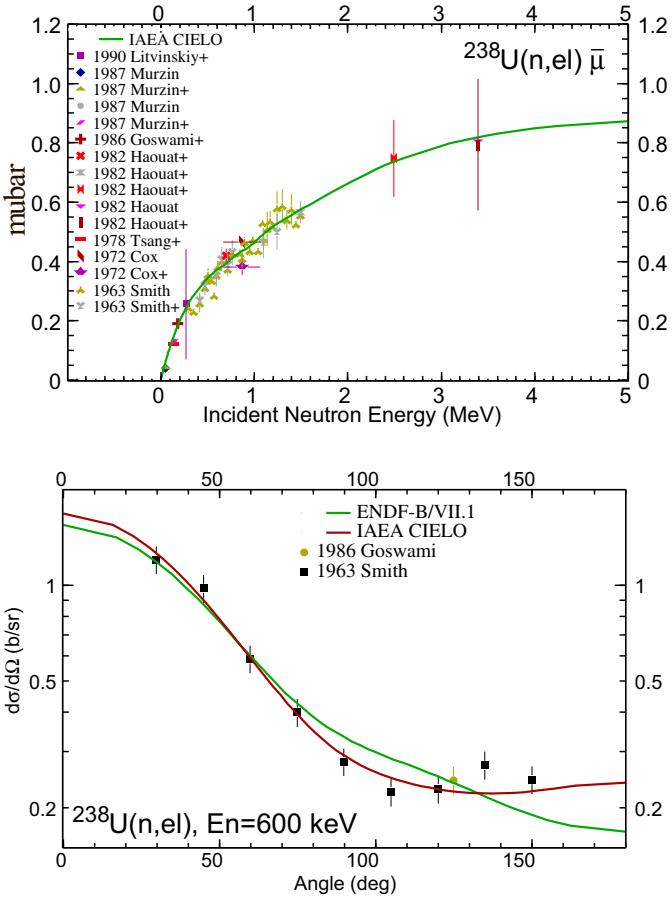


FIG. 19. (Color online) Average cosine of neutron elastic scattering $\overline{\mu}$ on $^{238}U$ (top). Angular distribution of neutron elastic scattering at 650 keV incident energy (bottom) on $^{238}U$. Experimental data have been taken from EXFOR [91].

The average cosine of scattering $\overline{\mu}_{el}$ is a commonly employed measure of the anisotropy of elastic scattering, which roughly determines the forward scattering. Experimental data derived from measured angular distributions of resolved elastic scattering for energies lower than 3.4 MeV are in excellent agreement with the smooth curve predicted by the EMPIRE calculations in Fig. 19(top). Such agreement demonstrates the good quality of the optical model potential employed.

Fig. 19(bottom) presents calculated elastic angular distribution for incident neutron energies of 650 keV compared to the Smith 1963 data. An excellent agreement with data is shown for the IAEA CIELO compound-nucleus (CN) anisotropic calculation leading to a large increase of neutrons scattered in the backward direction for angles above 150 degrees. Young's calculations that defined the ENDF/B-VII.1 evaluation probably assumed isotropic CN elastic angular distribution, therefore, elastically scattered neutrons were severely underestimated in the backward direction. While the absolute number of neutrons scattered backward is small, those neutrons have a large impact on fast critical assemblies that contain $^{238}$U (or natural uranium) in the core (*e.g.*, Jemima benchmarks) or use it as a reflector (*e.g.*, Flaptop benchmarks). Note that the discussed differences in backward elastic scattering can not be seen in the comparison of the average cosine of scattering $\overline{\mu}_{el}$ shown in Fig. 19(top). Only higher-order Legendre even polynomial coefficients of the elastic scattering distribution are sensitive to the backward scattering.

The assumed collective levels in the continuum taken from Young *et al.* lead to improved description of Kammerdiener experimental data [98] on neutron emission spectra at 14 MeV as shown in Fig. 20, as well as to improved Monte Carlo simulations of the time-of-flight spectra in pulsed-sphere experiments for the $^{238}$U target [99, 100] (see also Sec. VII C). It is worth noting that the same collective levels were giving higher emission cross section in the ENDF/B-VII.1 evaluation. ENDF/B-VII.1 evaluation was reproducing measured double-differential data by Baba *et al.* [183], but the evaluated ENDF/B-VII.1 $^{238}$U(n,f) PFNS had an un-physically low average fission-neutron energy for 14 MeV incident neutrons as discussed in Sec. VII C. Such defect compensated for the overestimation of the inelastic spectra. This work achieved a consistent description of measured double-differential cross sections on thin $^{235}$U and $^{238}$U targets by Kammerdiener [98] using the same set of collective levels, but the cor-

rected PFNS taken from the JENDL-4 library [6]. Such consistency is reassuring, but the ultimate solution of the data discrepancy observed in Fig. 20 may require new experimental efforts, and also revisiting theoretical calculations [180–182] to properly consider the effect of PFNS on the comparison with measured data.

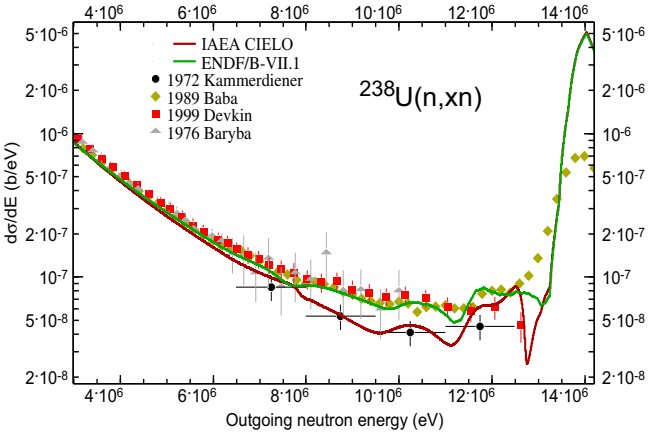


FIG. 20. (Color online) Evaluated neutron emission spectra on $^{238}$U target at 14.1 MeV incident neutron energy vs available experimental data [98, 183–185].

### D. Fission Neutron Multiplicities and Spectra in $^{238}$U($n$,f)

The prompt fission neutron multiplicities $\bar{\nu}_p$ in the fast region are shown in Fig. 21. The starting $\bar{\nu}_p$ values were also taken from ENDF/B-VII.1, but modified slightly based of the review of the available experimental data and the performance in integral benchmarks as shown in Fig. 21 for incident neutron energies from 500 keV up to 5 MeV. Resulting $\bar{\nu}_p$ energy dependence follows closely the Frehaut data that includes an inflexion point near 3 MeV [50]. This behaviour is not shown by other data sets and also disagrees with JENDL-4 and JEFF evaluations, which show an almost linear dependence with the incident neutron energy. The changes made due to the matching of integral benchmarks were only a small fraction of the spread in experimental data. The total $\bar{\nu}_{tot}$ was the sum of the prompt and the delayed contributions.

Recently evaluated $^{238}$U PFNS by Rising *et al.* [134, 135] were adopted for IAEA CIELO for incident neutron energies of $E_n \leq 5$ MeV and are shown in Fig. 22.

The underlying evaluation provides not only $^{238}$U PFNS but also consistent PFNS of $^{229-237}$U isotopes. These consistent PFNS are obtained by fitting simultaneously Los Alamos model parameter systematics dependent on the neutron number of the uranium isotope to differential experimental PFNS of $^{233,235,238}$U via the Kalman filter. The resulting posterior observables are parameter systematics for the average total kinetic energy of the

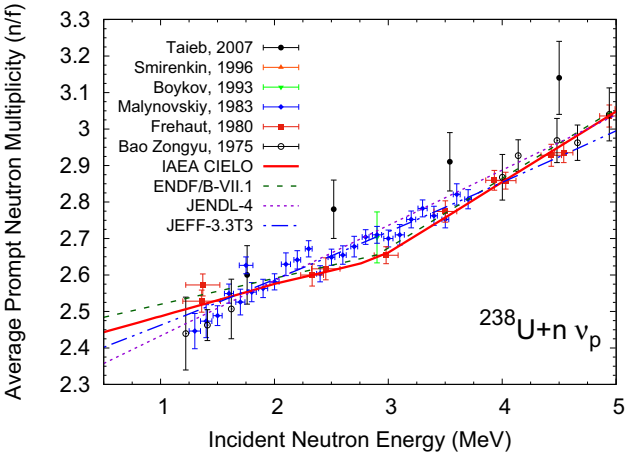


FIG. 21. (Color online) Neutron multiplicity $\bar{\nu}_p(E)$ for $^{238}$U($n$,f) reaction for incident neutron energies from 500 keV up to 5 MeV. Several experimental data sets taken from EXFOR [91] are compared to ENDF/B-VII.1, JENDL-4, JEFF-3.3, and IAEA CIELO evaluations.

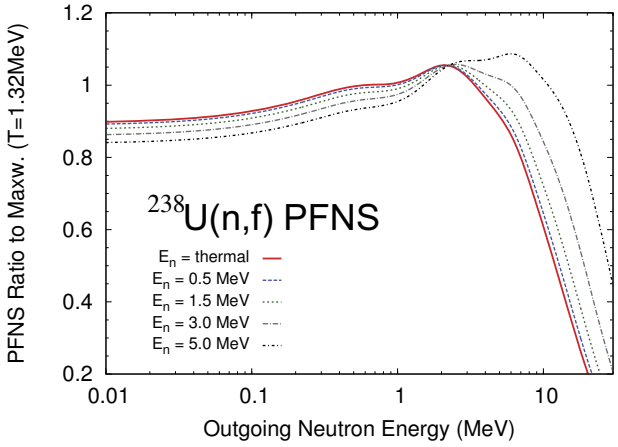


FIG. 22. (Color online) IAEA CIELO evaluated $^{238}$U PFNS spectra are shown for $E_n$ from thermal up to 5 MeV in ratio to a Maxwellian with temperature $T$=1.32 MeV.

fission fragments, the average energy released, the average level density parameter and the anisotropy parameter for $^{229-238}$U isotopes. These parameter systematics are then used to calculate corresponding evaluated PFNS via the Los Alamos model. The resulting $^{235}$U PFNS at thermal by Rising *et al.* [134, 135] agree very well with evaluations adopted for IAEA CIELO [8, 116]. Thus the IAEA CIELO $^{235}$U and $^{238}$U PFNS are consistent with each other.

The IAEA CIELO $^{238}$U PFNS, similarly to the evaluated $^{235}$U PFNS in the middle of Fig. 11, become systematically harder with increasing $E_n$ up to 5 MeV as seen in Fig. 22. This systematic hardening is caused by the $E_n$-dependence of the Los Alamos model. However, the parameter systematics of [134, 135] are only valid for the first chance fission contribution to the PFNS and should not be used to provide evaluated PFNS for $E_n$ >5 MeV.

Hence, ENDF/B-VII.1 PFNS were adopted for the

IAEA CIELO evaluation for $E_n$ >5 MeV and JENDL-4.0 PFNS above 8 MeV. There are compelling indications that the adopted ENDF/B-VII.1 PFNS from 5 to 8 MeV does not reproduce existing PFNS measurements showing an onset of very soft $^{238}$U($n$,$n'f$) neutrons above 5 MeV as pointed out by Maslov. It could be a better solution to follow JENDL-4 PFNS above 5 MeV, but extended testing would be needed. Additional work will be needed to reevaluate $^{238}$U($n$,f) PFNS above 5 MeV; new experimental data (*e.g.*, from a Chi-Nu LANL facility) are highly desirable.

### E. Gamma Multiplicities and Spectra in $n+^{238}$U

As for $^{235}$U the $\gamma$-ray multiplicities and spectra for individual reactions, these are obtained from model calculations. The contribution from the fission reaction was evaluated by I. Stetcu, P. Talou and M.B. Chadwick for the ENDF/B-VIII.0 library, based on experimental data and prompt fission emission modelling[139]. A general description of the evaluation procedure is available in the accompanying paper [139].

An example of the total $\gamma$-ray emission spectrum induced by 2 MeV neutrons is shown in Fig. 23. The bump observed in the new evaluation from 1 MeV to 2 MeV of emitted photon energy is due to the contribution from neutron inelastic scattering, which is dominant in that energy region as discussed in Sec. IV C.

ENDF/B-VII.1 evaluation lumped all gammas, while a new ENDF/B-VIII.0 evaluation successfully combined fission gammas with gammas produced by other reactions.

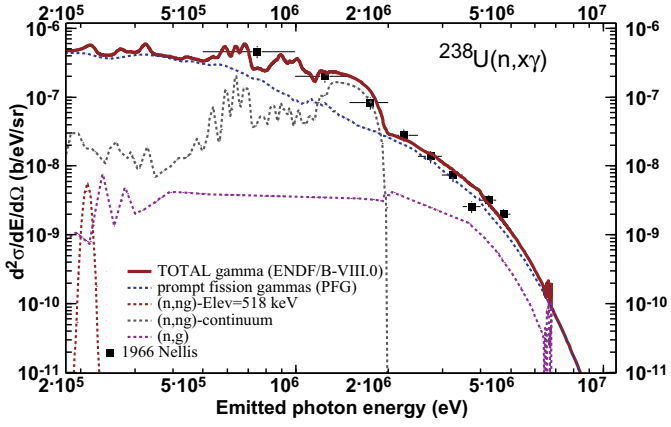


FIG. 23. (Color online) Total $\gamma$-ray emission spectrum at 55 degrees induced by 2 MeV neutrons incident on $^{238}$U compared with data by Nellis *et al.* [186].

## V. EVALUATED DATA FILE ASSEMBLY AND DATA UNCERTAINTIES

ENDF-formatting of the results of EMPIRE calculations is done with the EMPEND code, which is a standard module of the EMPIRE package. The non-threshold absorption reactions which are non-zero at the first calculated point are extrapolated to thermal as $1/v$. Elastic angular distributions are extrapolated flat down to thermal from the first calculated point. Nevertheless, the formatted file obtained in this way is incomplete since not all quantities are calculated, or calculated accurately enough. Additional data sources and utility codes are employed in the file-assembly process. Specific features of the file assembly are given below.

The resonance parameters are inserted with the ENDRES code of the EMPIRE package, taking care to match consistently the energy boundaries between the resonance and the fast energy range.

Covariance matrix prior is assembled by random sampling of the model parameters. This affects all cross sections, including the differential and double differential ones, which opens the door for constructing cross-reaction correlations. In fact, all reactions have covariances, some in the form of "lumped reactions", *e.g.*, inelastic covariances are given in MT51 (first inelastic level) and MT851 (remaining inelastic levels+continuum). This feature is extremely important because it allows the preservation of unitarity. The covariance matrix of the total cross section is the sum of all partial covariance cross sections, including all cross correlations between the reactions, which is consistent with the ENDF philosophy.

In addition to the cross sections, the global covariance matrix prior also includes the covariances of the average cosine of scattering $\bar{\mu}_{el}$ in the laboratory system ($P_1$ Legendre polynomial coefficient) and of the $P_2$ coefficient at several energy intervals, including cross-correlations. Note that the covariances of $P_1$ and $P_2$ Legendre polynomial coefficients with the elastic cross section (proportional to $P_0$) were usually not given. Therefore, very important correlations between angular distributions and elastic cross sections are missing in the existing evaluated files.

Although the main structures observed in the shape of the capture and fission cross sections are modelled with the use of tuning parameters within EMPIRE, the nuclear models are far from being perfect and cannot describe certain features that might be present in the data. Additionally, models feature a relatively small number of parameters describing many data points. Therefore, the model covariance matrix is typically too stiff (too rigid). To soften the correlations the variance of all quantities in the prior was increased by adding a 3% statistical uncertainty on the model-covariance matrix diagonal for all energies in the evaluation grid.

The prior mean values and the covariances were fed to the generalized least-squares code GANDR, after which experimental data are introduced in the Bayesian approach. Since the prior is chosen such that it represents well the experimental data, the cross sections are not expected to change much. The main differences occur in the uncertainties and correlations.

Details of the above procedures specific to each nuclide are described below.

### A. $^{235}$U Target

The new resonance evaluation was produced at ORNL as described in Sec. III A. In the unresolved resonance range the average parameters were adopted from ENDF/B-VII.1, but these are only used for self-shielding calculations because the cross sections are tabulated explicitly. The existing resonance evaluation was merged into the IAEA CIELO file.

The full covariance matrix of the resolved resonance parameters is too big to be practically useful. Note that the ideal solution could be to use the resonance parameter covariance matrix (ENDF File 32) only up to 100 eV, the remainder being given in group-wise form (ENDF File 33, LB=5) on a suitable fine energy grid. However, implementation challenges and time constrains prevented the use of such solution. Therefore, the cross section covariances were generated on a fine energy grid and inserted into the final ENDF file using ENDF File 33 format. The covariances in the unresolved resonance region are evaluated together with those for the fast energy range.

The fission cross section is the Standard at the thermal energy, from 7.8 to 11 eV, and in the energy range from 0.15 MeV to 200 MeV, but it was evaluated at lower energies along with the Standards on a coarse energy grid as bin-averaged values down to 100 eV. Above 150 keV, in the region of the Standards, the matching of the current evaluation is exact. At lower energies in the resolved resonance region there exist some minor deviations, which may require a re-evaluation of the resonance parameters, but this is left for future work.

In the unresolved resonance range the cross section shape is taken from the ENDF/B-VII.1 library, rescaled such that consistency with group-averaged values in Standards is preserved. Above the unresolved resonance range up to 75 keV the shape is from a broad average of the linearised Weston data, rescaled in a similar manner. Above 75 keV the data are taken from the Standards 2017 directly. There remain discrepancies from 5 keV up to 75 keV between the shape of fission cross section (that reflects a broad average) and measured high-resolution data (*e.g.*, by n_TOF collaboration). Unfortunately, to address such differences a new comprehensive evaluation of capture and fission yields in the URR is needed that would describe measured data using the unresolved-resonance formalism.

The matching of the capture cross section with experimental data is done at the level of the nuclear model calculation as described in the previous Section. No additional tuning was performed during the file assembly.

The evaluation of the average number of prompt neutrons per fission $\bar{\nu}_p(E)$ is described in Sec. III A 4.

The prompt-fission neutron spectra consist of the following:

- Standards 2017 for incident thermal neutrons.
- LANL evaluation (without Chi-Nu data [117]) below 5 MeV.
- LANL evaluation above 5 MeV using Chi-Nu experimental data [117].
- The 20 MeV PFNS is duplicated at 30 MeV for completeness; new evaluation of PFNS is required above 20 MeV.

The prompt-fission gamma multiplicities and spectra were provided by I. Stetcu ad M.B. Chadwick (LANL). A detailed description of the evaluation process is included in the accompanying paper describing the ENDF/B-VIII.0 library [139].

The covariance matrix prior was generated using the EMPIRE code by random sampling of the parameters listed in Table VI. Parameter uncertainties are loosely based on RIPL uncertainties [53]; their uncertainties have been extended to cover the range of scaling of those parameters used to fit the experimental data. For a prior calculation it is important that uncertainty bands of the model cover all selected experimental data. In other words, we enforce the least-squares requirement that model calculations and data should be statistically consistent.

TABLE VI. Input nuclear reaction model parameters for the $^{235}$U calculation and their uncertainties used in EMPIRE for random sampling to generate the covariance matrix prior.

| EMPIRE input parameter | Symbol | Value | Unc.(%) | Nucleus |
|---|---|---|---|---|
| Preeq. mean-free path | PCROSS | 1.86 | 15 | |
| Preeq. level density normal. | GTILNO | 0.80 | 20 | $^{236}$U |
| Preeq. level density normal. | GTILNO | 0.98 | 5 | $^{235}$U |
| Preeq. $\Gamma_n$ normal. | TUNEPE | 1.40 | 10 | $^{235}$U |
| Preeq. $\Gamma_\gamma$ normal. | TUNEPE | 1.15 | 10 | $^{236}$U |
| Level density normalization | ATILNO | 0.99 | 5 | $^{236}$U |
| Level density normalization | ATILNO | 0.99 | 10 | $^{235}$U |
| Level density normalization | ATILNO | 0.99 | 10 | $^{234}$U |
| Level density normalization | ATILNO | 0.74 | 20 | $^{233}$U |
| Level density normalization | ATILNO | 0.80 | 20 | $^{232}$U |
| $\Gamma_\gamma$ normalization | TUNE | 1.40 | 20 | $^{236}$U |
| $\Gamma_n$ normalization | TUNE | 1.00 | 10 | $^{236}$U |
| $\Gamma_n$ normalization | TUNE | 1.00 | 10 | $^{235}$U |
| $\Gamma_n$ normalization | TUNE | 1.00 | 10 | $^{234}$U |
| $\Gamma_p$ normalization | TUNE | 1.00 | 15 | $^{236}$U |
| $\Gamma_\alpha$ normalization | TUNE | 1.00 | 15 | $^{236}$U |
| $\Gamma_f$ normalization | TUNEFI | 1.00 | 1–3 | $^{236}$U |
| $\Gamma_f$ normalization | TUNEFI | 1.00 | 3 | $^{235}$U |
| $\Gamma_f$ normalization | TUNEFI | 1.00 | 3 | $^{234}$U |
| $\sigma_{el}$ model defect uncertainty | ELARED | 1.00 | 3 | |
| $\sigma_{abs}$ model defect uncertainty | FUSRED | 1.00 | 3 | |
| Real vol. OMP depth normal. | UOMPVV | 1.0 | 2 | $^{235}$U |
| Imag.vol. OMP depth normal. | UOMPWV | 1.0 | 10 | $^{235}$U |
| Imag.surf. OMP depth normal. | UOMPWS | 1.0 | 10 | $^{235}$U |
| Vol. OMP diffuseness normal. | UOMPAV | 1.0 | 2.5 | $^{235}$U |
| Surf. OMP diffuseness normal. | UOMPAS | 1.0 | 2.5 | $^{235}$U |
| Dynamic-deformation normal. | DEFDYN | 1.0 | 5 | $^{235}$U |
| Static-deformation normal. | DEFSTA | 1.0 | 5 | $^{235}$U |

Experimental data from EXFOR were used to constrain the fit by the generalised least-squares method (GANDR code). The list of selected total cross section measurements on $^{235}$U target is shown in Table VII.

Systematic uncertainties of 2% were added to each measurement to account for unknown errors. In addition, a 3% global systematic uncertainty was added to consider possible unrecognized systematic uncertainties that introduce correlations between experiments. The covariance plot of the total cross section is shown on Fig. 24(a). Co-

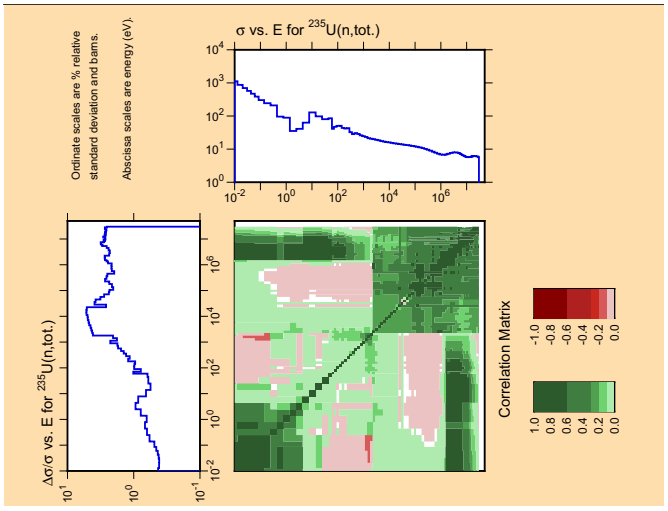


(a) $^{235}$U(n,tot) covariance matrix.

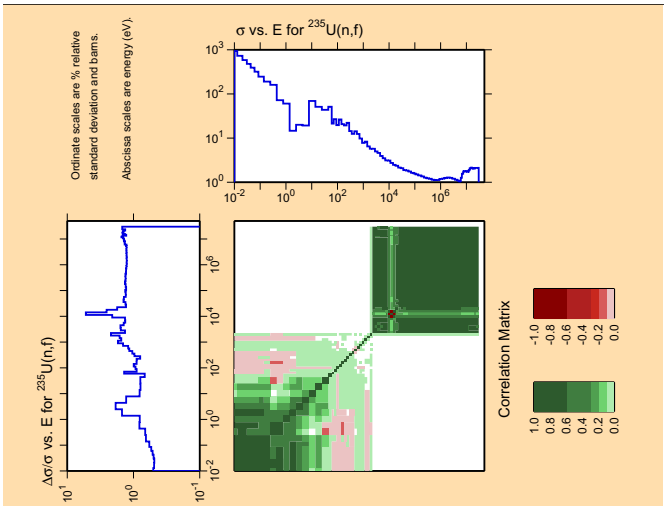


(b) $^{235}$U(n,f) covariance matrix.

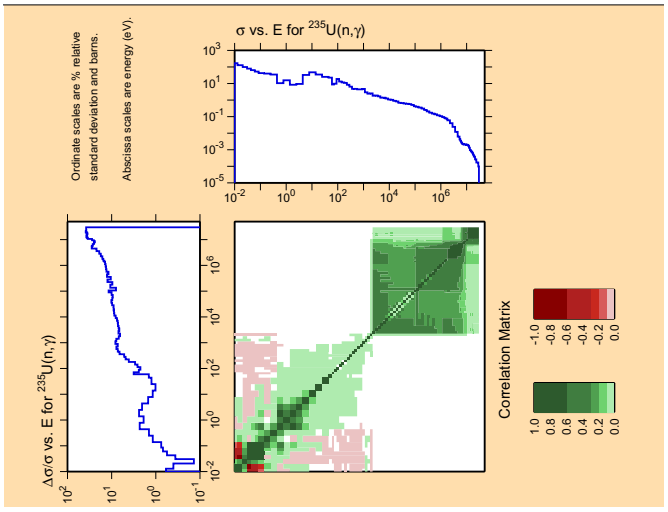


(c) $^{235}$U(n,$\gamma$) covariance matrix.

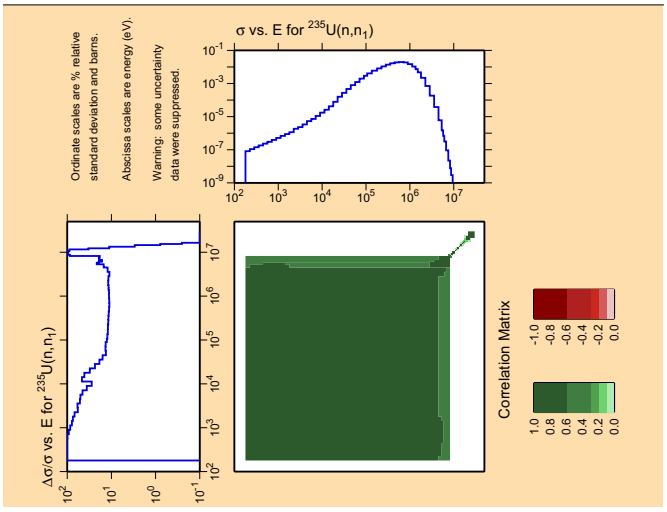


(d) $^{235}$U(n,n') covariance matrix.

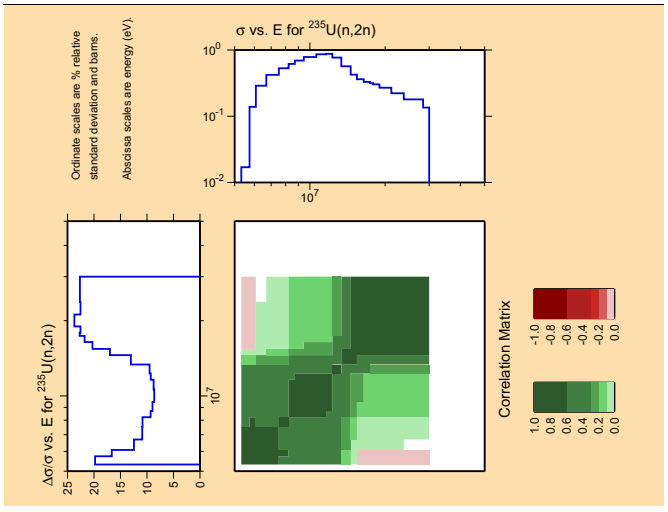


(e) $^{235}$U(n,2n) covariance matrix.

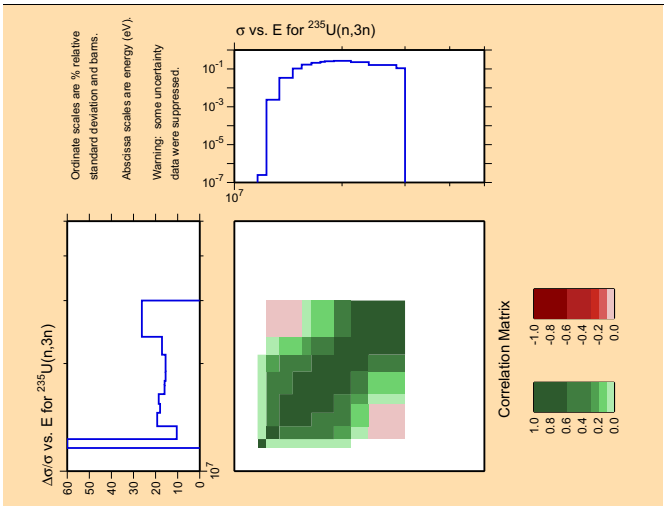


(f) $^{235}$U(n,3n) covariance matrix.

FIG. 24. (Color online) Selected evaluated cross section covariance matrices for neutron-induced reactions on $^{235}$U plotted with NJOY.

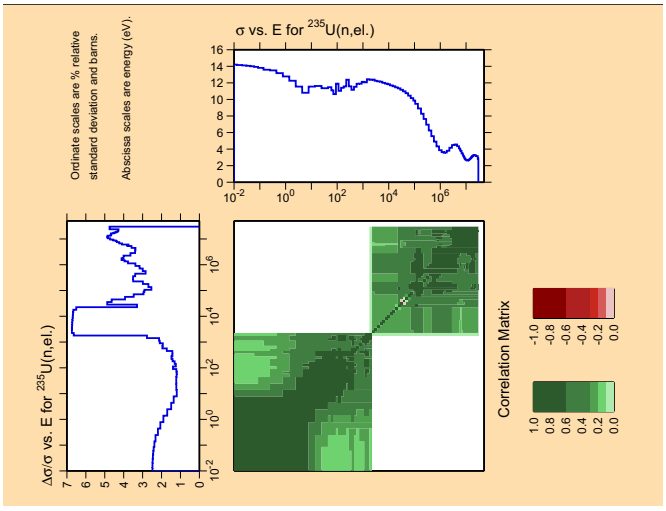


(a) $^{235}$U(n,el) covariance matrix.

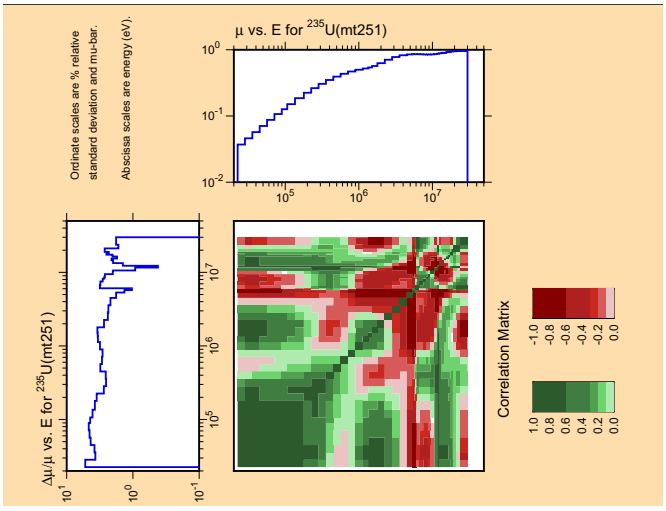


(b) $\bar{\mu}_{el}$ covariance matrix.

FIG. 25. (Color online) Cross section and $\bar{\mu}_{el}$ covariance matrices for elastic neutron scattering on $^{235}$U plotted with NJOY.

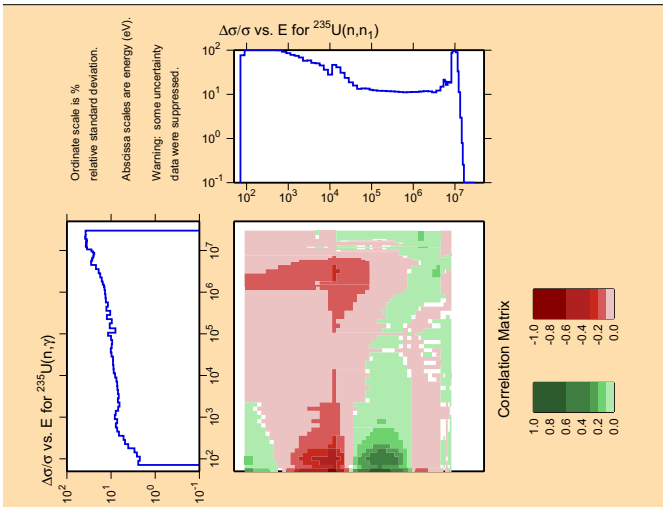


(a) Cross-reaction $^{235}$U(n,$\gamma$)–$^{235}$U(n,n') covariance matrix.

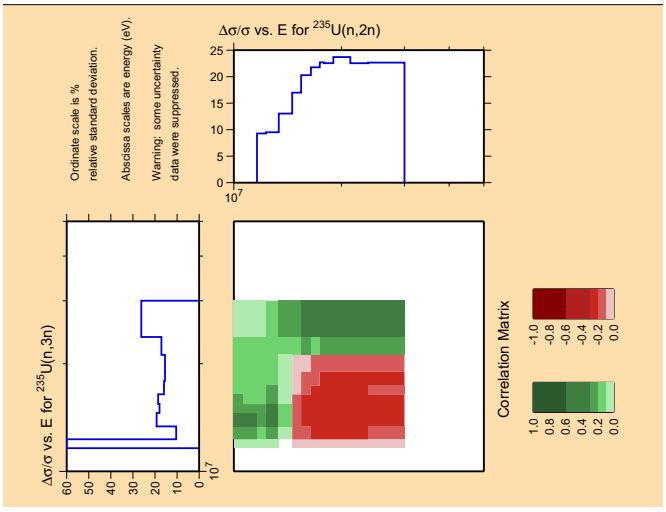


(b) Cross-reaction $^{235}$U(n,2n)–$^{235}$U(n,3n) covariance matrix.

FIG. 26. (Color online) Selected evaluated cross-reaction covariance matrices for neutron-induced reactions on $^{235}$U plotted with NJOY.

variance matrix of the total cross section is the sum of the partials. This is possible because all reaction channels have covariances (some in the form of lumped reactions, *e.g.*, MT851=MT52+MT53+...+MT91 uncertainties) and include cross-reaction components, many of them anti-correlated; without these the uncertainty of the total cross section would be grossly overestimated. Note that the inelastic cross section with threshold at 77 eV gives rise to weak correlations between the resonance and the fast energy region, even though such correlations are not present in the other resonant reaction channels.

The fission cross sections and covariances from Standards 2017 were input to GANDR. To avoid double-counting, the variance of fission in the prior was increased by 20% to make it non-informative. Then, the fission Standards evaluation was used in the Bayesian approach as a pseudo-experimental data. An additional systematic uncertainty of 1.2% was added to the covariance matrix of the Standards 2017 to account for unrecognized systematic uncertainties (USU), as recommended in the Standards 2017 documentation [14]. The evaluated fission co-

TABLE VII. Experimental data taken from EXFOR [91] for the total cross section of $^{235}$U used in the fitting procedure within the GANDR system.

| First author | Year | EXFOR | Comment |
|---|---|---|---|
| J.M. Peterson [187] | 1960 | 11108044 | |
| C.A. Uttley [188] | 1966 | 21088004 | $25 < E < 960$ keV |
| D.G. Foster jr [189] | 1971 | 10047096 | |
| J. Cabe [190] | 1973 | 20480017 | |
| | | 20480016 | (exclude) |
| | | 20480018 | |
| F.L. Green [191, 192] | 1973 | 10588002 | |
| R.B. Schwartz [193] | 1974 | 10280005 | every $2^{nd}$ point |
| V.P. Vertebniy [102] | 1980 | 40609002 | $E = 24.5$ keV |
| W.P. Poenitz [162] | 1981 | 10935006 | $E > 200$ keV |
| W.P. Poenitz [163] | 1983 | 12853054 | |

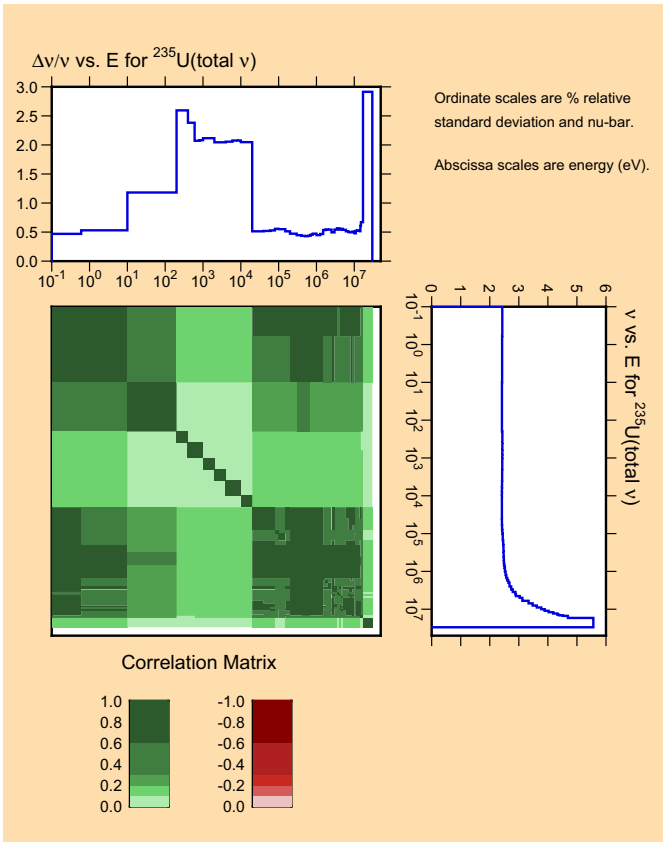


(a) $\bar{\nu}_{tot}$ covariance matrix for $^{235}$U($n$,f) reaction.

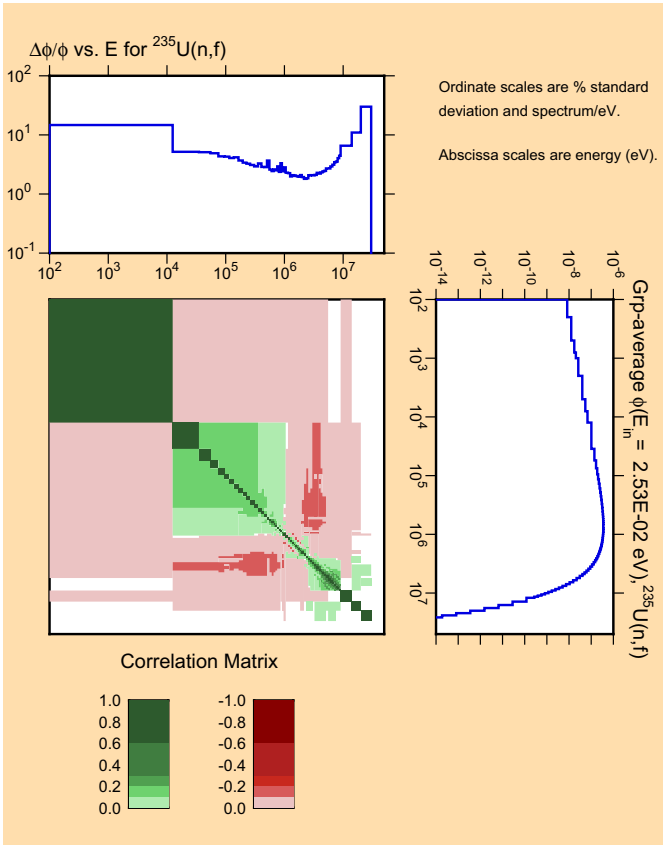


(b) $^{235}$U($n_{th}$,f) PFNS covariance matrix for thermal neutrons.

FIG. 27. (Color online) Evaluated $\bar{\nu}_{tot}$ and PFNS covariance matrices for neutron-induced fission on $^{235}$U plotted with NJOY.

variance plot is shown in Fig. 24(b). The uncertainty is mostly determined by the Standards 2017 and amounts to 1.2–2% over most of the energy range, but is lower at thermal because the cross section there is well known from the Thermal Neutron Constant fit [14], and the experiments are specific of the thermal region so the estimated USU does not apply [14].

Only the radiative capture data of Jandel [32] (EXFOR entry 14149003) in the energy range $2 < E < 60$ keV were considered for GANDR fitting. Other relevant measurements in EXFOR involve measured cross section ratio of capture to fission. These ratio measurements should be added at a later time. The capture covariance plot is shown in Fig. 24(c). The capture cross section has much larger uncertainty than fission, being around 10% in the fast neutron range. In the high-energy end, where the cross section decreases, the uncertainty steadily increases. Capture experiments for incident energies of 14 MeV were not considered in the present evaluation. Note that the USU for capture on fissile materials was estimated at 2.4%.

Inelastic experimental data [92–95] have too large uncertainties and are too sparse in energy to constrain the evaluated cross sections (see Fig. 6) and were not included in the fit. The uncertainties of the inelastic cross sections are given separately for the first discrete level (MT51), which has a very low threshold of 77 eV, and for the remaining discrete levels and the continuum (MT851=MT52+...+MT91). The evaluated covariance plot of the first discrete level is shown in Fig. 24(d). The uncertainty remains about 10% from 0.1 up to 6–7 MeV. Note that the uncertainty of the first inelastic level gives only a minor contribution to the overall inelastic uncertainty (MT4 uncertainty). The total inelastic uncertainty should be estimated as the sum of absolute covariances for MT51 and MT851 contributions, correspondingly.

The two-neutron emission cross section measurement by Frehaut [96] (revised in 2016, EXFOR entry 21568004) was considered. It includes the normalisation correction for the Standards 2006. However, the data points below 8.5 MeV were rejected because of experimental uncertainties due to the difficulty in discriminating between neutrons from the ($n$,2$n$) and the fission reaction. This difficulty may lead to an underestimation of the measured ($n$,2$n$) cross sections in many actinides as can be also seen for the $^{238}$U target, where many other measurements are available. The measurement of Mather [97] (EXFOR entry 20795010) was rejected due to unreasonably large discrepancy with the Frehaut data and the shape, which looks un-physical and was in contradiction with the model calculation. The ($n$,2$n$) covariance plot is shown in Fig. 24(e). A typical uncertainty shape (inverted bell) can be seen with maxima near the threshold and at higher energies; the minimum uncertainty of 9-10% corresponds to the region of the maximum cross section from 9–12 MeV.

There are only two data sets for the three-neutron emission cross sections in EXFOR. The data by Veeser [201] (EXFOR entry 10795002) were used in the fit, while the data by Mather [97] (EXFOR entry 20795011) were rejected by similar arguments as for the two-neutron emission reaction. The covariance plot is shown in Fig. 24(f). A typical uncertainty around 20% can be seen from 16 up to 24 MeV.

Fig. 25 shows the covariance matrix plot of the elastic cross section and the average cosine of elastic scattering $\bar{\mu}_{el}$. Integrated elastic experimental data [198, 199] are either discrepant or have too large uncertainties to constrain the evaluated cross sections and were not included in the fit. The elastic covariance in Fig. 25(a) is clearly split in two uncorrelated blocks: the RRR and the fast neutron region. Uncertainties in elastic cross sections are constrained by the optical model and the total cross section data through correlations; uncertainties are from 2% to 3% in the RRR, but reaches 7% in the URR, then decreasing to less than 5% in the fast neutron range.

Covariance of the average cosine of elastic scattering $\bar{\mu}_{el}$ ($P_1$ Legendre polynomial coefficient) shows strong anti-correlations in Fig. 25(b) probably due to normalization constrains of the Legendre polynomial coefficients to the elastic cross section. Unfortunately, NJOY does not process the covariances of the higher-order $P_n$, $n > 1$ Legendre polynomial coefficients and their cross-correlations that were evaluated and are available in the IAEA CIELO file.

Note that all cross section covariances include the cross-reaction terms and the total is the sum of all individual reaction contributions. As an example, the cross-reaction covariances are shown between the capture and the inelastic cross sections in Fig. 26(a) and between the ($n$,2$n$) and ($n$,3$n$) cross sections in Fig. 26(b). Strong anti-correlations between capture and the inelastic cross section on the first (isomeric) level are observed in Fig. 26(a) below 1 keV, where these are practically the only two reaction channels open. Note that the upper panel of Fig. 26(b) should contain the relative ($n$,2$n$) uncertainty, but there is a either a processing problem or a NJOY problem that requires further investigation. Finally, note again that failure to consider cross-reaction covariances would lead to a gross overestimation of the uncertainty of the total cross section, and will also affect the proper redistribution of physical quantities during subsequent data adjustments to produce adjusted evaluated libraries for specific applications.

The covariance matrix of the average number of prompt neutrons emitted per fission were prepared using the ENDF/B-VII.1 evaluation as a starting point. The uncertainties at the thermal energy were adjusted for consistency with the Standards 2017. Above the thermal range up to 75 eV the statistical uncertainties of the experimental data of Reed [46] and Simon [49] were used. Finally, the total uncertainties were taken as a combination of statistical uncertainties with the fully correlated USU of 0.4% covering the whole energy range. The covariance matrix is shown in Fig. 27(a).

The covariance matrix of the PFNS at the thermal point was evaluated by Trkov and Capote and is shown in Fig. 27(b). Uncertainties were scaled[2] to consider the unrecognized shape uncertainty [14], the minimum uncertainty (about 1.8%) is reached around 2 MeV of outgoing neutron energy. The uncertainties for outgoing neutron energies from 9 up to 14 MeV are about 7%, which were estimated from the uncertainty of the measured $^{90}$Zr(n,2n) spectrum-average cross section used in the fitting of the PFNS high-energy tail. Uncertainties increase above 15 MeV of outgoing neutron energy up to 30% as no data are available at those high energies. However, the number of emitted neutrons with energy larger than 15 MeV are well below 0.1% of the total number of emitted neutrons.

The uncertainties in the number of delayed neutrons per fission were adopted from the work by Keepin [114] as tabulated by Tuttle [115]. The uncertainties are given for the thermal and the fast incident neutron energies. The uncertainties of the total number of neutrons emitted per fission are the sum of the prompt and the delayed contribution.

Cross-material covariances between $^{235}$U, $^{238}$U and $^{239}$Pu are also available from the Neutron Standards fit of differential cross section measurements [14], with positive correlations particularly strong between corresponding fission channels due to ratio measurements.

### B. $^{238}$U Target

The average resonance parameters in the unresolved resonance range are only used for self-shielding calculations. As in the case of $^{235}$U, the resonance parameter covariance matrix is too big to be practically useful. Since the resonance parameters in the JEFF-3.3 library are based on the same resonance analysis, the cross section covariance matrix in group representation was adopted from this library. The covariances in the unresolved resonance region were evaluated together with those for the fast energy range.

The fission cross section of $^{238}$U is the Standard from 2 MeV to 200 MeV and was evaluated with the Standards down to 500 keV [14] using a denser energy grid from 500 keV up to 2 MeV to describe the below-threshold fission resonances. It was adopted in full for the energy range of the evaluation. This is justified because the model calculation is very close to the Standards 2017 (within 3%), so the replacement does not destroy the internal consistency of the competing reaction channels in the model calculation. The small average fission cross section in the unresolved resonance range of the order of 0.1 mb has been adopted from an estimate by Trkov as described

[2] A PFNS covariance matrix was multiplied by a factor of 4.8 so that the uncertainty of the PFNS average energy was increased up to 10 keV.

in Sec. IV A, based on available broad average fission cross section data in EXFOR.

The capture cross sections were evaluated within the Standards up to 2 MeV and included in the analysis the most recent high-accuracy measurement at JRC-Geel [143]. The cross sections from Standards 2017 [14] were adopted in full above the resonance range from 20 keV up. This is again justified because the model parameters were tuned such that the calculated capture cross section closely agree with the Standards. The comparison of IAEA CIELO capture cross sections with the Standards 2017 is shown in Fig. 28, which shows complete agreement, except for the resonance range below 20 keV, where minor differences remain.

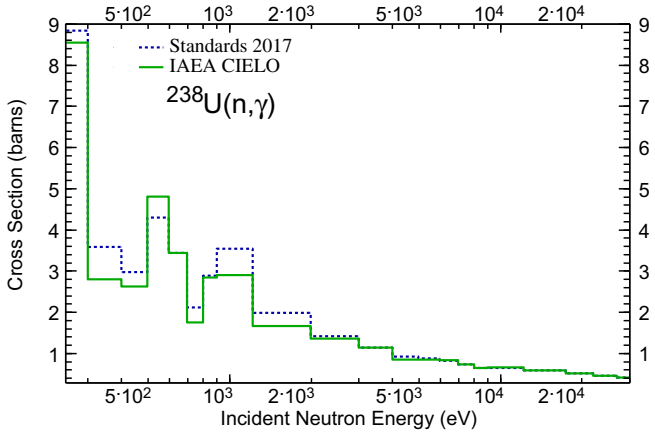


FIG. 28. (Color online) Comparison of the capture cross section of $^{238}$U and the Standards 2017 evaluation in group-wise representation. In the reference region (20 keV up to 2.2 MeV) the matching is exact.

Various quantities related to fission were evaluated separately or borrowed from other sources, namely the delayed average number of neutrons per fission $\bar{\nu}_d$, delayed neutron spectra and prompt fission gamma multiplicities and spectra. The delayed neutron constants were taken from the ENDF/B-VII.1 library.

The covariance matrix prior was generated by random sampling of the parameters listed in Table VIII. Parameter uncertainties are loosely based on RIPL uncertainties [53]; their uncertainties have been extended to cover the range of scaling of those parameters used to fit the experimental data. As mentioned before, for a prior calculation it is important that uncertainty bands of the model cover all selected experimental data.

In order to evaluate the covariances the experimental data from EXFOR was fed to the generalised least-squares code GANDR using the model calculated covariance as a prior. The list of selected total cross section measurements is shown in Table IX.

Systematic uncertainties of 2% were added to each measurement to account for unknown errors. In addition, a 3% global systematic uncertainty was added to consider possible unrecognized systematic uncertainties that introduce correlations between experiments. The covariance

TABLE VIII. Input nuclear model parameters for the $n+^{238}$U calculation and their uncertainties used in EMPIRE for random sampling to generate the covariance matrix prior.

| EMPIRE input parameter | Symbol | Value | Unc.(%) | Nucleus |
|---|---|---|---|---|
| Preeq. mean-free path | PCROSS | 1.82 | 20 | |
| Level density normalization | ATILNO | 0.960 | 5 | $^{239}$U |
| Level density normalization | ATILNO | 0.970 | 10 | $^{238}$U |
| Level density normalization | ATILNO | 0.807 | 20 | $^{237}$U |
| Level density normalization | ATILNO | 0.980 | 10 | $^{236}$U |
| Level density normalization | ATILNO | 1.05 | 10 | $^{235}$U |
| Preeq. level density normal. | GTILNO | 1.00 | 10 | $^{238}$U |
| $\Gamma_\gamma$ normalization | TUNE | 3.1 | 5 | $^{239}$U |
| $\Gamma_n$ normalization | TUNE | 1.00 | 10 | $^{239}$U |
| $\Gamma_n$ normalization | TUNE | 1.00 | 10 | $^{238}$U |
| $\Gamma_n$ normalization | TUNE | 1.00 | 10 | $^{237}$U |
| $\Gamma_p$ normalization | TUNE | 1.00 | 15 | $^{239}$U |
| $\Gamma_\alpha$ normalization | TUNE | 1.00 | 15 | $^{239}$U |
| $\Gamma_f$ normalization | TUNEFI | 1.00 | 3 | $^{239}$U |
| $\Gamma_f$ normalization | TUNEFI | 1.00 | 3 | $^{238}$U |
| $\Gamma_f$ normalization | TUNEFI | 1.00 | 3 | $^{237}$U |
| $\sigma_{tot}$ model defect uncertainty | TOTRED | 0.995 | 5 | |
| Real vol. OMP depth normal. | UOMPVV | 1.0 | 2 | $^{238}$U |
| Imag.vol. OMP depth normal. | UOMPWV | 1.0 | 10 | $^{238}$U |
| Imag.surf. OMP depth normal. | UOMPWS | 1.0 | 10 | $^{238}$U |
| Vol. OMP diffuseness normal. | UOMPAV | 1.0 | 2.5 | $^{238}$U |
| Surf. OMP diffuseness normal. | UOMPAS | 1.0 | 2.5 | $^{238}$U |
| Dynamic-deformation normal. | DEFDYN | 1.0 | 5 | $^{238}$U |
| Static-deformation normal. | DEFSTA | 1.0 | 5 | $^{238}$U |

TABLE IX. Experimental data taken from EXFOR [91] for the total cross section of $^{238}$U used in the fitting procedure within the GANDR system.

| First author | Year | EXFOR | Comment |
|---|---|---|---|
| R. Batchelor [194] | 1965 | 21019013 | |
| D.G. Foster Jr [189] | 1971 | 10047099 | |
| M. Baba [195] | 1973 | 21092002 | |
| R.B. Schwartz [193] | 1974 | 10280006 | (every 2-nd point) |
| W.P. Poenitz [158] | 1981 | 10935007 | |
| I. Tsubone [164] | 1984 | 21813002 | |
| Yu.V. Grigoriev [196] | 1990 | 41154002 | ($E > 15$ keV) |
| W.P. Abfalterer [197] | 2001 | 13753030 | |

plot of the total cross section is shown on Fig. 29(a). The uncertainties are small in the thermal, raising then to around 3% in the fast energy region, where the total cross section is well-defined from existing experimental data.

The fission cross sections are Standards or (below 2 MeV) evaluated with the Standards, therefore, the statistical uncertainty in the prior covariance matrix was increased by 20% to diminish the constraints imposed from the model-parameter based prior. The fission cross sections and the corresponding covariances were fed to GANDR in the Bayesian approach to be combined consistently with the covariances for the other reactions. The evaluated covariance matrix is shown in Fig. 29(b). Uncertainties below the fission threshold are 20% on average.

The capture cross sections were also evaluated with the Standards up to 2.1 MeV. The covariances below 20 keV were evaluated as part of the resonance analysis, so only the cross sections and the corresponding covariance matrix in the range 20 keV$< E <$2.1 MeV were fed to GANDR. The evaluated covariance matrix is shown in Fig. 29(c).

As in the case of $^{235}$U, inelastic experimental data were

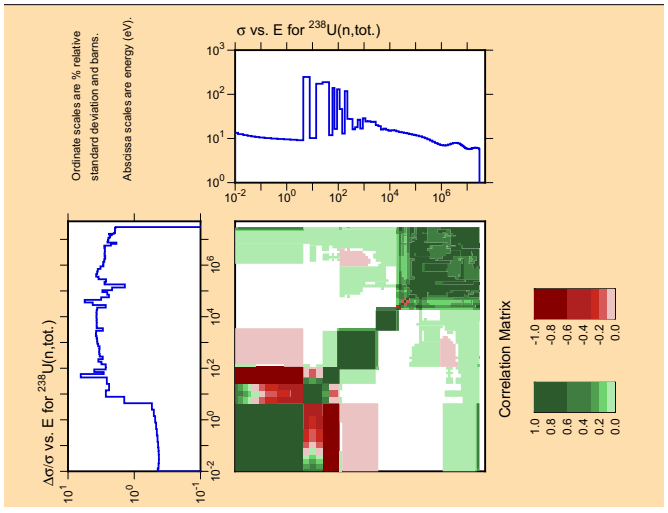


(a) $^{238}$U(n,tot) covariance matrix.

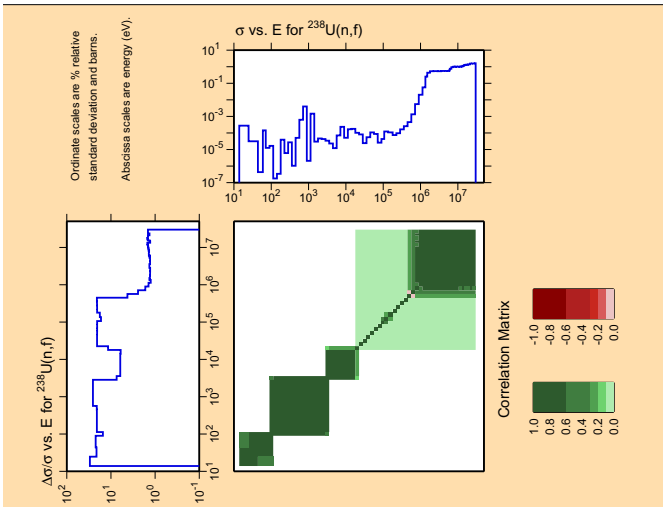


(b) $^{238}$U(n,f) covariance matrix.

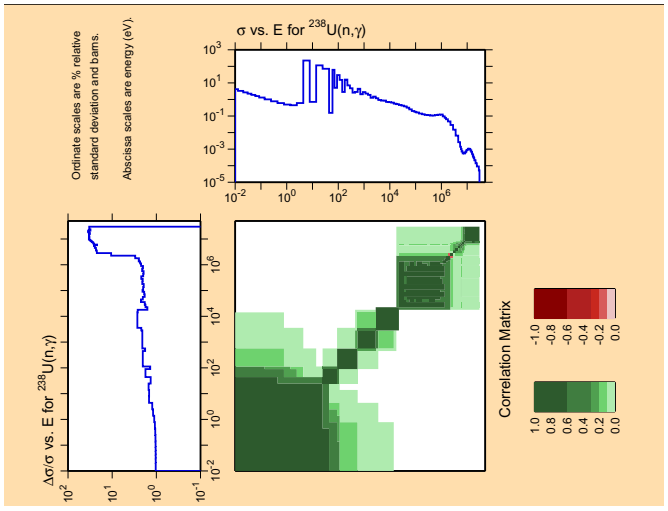


(c) $^{238}$U(n,$\gamma$) covariance matrix.

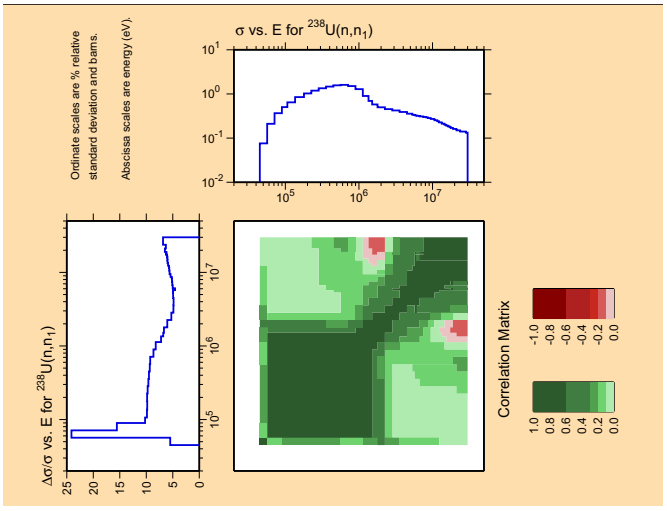


(d) $^{238}$U(n,n') covariance matrix.

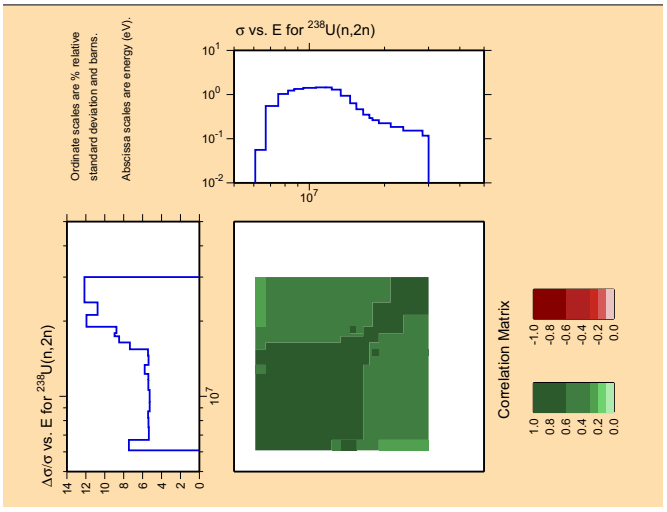


(e) $^{238}$U(n,2n) covariance matrix.

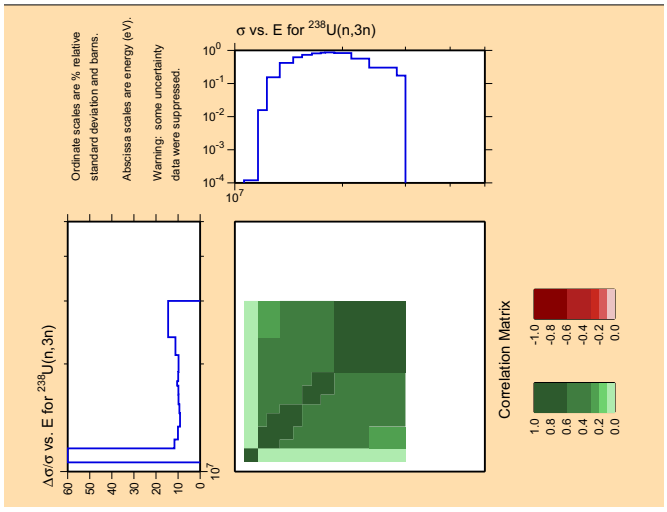


(f) $^{238}$U(n,3n) covariance matrix.

FIG. 29. (Color online) Selected evaluated cross section covariance matrices for neutron-induced reactions on $^{238}$U plotted with NJOY.

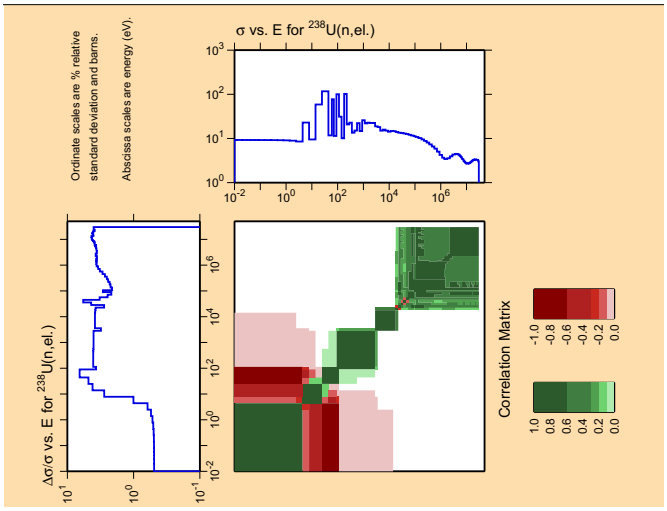


(a) $^{238}$U(n,el) covariance matrix.

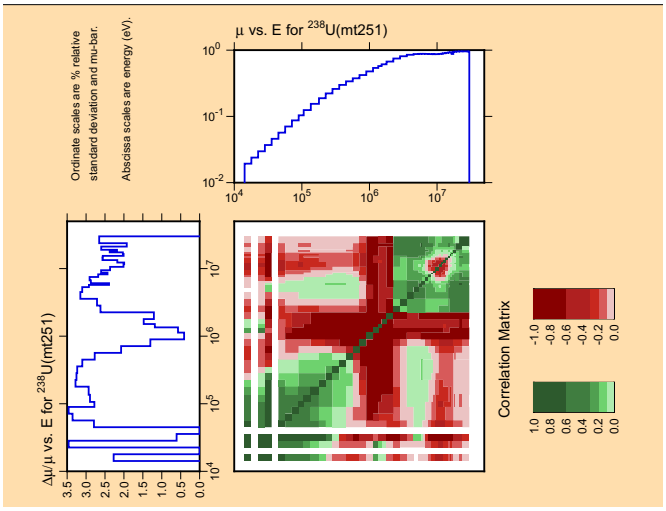


(b) $\bar{\mu}_{el}$ covariance matrix.

FIG. 30. (Color online) Cross section and $\bar{\mu}_{el}$ covariance matrices for elastic neutron scattering on $^{238}$U plotted with NJOY.

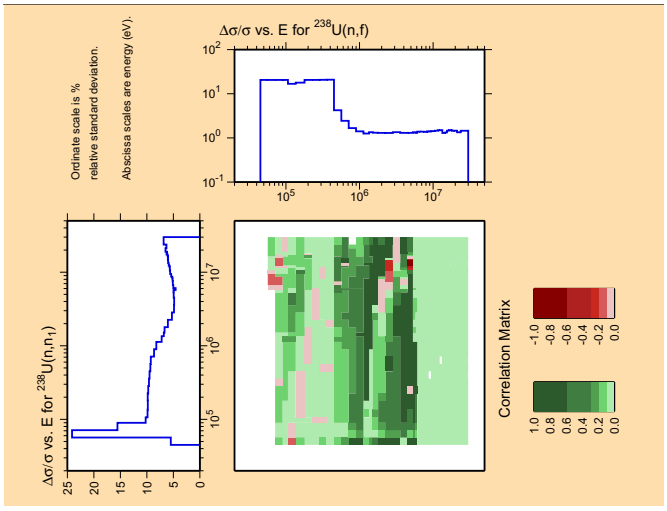


(a) Cross-reaction $^{238}$U(n,f)–$^{238}$U(n,n') covariance matrix.

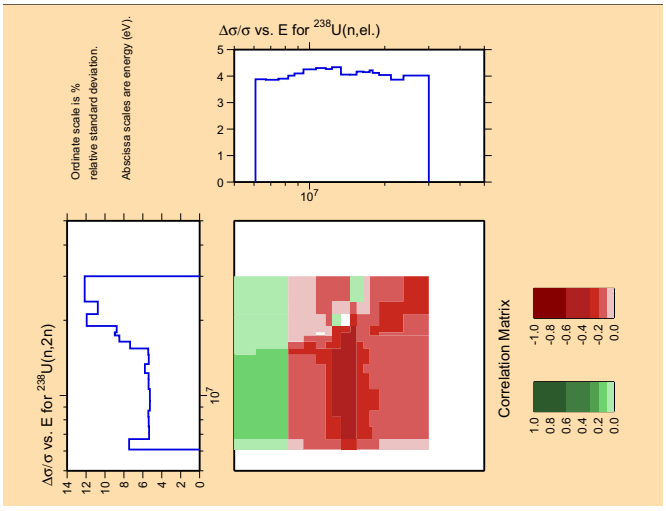


(b) Cross-reaction $^{238}$U(n,2n)–$^{238}$U(n,el) covariance matrix.

FIG. 31. (Color online) Selected evaluated cross-reaction covariance matrices for neutron-induced reactions on $^{238}$U plotted with NJOY.

considered too scattered to constrain the evaluated cross sections. The uncertainties of the inelastic cross sections are given separately for the first discrete level (MT51), and for the remaining discrete levels and the continuum (MT851=MT52+...+MT91). The evaluated covariance plot of the first discrete level is shown in Fig. 29(d). The uncertainty minimum is about 6% in the region of the maximum cross section. Note that for $^{238}$U the uncertainty of the first inelastic level gives a major contribution to the overall inelastic uncertainty (MT4 uncertainty). The total inelastic uncertainty should be estimated as the sum of absolute covariances for MT51 and MT851 contributions, correspondingly.

Several consistent data sets for the (n,2n) reaction are available in EXFOR and are listed in Table X. New experimental data by Krishichayan *et al.* [209] helped in reducing the evaluated uncertainty to about 6% in the region of the maximum of the excitation function. The evaluated covariance matrix plot is shown in Fig. 29(e).

TABLE X. Experimental data for $^{238}$U(n,2n) fitting procedure with GANDR. The asterisk * indicates renormalized data to the current dosimetry standards [202, 203].

| First author | Year | EXFOR | Comment |
|---|---|---|---|
| J.D. Knight* [204] | 1958 | 12459021 | renorm. STD 2006 |
| L.R. Veeser [201] | 1978 | 10795004 | |
| H. Karius [205] | 1979 | 20499002 | |
| J. Frehaut* [96] | 1980 | 20416021 | renorm. STD 2006 |
| N.V. Kornilov [206] | 1980 | 30561002 | |
| C. Konno [207] | 1993 | 22637090 | |
| X. Wang [208] | 2010 | 32677002 | |
| Krishichayan* [209] | 2015 | 99999001 | renorm. IRDFF |
| A.A. Filatenkov [210] | 2016 | 41614240 | |

Three data sets for the three-neutron emission reaction are available in EXFOR and are listed in Table XI. The evaluated covariance matrix plot is shown in Fig. 29(f).

Fig. 30 shows the covariance matrix plot of the elastic

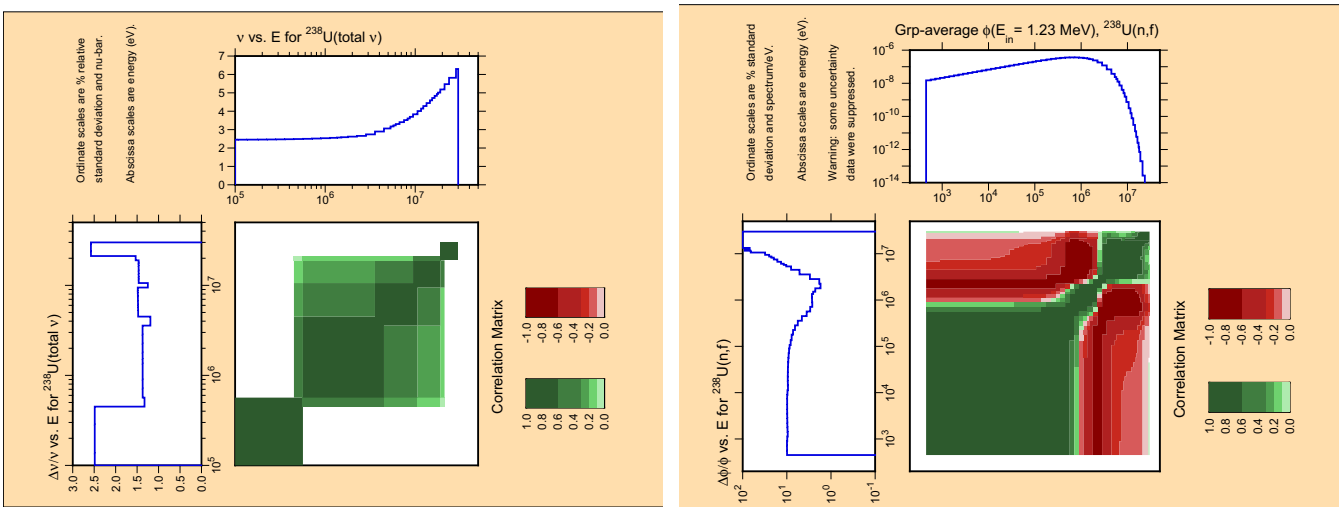


(a) $\bar{\nu}_{tot}$ covariance matrix for $^{238}$U($n$,f) reaction. (b) $^{238}$U($n$,f) PFNS covariance matrix in the fast range.

FIG. 32. (Color online) Evaluated $\bar{\nu}_{tot}$ and PFNS covariance matrices for neutron-induced fission on $^{238}$U plotted with NJOY.

TABLE XI. Experimental data for $^{238}$U(n,3n) fitting procedure with GANDR.

| First author | Year | EXFOR |
|---|---|---|
| J. Frehaut [96] | 2016 | 20416022 |
| X. Wang [211] | 2013 | 32709002 |
| A. Wallner [212] | 2014 | 20499022 |

cross section and the average cosine of elastic scattering $\bar{\mu}_{el}$. Again it was considered that the integrated elastic experimental data are either discrepant or have too large uncertainties to constrain the evaluated cross sections and were not included in the fit. The elastic covariance in Fig. 30(a) is split in three uncorrelated blocks: the RRR, a region around 10 keV, and the fast neutron region. Uncertainties in elastic cross sections are constrained by the optical model and the total cross section data through correlations; uncertainties are around 4% above 1 eV.

Covariance of the average cosine of elastic scattering $\bar{\mu}_{el}$ ($P_1$ Legendre polynomial coefficient) shows strong anti-correlations in Fig. 30(b) probably due to normalization constrains of the Legendre polynomial coefficients to the elastic cross section. Evaluated uncertainties are relatively large.

As in the case of $^{235}$U, all cross section covariances include the cross-reaction terms and the total is the sum of all individual reaction contributions. As an example, the cross-reaction covariances are shown between the fission and the first discrete level inelastic cross sections in Fig. 31(a) and between the ($n$,2$n$) and the elastic cross sections in Fig. 31(b). Later plot shows strong anti-correlations between 6–12 MeV probably due to unitarity constrains. Failure to consider cross-reaction covariances would lead to a gross overestimation of the uncertainty of the total cross section.

The starting value for the covariance matrix of the average number of prompt neutrons emitted per fission was the ENDF/B-VII.1 library. The uncertainty below 0.5 MeV of incident neutron energy was assigned arbitrarily as 2%. Fission in this energy region is practically negligible, so the precise value of the uncertainty estimate is not important. The covariance matrix is shown in Fig. 32(a). Above 2 MeV the prompt $\bar{\nu}_p$-uncertainty is about 1.5%, reflecting the spread in measured data (see Fig. 21). The uncertainties in the number of delayed neutrons per fission $\bar{\nu}_d$ were again adopted from the work by Keepin [114] as tabulated by Tuttle [115]. The uncertainties are given for the thermal and the fast incident neutron energies. The uncertainties of the total number of neutrons emitted per fission $\bar{\nu}_{tot}$ are the sum of the prompt and the delayed contribution.

The covariance matrix of the PFNS was evaluated within the IAEA CRP on the Prompt-Fission Neutron Spectra of Actinides [10] and is shown in Fig. 32(b). A minimum uncertainty of about 1% reflects the evaluation method based on model data with small variability of possible model shapes.

## VI. RPI QUASI-DIFFERENTIAL BENCHMARK FOR $n+^{238}$U

The RPI quasi-differential experiment was described in Ref. [213] and used in the evaluation process to verify the calculated double differential scattering cross sections. In this experiment the neutron beam that, incident on the $^{238}$U sample, scattered or caused fission; the resulting neutrons were detected by an array of neutron detectors surrounding the sample. The effective energies covered the range from 0.5 to 20 MeV. The measured data were compared with detailed simulations of the experiment performed with different evaluations of $^{238}$U.

An important aspect of this experiment is that all emitted neutrons are detected, including those from elastic and inelastic scattering, fission neutrons and multiple scattering contribution. Comprehensive neutron detection avoids typical uncertainties introduced by splitting the neutron yield into elastic, inelastic and fission neutron contribu-

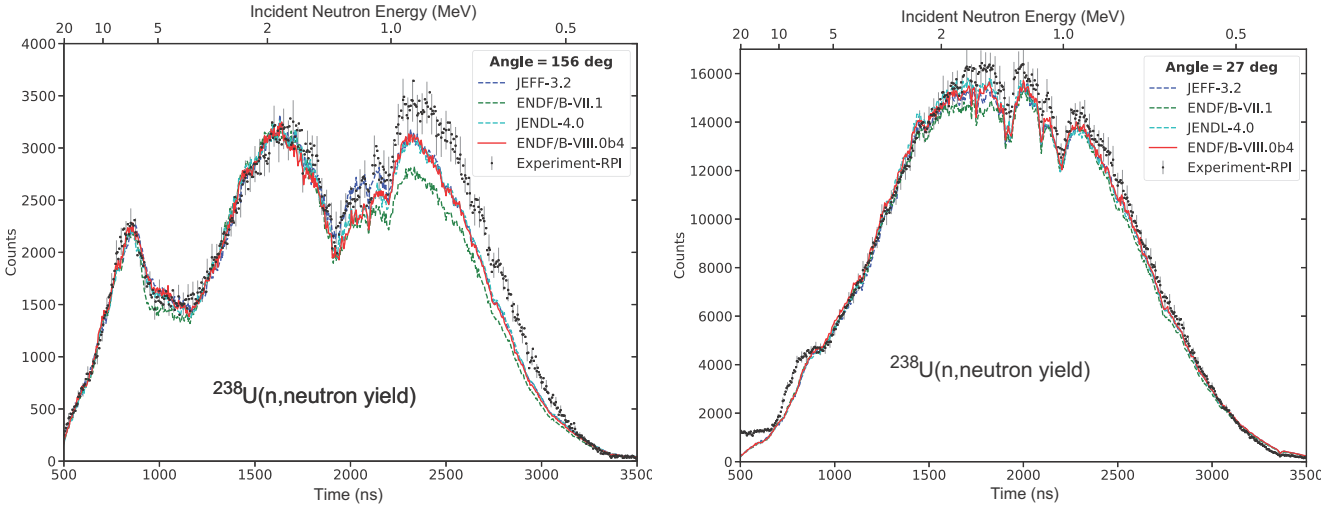


FIG. 33. (Color online) The measured time of flight of neutrons detected at 156 deg (left) and 27 deg (right) relative to the neutron beam incident on $^{238}$U. The upper x-axis approximately corresponds to the incident neutron energy, see Ref. [213] for more details.

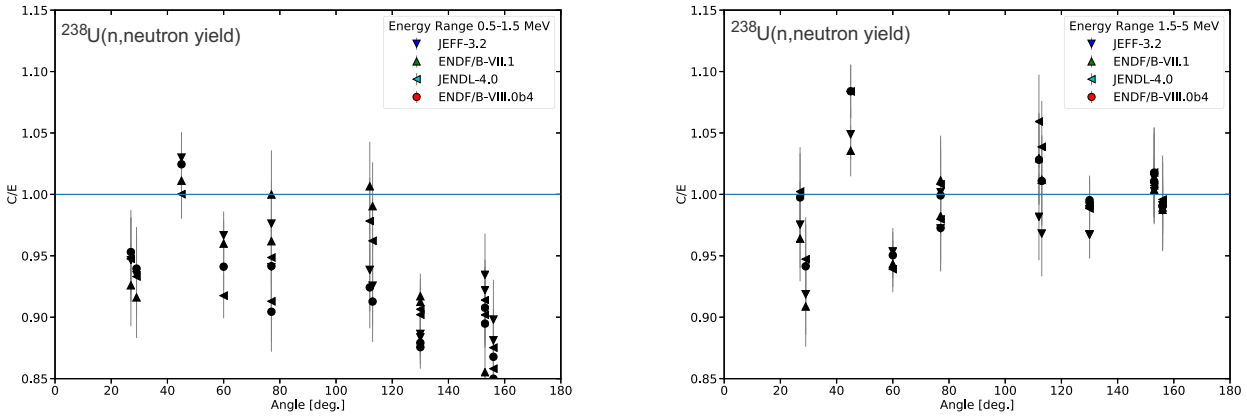


(a) Detected $E_n$ in the range from 0.5 to 1.5 MeV

(b) Detected $E_n$ in the range from 1.5 to 5 MeV

FIG. 34. (Color online) The C/E for $n+^{238}$U as a function of the angle of the emitted neutrons. The contributions to the first energy range (left) come mostly from the scattering, while the contributions to the second energy range (right) come from the scattering and fission neutrons. The uncertainty bars are dominated by the normalization uncertainty of the experiment.

tions. The disadvantage is that the cross sections cannot be inferred from the measurements directly, but this is compensated by the high sensitivity of measured data to the neutron production cross sections. In many experiments neutron production is swamped by the elastic component. In the present case the elastic contribution becomes very low at certain angles, raising the importance of other minor channels, including the inelastic scattering. This experiment could be seen as a quasi-differential benchmark for validating nuclear data, where experimental set-up is simple and very well documented. This allows for an accurate Monte Carlo simulation directly in the time domain.

As was previously shown [213], one of the issues observed with the ENDF/B-VII.1 library was the low scattering cross section at back angles in the energy range of 0.5-1.5 MeV. Simulations with the IAEA CIELO data shown in Fig. 33(left) for back scattering to 156 deg indicate that the agreement with the experiment was improved. The comparison for the forward angle of 27 deg in Fig. 33(right) shows good agreement between the experiment and simulation. The total counts observed indicate the dominance of the forward scattering. Details of the new physics introduced to the EMPIRE code were described in Refs. [68, 69]. The C/E as a function of the angle was calculated by integrating the experimental data (E) and simulation (C) with respect to time-of-flight; C/E in the energy range of 0.5–1.5 MeV is shown in Fig. 34(left) and in the energy range from 1.5–5 MeV in Fig. 34(right). The improvement at back angles relative to ENDF/B-VII.1 is noticeable, while at other angles the new evaluation performs similar to other evaluations and performs well considering the systematic uncertainties of the experiment.

## VII. INTEGRAL BENCHMARKS: CRITICALITY AND FUSION

Nuclear power applications have traditionally relied heavily on computational means to optimize designs, ensure safety and determine quantities of interest that are difficult to measure directly. Accurate nuclear data that reproduce integral observables are of utmost importance in evaluated libraries for specific applications.

Requirements for criticality safety gave rise to an international project aimed at collecting detailed and verified information about reactor experiments performed in different worldwide laboratories over several decades. This information can be used for the validation of computational methods, as well as nuclear data. The latest issue of the Handbook of International Criticality Safety Benchmarks Evaluation Project (ICSBEP) [17] contains 558 evaluations spanning 4798 critical, near-critical or subcritical configurations. The current scope of testing was limited to selected critical benchmark cases from the ICSBEP collection. Preliminary results with an earlier version of the IAEA CIELO evaluations were reported at the ND2016 Conference [52]. The calculations were repeated with the current ENDF/B-VIII.0 library that includes the IAEA CIELO evaluations.

### A. $^{235}$U Bare Fast Assemblies

There were fourteen bare highly-enriched uranium benchmarks in ICSBEP that were found potentially suitable for the testing. The list is given in Table XII.

TABLE XII. List of highly-enriched uranium (HEU) fuel bare assemblies from the ICSBEP Handbook [17].

| No. | ICSBEP Label | Short name | Common name |
|---|---|---|---|
| 1 | HEU-MET-FAST-001 | hmf001 | Godiva |
| 2 | HEU-MET-FAST-008 | hmf008 | VNIIEF_bare |
| 3 | HEU-MET-FAST-015 | hmf015 | VNIIEF_UnrCy1 |
| 4 | HEU-MET-FAST-065 | hmf065 | VNIIEF_UnrCy2 |
| 5 | HEU-MET-FAST-018 | hmf018 | VNIIEF_Sphere |
| 6 | HEU-MET-FAST-051 | hmf051-01 | ORCEF-01 |
| 7 | HEU-MET-FAST-051 | hmf051-02 | ORCEF-02 |
| 8 | HEU-MET-FAST-051 | hmf051-03 | ORCEF-03 |
| 9 | HEU-MET-FAST-051 | hmf051-15 | ORCEF-15 |
| 10 | HEU-MET-FAST-051 | hmf051-16 | ORCEF-16 |
| 11 | HEU-MET-FAST-051 | hmf051-17 | ORCEF-17 |
| 12 | HEU-MET-FAST-100 | hmf100-1 | ORSphere-1 |
| 13 | HEU-MET-FAST-100 | hmf100-2 | ORSphere-2 |
| 14 | HEU-MET-FAST-080 | hmf080 | Caliban |

Differences $\Delta k_{\rm eff}$ between the calculated multiplication factors and the reference benchmark values in the pcm units (parts per 100,000) are shown in Fig. 35 for ENDF/B-VII.1 [4] and JEFF-3.2 [5] evaluations, together with the IAEA CIELO results documented in this work.

Godiva (HEU-MET-FAST-001) is the only benchmark from Los Alamos National Laboratory included in this exercise . Many libraries were tuned to Godiva and its calculated $\Delta k_{\rm eff}$ lies somewhere in the middle of the calculated results for all fourteen benchmarks. Godiva $\Delta k_{\rm eff}$ is in excellent agreement with the calculated one for the equivalent Russian spherical benchmark HEU-MET-FAST-018 from VNIIEF, Sarov, Russia. It should be noted that such level of $\Delta k_{\rm eff}$ agreement is achieved in the libraries by final tuning of the prompt $^{235}$U $\bar{\nu}_p$ in the 1–2 MeV region by about 0.05%. Such tuning is not reflected in the evaluated uncertainties and is well within the uncertainties of measured differential data (see Fig. 10). Unfortunately, the situation is highly unsatisfactory for the remaining benchmarks. They are all extremely sensitive to the $^{235}$U nuclear data. The sensitivity profiles available in the NEA Data Bank's DICE package for the cross sections are very similar. The sensitivities to angular distributions are currently not available for all benchmarks, so a test was performed by a direct perturbation of the $P_1$ elastic scattering coefficient. The effect on the predicted reactivity was strong, but practically equal for all benchmarks. Sensitivities to higher threshold reaction cross sections are small, so the differences in the emission spectra are not expected to affect criticality selectively for specific benchmarks. In short, any change in the $^{235}$U data affects all benchmarks about equally. Therefore, it is not possible to explain large discrepancies (well beyond quoted uncertainties and especially a large spread in the calculated $\Delta k_{\rm eff}$) by nuclear data deficiencies.

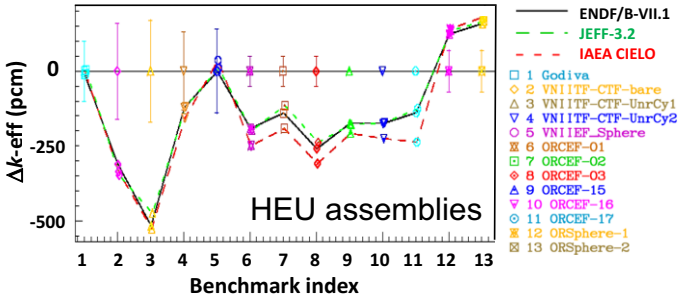


FIG. 35. (Color online) Benchmark results for highly-enriched uranium (HEU) bare assemblies from ICSBEP benchmarks [17]. Symbols linked by lines show the calculated $\Delta k_{\rm eff}$ values using different libraries.

An action would be appreciated by the ICSBEP curators requesting the benchmark evaluators to identify possible reasons for such large discrepancies and to revise benchmark specifications, quoted benchmark uncertainties, or the corresponding MCNP computational models, if needed. Particularly:

- The Russian bare cylinders and spheres HEU-MET-FAST-008, HEU-MET-FAST-015, HEU-MET-FAST-065, and HEU-MET-FAST-018 show a spread of more than 500 pcm with a bias to a lower reactivity using exactly the same nuclear data as the benchmarks mentioned above that showed good agreement. Therefore, HEU-MET-FAST-008, HEU-

MET-FAST-015, HEU-MET-FAST-065 benchmark specifications or computational models require attention if we assume that HEU-MET-FAST-001 and HEU-MET-FAST-018 are acceptable.

- The Oak Ridge cylinders HEU-MET-FAST-051 have a relatively small spread, but they are calculated lower compared to Godiva (HEU-MET-FAST-001) by about 250 pcm. The HEU-MET-FAST-051 suite actually includes 17 cases. Since they all show similar trends, only six are included in the analysis. Some of them show unreasonably small uncertainties. On the other hand, the Oak Ridge sphere HEU-MET-FAST-100 cases are high when compared to Godiva by about 200 pcm. Overall, the Oak Ridge benchmarks also have a spread of nearly 500 pcm. Therefore, these ORNL's benchmark specifications or computational models may require some attention.
- The French Caliban cylindrical assembly HEU-MET-FAST-080 is by far the highest, differing by nearly 1000 pcm from the average. A quick review of the input model and the benchmark specifications (O. Cabellos, Private communication, December 2016) reveals that the fissile material mass calculated from the volumes and the densities is 0.5% higher than specified in the benchmark description. This would account for about 400 pcm, which would still leave a discrepancy of about 500 pcm. Therefore, it is our opinion that this benchmark needs a complete review.

From the above it seems necessary to assess the unrecognized systematic uncertainty of $^{235}$U benchmarks. Such approach may lead to additional benchmark uncertainties, which could be important for those cases with unreasonable low-declared uncertainties.

The reactivity prediction of the current $^{235}$U evaluation has been slightly tuned (by less than ±50 pcm compared to the original Young least-squares adjustment [65]) to match the benchmark reactivity value of Godiva, which is somewhere in the middle of predicted reactivities of all benchmarks. This seems to counteract the nubar adjustment made in the ENDF/B-VII.1 library, but unfortunately precise details of that adjustment are not available. Assuming that Godiva is representative of the highly enriched bare assemblies, we think that the present $^{235}$U evaluation represents the best knowledge of the nuclear properties of $^{235}$U in the fast energy range in terms of integral performance as well as in terms of measured differential data, consistent with the $^{235}$U($n$,f) standards cross sections [14].

### B. Other Selected Fast Assemblies Containing $^{235}$U and $^{238}$U

A short list of fast-neutron benchmarks was selected, which are traditionally used to test the performance of uranium nuclear data including both $^{235}$U and $^{238}$U isotopes. The IAEA CIELO $^{235}$U evaluated data file was complemented by the IAEA CIELO evaluated $^{238}$U file [69, 175, 176] for this exercise. All other relevant isotopes (mainly $^{234}$U) were kept fixed to the ENDF/B-VIII.0 evaluations [139]. The benchmark list is given in Table XIII and includes different types of fast assemblies with regard to fuel material, reflectors, enrichment and spectral characteristics. From our experience, these benchmarks are considered to be fairly reliable, since they have been analyzed by many authors and reported in a variety of publications. We also included Godiva (HEU-MET-FAST-001) results as a reference.

TABLE XIII. List of main benchmarks for $^{235}$U and $^{238}$U data validation.

| No. | ICSBEP label | Short name | Common name |
|---|---|---|---|
| 1 | HEU-MET-FAST-001 | hmf001 | Godiva |
| 2 | HEU-MET-FAST-028 | hmf028 | Flattop-25 |
| 3 | IEU-MET-FAST-007 | imf007d | Big_Ten(d) |
| 4 | IEU-MET-FAST-001 | imf001-001 | Jemima-1 |
| 5 | IEU-MET-FAST-001 | imf001-002 | Jemima-2 |
| 6 | IEU-MET-FAST-001 | imf001-003 | Jemima-3 |
| 7 | IEU-MET-FAST-001 | imf001-004 | Jemima-4 |

The calculated $\Delta k_{\rm eff}$ is plotted in Fig. 36 as a function of parameter $E_\alpha$, which is defined as the energy of the average neutron lethargy causing fission. $E_\alpha$ works as a spectral parameter, weighted by the fission cross section at a given energy, and is easily retrievable from MCNP outputs. From independent studies we know that the softest neutron spectrum in this list corresponds to the Big_Ten assembly which is very sensitive to neutron energies from 10 keV to 50 keV. On the other end, the hardest neutron spectrum corresponds to the Godiva assembly which is very sensitive to neutron energies above 100 keV with a mean neutron energy around 700 keV. The Flattop-25 and Jemima assemblies are between those two extreme cases.

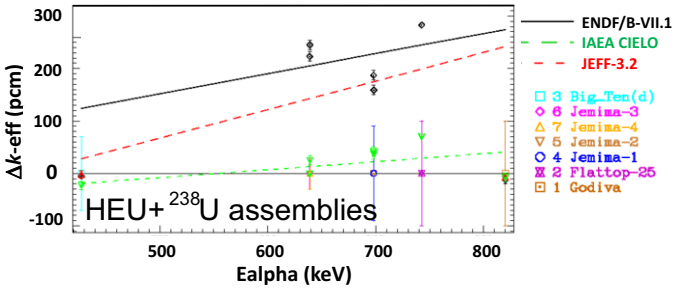


FIG. 36. (Color online) Selected fast $^{235}$U cores with $^{238}$U contents from ICSBEP benchmarks [17]. Symbols show the calculated values using different libraries; lines show the derived trends for $\Delta k_{\rm eff}$ as a function of $E_\alpha$.

From this plot it is evident that the new evaluation solves many of the outstanding problems in the older evaluations:

- The over-prediction of reactivity in the Flattop-25 assembly (highly-enriched uranium reflected by natural uranium) is eliminated without affecting the criticality prediction of Godiva and Big_Ten, the later having a softer spectrum due to the presence of graphite and natural uranium reflector.
- Major improvement is achieved in predicting the reactivity of the Jemima assemblies with uranium fuel of intermediate enrichment.

Derived trends of $\Delta k_{\rm eff}$ vs $E_\alpha$ for each library are also plotted in Fig. 36 as a black solid line (for ENDF/B-VII.1), and red and green dashed lines (for current evaluation and JEFF-3.2 evaluation, respectively). The red dashed line shows that the fitted trend for the current IAEA CIELO $^{235}$U and $^{238}$U file is practically flat and well within quoted experimental uncertainties, representing a considerable improvement compared to previous evaluations. It is worth noting that the improved trend show in Fig. 36 is mainly due to the improvements in elastic and inelastic scattering in the $^{238}$U evaluation.

### C. Lawrence Livermore Pulsed Sphere Experiments with 14 MeV Neutrons

Pulsed sphere experiments carried out at the Lawrence Livermore National Laboratory (LLNL) used a 14 MeV neutron source to measure the neutron leakage spectra from $^{238}$U spheres by the time-of-flight (TOF) technique [214–216]. Neutrons at the nominal energy of 14 MeV were generated via the $^3$H(d,n)$^4$He reaction from a 400 keV deuteron beam impinging on a tritium-loaded titanium target positioned in the center of the sphere. The LLNL pulsed sphere (LPS) benchmark experiments were evaluated several times [100, 217–221]. The latest evaluation was performed using MCNP (Monte Carlo n-particle) transport code inputs of Stephanie C. Frankle provided by the Los Alamos National Laboratory. In the input the experimental geometry was not modelled explicitly and some simplifications were introduced: i) neutron detectors were modelled as ring detectors and ii) concrete pit walls and collimators inside the beamline were not included in the model. However, a thin layer of a black absorber was added instead of the collimator [219].

Additional analysis was performed by Goričanec *et al.* to study the effect of the uncertainties on the flight path length, the angular positioning of the detectors, the concrete pit walls and the detailed structure of the collimator by developing a full 3D model of the experimental set-up [222]. The analysis confirmed the adequacy of the simplified model. In Ref. [218] the measured and calculated background spectra are reported. There is an additional peak visible at 2.8 MeV, which originates from the D-D reaction on the accumulated deuterium in the target, therefore, the comparison of experiments and calculations below 4 MeV is considered less reliable.

The comparison of measured and calculated neutron spectrum in the case of the experimental configuration with a thicker sphere (2.8 mfp), recommended by S. C. Frankle to be used for benchmarking, is presented in Fig. 37.

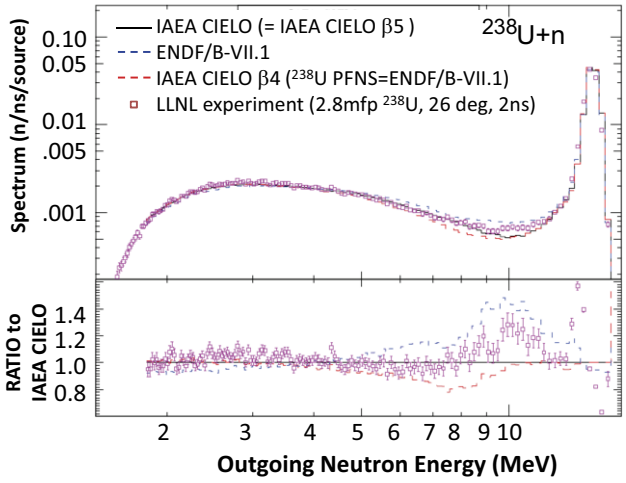


FIG. 37. (Color online) Comparison of leakage neutron spectrum TOF measurements (squares) to reference benchmark model calculations for the recommended experimental configuration using the full IAEA CIELO evaluation (solid), the ENDF/B-VII.1 (dashed blue), and the IAEA CIELO evaluation with $^{238}$U PFNS from the ENDF/B-VII.1 library.

Calculations using different neutron cross section libraries were performed: ENDF/B-VII.1, IAEA CIELO $\beta4$, and IAEA CIELO $\beta5$ (adopted as the final IAEA CIELO evaluation). The difference between the IAEA CIELO versions is that in the $\beta5$ version a fission spectrum of prompt neutrons above 8 MeV is taken from the JENDL-4 nuclear data library, while $^{238}$U PFNS from the ENDF/B-VII.1 library were used for all energies in the IAEA CIELO $\beta4$ library. Deviations between measurements and calculations can be observed; among different evaluations the IAEA CIELO $\beta5$ gives the best agreement with the experimental results and the ENDF/B-VII.1 file - the worse agreement - illustrating the relatively large impact of the $^{238}$U($n$,f) prompt fission spectrum on LPS neutron leakage for 5–10 MeV of outgoing neutron energy.

The overall conclusion is that the new IAEA CIELO file ($\beta5$) for $^{238}$U performs well, and certainly better than ENDF/B-VII.1. The importance of replacing the PFNS above 8 MeV with the data from JENDL is manifested by the improved agreement with measured data in the leaked neutron energy range from 5 MeV to 10 MeV. Note that the new IAEA CIELO evaluation still underestimates the experimental data from 10–12 MeV probably due to the missing strength of inelastic scattering to the continuum.

## VIII. CONCLUSIONS

New evaluations of neutron-induced reactions on $^{235}$U and $^{238}$U up to 30 MeV incident energy range have been produced under the IAEA coordination within the CIELO project [1–3]. Theory based calculations - performed with the code EMPIRE–3.2 Malta - combined with the latest experimental data for the capture channel, with newly measured and evaluated PFNS, and with nonmodel evaluation of experimental data from the Neutron Standards, accurately reproduce both differential and integral measured data. This was possible by improving the reaction modelling, by using the latest nuclear structure information provided by experiments and microscopic studies, by using the newest and more accurate experimental differential data, and by constraining model parameters using the feedback from criticality calculations of carefully selected benchmark experiments. These aspects are of great importance for the ongoing international projects dedicated to the nuclear data development and nuclear data evaluation.

The present IAEA CIELO $^{235}$U and $^{238}$U evaluated data files represent an excellent starting point towards a significantly improved evaluated data for major uranium isotopes. These evaluated files have been adopted by the ENDF project to become part of the new ENDF/B-VIII.0 library [139].

## ACKNOWLEDGEMENTS

We thank the Nuclear Energy Agency for administrative support for the WPEC Subgroup 40 collaboration and for starting the CIELO project, in particular we thank NEA colleagues E. Dupont, O. Cabellos and F. Michel-Sendis for their encouragement and assistance.

Authors acknowledge an important contribution made by the IAEA Neutron Standards committee, and by all contributors to the IAEA Prompt Fission Neutron Spectra project.

The work of M.S. was partially supported by the European Commission under the contract CHANDA (EURATOM No. FP7-605203). Work at Brookhaven National Laboratory was sponsored by the Office of Nuclear Physics, Office of Science of the U.S. Department of Energy under Contract No. DE-AC02-98CH10886 with Brookhaven Science Associates, LLC. Work at ORNL was supported by the US Department of Energy (DOE), Nuclear Criticality Safety Program (NCSP) funded and managed by the National Nuclear Security Administration for DOE. R.C. and E.S.S. would like to thank their optical model coworkers J.M. Quesada, D.S. Martyanov, and S. Chiba for fruitful collaboration on the development of optical model potentials that are the backbone of our cross section calculations. R.C. and D.N. would like to thank D.L. Smith for suggestions and advice on both the PFNS evaluation and uncertainty quantification issues. Special thanks go to M.B. Chadwick, M. White, T. Kawano, S. Hilaire, P. Romain, and B. Morillon for many enlightening discussions, and to A.C. (Skip) Kahler for an enormous number of calculated benchmark results for cross-checking and validation.

[1] OECD, Nuclear Energy Agency, "Collaborative International Evaluated Library Organisation (CIELO) Pilot Project," WPEC Subgroup 40 (SG-40) (see https://www.oecd-nea.org/science/wpec/sg40-cielo/).

[2] M. B. Chadwick, E. Dupont, E. Bauge *et al.*, "The CIELO Collaboration: Neutron Reactions on $^{1}$H, $^{16}$O, $^{56}$Fe, $^{235,238}$U, and $^{239}$Pu," Nucl. Data Sheets **118**, 1–25 (2014).

[3] R. Capote and A. Trkov (coordinators), "IAEA CIELO Data Development Project," within the International Pilot Project of the OECD/NEA [1] (see https://www-nds.iaea.org/CIELO/).

[4] M. B. Chadwick, M. W. Herman, P. Obložinský *et al.*, "ENDF/B-VII.1 nuclear data for science and technology: cross sections, covariances, fission product yields and decay data," Nucl. Data Sheets **112**, 2887–2996 (2011).

[5] JEFF Scientific Working Group, "Joint Evaluated Fission and Fusion File (JEFF) release 3.2," OECD, NEA, March 5 (2014).

[6] K. Shibata *et al.*, "JENDL-4.0: A New Library for Nuclear Science and Engineering," J. Nucl. Sci. Techn. **48**, 1–30 (2011).

[7] Chinese Evaluated Nuclear Data Library CENDL-3.1, China Nuclear Data Center, CD-ROM released on 24 December 2009.

[8] A. Trkov, R. Capote, "Evaluation of the Prompt Fission Neutron Spectrum of Thermal-neutron Induced Fission in U-235", Phys. Proc. **64**, 48–54 (2015).

[9] R. Capote, A. Trkov, V.G. Pronyaev, "Current Issues in Nuclear Data Evaluation Methodology: $^{235}$U Prompt Fission Neutron Spectra and Multiplicity for Thermal Neutrons," Nucl. Data Sheets **123**, 8–15 (2015).

[10] R. Capote, Y.-J. Chen, F.-J. Hambsch *et al.*, "Prompt fission neutron spectra of actinides," Nucl. Data Sheets **131**, 1–106 (2016).

[11] A. J. Plompen, T. Kawano, R. Capote Noy, "Inelastic scattering and capture cross-section data of major actinides in the fast neutron region," Report **INDC(NDS)-0597**, IAEA, Vienna 2012. Available online at https://www-nds.iaea.org/publications/indc/indc-nds-0597.pdf.

[12] S. Badikov *et al.*, "International Evaluation of Neutron Cross-Section Standards," Report **STI/PUB/1291**, IAEA, Vienna 2008.

[13] A. D. Carlson, V. G. Pronyaev, D. L. Smith *et al.*, "Inter-

national Evaluation of Neutron Cross Section Standards," Nucl. Data Sheets **110**, 3215–3324 (2009).
[14] A. D. Carlson, V. G. Pronyaev, R. Capote *et al.*, "Evaluation of Neutron Data Standards," Nucl. Data Sheets **148**, 143–188 (2018).
[15] M. W. Herman, R. Capote, B. V. Carlson, P. Obložinský, M. Sin, A. Trkov, H. Wienke, V. Zerkin, "EMPIRE: Nuclear Reaction Model Code System for Data Evaluation," Nucl. Data Sheets **108**, 2655–2715 (2007).
[16] M. Herman *et al.*, "EMPIRE-3.2 Malta User's Manual," Report **INDC(NDS)-0603**, IAEA, Vienna 2013. Available online at https://www-nds.iaea.org/publications/indc/indc-nds-0603.pdf.
[17] ICSBEP 2016: International Handbook of Evaluated Criticality Safety Benchmark Experiments, Nuclear Energy Agency, OECD, Paris 2016. See http://www.oecd-nea.org/science/wpncs/icsbep/handbook.html.
[18] R. E. MacFarlane, D. W. Muir, R. M. Boicourt, A. C. Kahler, "The NJOY Nuclear Data Processing System, Version 2012," LANL Report **LA-UR-12-27079**, Los Alamos 2012.
[19] "MCNP—A General Monte Carlo Code for Neutron and Photon Transport, Version 5," LANL Report **LA-UR-05-8617**, Los Alamos 2005.
[20] D. W. Muir, "Global Assessment of Nuclear Data Requirements," IAEA, Vienna 2001. Code and documentation available online at https://www-nds.iaea.org/gandr/.
[21] R. Capote, D. L. Smith, A. Trkov, "Nuclear Data Evaluation Methodology Including Estimates of Covariances," EPJ Web of Conf. **8**, 04001 (2010).
[22] A. Trkov, R. Capote, I. Kodeli, L. Leal, "Evaluation of tungsten nuclear reaction data with covariances," Nucl. Data Sheets **109**, 2905–2909 (2008).
[23] A. Trkov *et al.*, "Covariances of Evaluated Nuclear Cross Section Data for $^{232}$Th, $^{180,182,183,184,186}$W and $^{55}$Mn," Nucl. Data Sheets **112**, 3098–3119 (2011).
[24] N. M. Larson, "Updated users' guide for SAMMY: Multilevel *R*-matrix fits to neutron data using Bayes' equations," Report **ORNL/TM-9179/R8** (2008).
[25] M. T. Pigni, R. Capote, A. Trkov, V. G. Pronyaev, "n+235U resonance parameters and neutron multiplicities in the energy region below 100 eV," EPJ Web of Conf. **146**, 02011 (2017).
[26] L. C. Leal *et al.*, "*R*-Matrix Analysis of $^{235}$U Neutron Transmission and Cross-Section Measurements in the 0- to 2.25-keV Energy Range," Nucl. Sci. Eng. **131**, 230–253 (1999).
[27] V. G. Pronyaev, R. Capote, A. Trkov, G. Noguere, A. Wallner, "New fit of Thermal Neutron Constants (TNC) for $^{233,235}$U, $^{239,241}$Pu and $^{252}$Cf(sf): microscopic vs Maxwellian data," ND2016, Brugges, Belgium, September 2016, EPJ Web of Conf. **146**, 02045 (2017).
[28] R. R. Spencer *et al.*, "Parameters of the 1.056-eV Resonance in $^{240}$Pu and the 2200 m/s Neutron Total Cross Sections of $^{235}$U, $^{239}$Pu, and $^{240}$Pu " Nucl. Sci. Eng. **96**, 318–329 (1987).
[29] D. Cano-Ott, Private communication (2016).
[30] Y. Danon, D. Williams, R. Bahran, E. Blain, B. McDermott, D. Barry, G. Leinweber, R. Block, M. Rapp, "Simultaneous Measurement of $^{235}$U Fission and Capture Cross Sections From 0.01 eV to 3 keV Using a Gamma Multiplicity Detector," Nucl. Sci. Eng. **187**, pp. 291–301 (2017).
[31] G. de Saussure *et al.*, "Multilevel Analyses of the $^{235}$U Fission and Capture Cross Sections," Phys. Rev. **C7**, 2018–2032 (1966).
[32] M. Jandel, T. A. Bredeweg, E. M. Bond *et al.*, "New precision measurements of the $^{235}$U(n,$\gamma$) cross section," Phys. Rev. Lett. **109**, 202506 (2012); EXFOR 14149.
[33] H. Weigmann *et al.*, "Measurements of eta of $^{235}$U for subthermal neutron energies," Int. Conf. on the Physics of Reactors, Marseille 1990, France, vol. 3, Part. PI, p. 33 (1990).
[34] F. D. Brooks *et al.*, "Eta and neutron cross sections of $^{235}$U from 0.03 to 200 eV," Atomic Energy Research Estabishment, Harwell, Report **AERE-M1670** (1966).
[35] R. Gwin *et al.*, "Measurements of the Neutron Fission Cross Sections of $^{235}$U ($E_n$ = 0.01 eV to 30 keV) and $^{239}$Pu ($E_n$ = 0.01 to 60 eV)," Nucl. Sci. Eng. **88**, 37–55 (1984).
[36] R. Gwin, Oak Ridge National Laboratory, Private communication (1997).
[37] L. W. Weston, J. H. Todd, "Subthreshold Fission Cross Section of $^{240}$Pu and the Fission Cross Sections of $^{235}$U and $^{239}$Pu," Nucl. Sci. Eng. **88**, 567–578 (1984).
[38] R. B. Perez *et al.*, "Simultaneous Measurements of the Neutron Fission and Capture Cross Sections for Uranium-235 for Neutron Energies from 8 eV to 10 keV," Nucl. Sci. Eng. **52**, 46–72 (1973).
[39] C. Wagemans *et al.*, "Subthermal fission cross-section measurements for $^{233}$U, $^{235}$U and $^{239}$Pu," *Proc. Int. Conf. Nucl. Data for Science and Technology*, Mito, Japan 1988, p. 91–95 (1988).
[40] R. A. Shrack, "Measurement of the $^{235}$U($n$,f) reaction from thermal to 1 keV," *Proc. Int. Conf. Nucl. Data for Science and Technology*, Mito, Japan 1988, p. 101–104 (1988).
[41] J. A. Harvey *et al.*, "High-Resolution Neutron Transmission Measurements on $^{235}$U, $^{239}$Pu, and $^{238}$U," *Proc. Int. Conf. Nucl. Data for Science and Technology*, Mito, Japan, 1988, p. 115–118 (1988).
[42] L. Leal, Private communication, see IAEA CIELO webpage, IRSN.v2 resonance parameter in u235ib02i2g6cnu3f2 file.
[43] M. Ishikawa, "Recommendation from ADJ2010 Adjustment," Kick-off Meeting of WPEC Subgroup 39, OECD, Paris, November 28-29, 2013. Available online at https://www.oecd-nea.org/science/wpec/sg39/Meeting2_Nov2013/01_ADJ2010_Recom_Ishikawa.pdf
[44] M. Fukushima, K. Yokoyama, O. Iwamoto, Y. Nagaya, "Benchmark tests for ENDF/B-VIII.0 beta1 using Sodium-void reactivity worth of FCA-XXVII-1," SG-39 Meeting, December 1-2, OECD, Paris, 2016. Available online at https://www.oecd-nea.org/science/wpec/sg39/Meeting_December2016/SG39_4_KYokoyama_1.pdf.
[45] C. Wagemans *et al.*, "New results on the $^{235}$U($n$,f) fission integrals," Report **IAEA/TECDOC-335**, 157–161 (1984).
[46] R. L. Reed *et al.*, "Prompt neutron multiplicity measurements for neutron-induced fission of $^{233}$U and $^{235}$U," Chicago Operations Office Report **COO-3058-39**, 3 (1973).
[47] R. E. Howe, R. W. Hockenbury, R. C. Block, "Prompt fission neutrons from eV resonances in $^{235}$U: Measurement

and correlation with other fission properties," PHYS. REV. **C13**, 195–205 (1976).
[48] R. Gwin *et al.*, "Measurements of the Energy Dependence of Prompt Neutron Emission from $^{233}$U, $^{235}$U, $^{239}$Pu, and $^{241}$Pu for $E_n$ = 0.005 to 10 eV Relative to Emission from Spontaneous Fission of $^{252}$Cf," NUCL. SCI. ENG. **87**, 381–404 (1984).
[49] G. Simon, J. Frehaut, "Measurements and interpretation of the mean prompt neutron number and the mean prompt fission gamma energy emitted in neutron resonances of fissile nuclei," *All Union Conf. on Neutron Phys.* (Kiev, September 1975) **vol. 5**, 337 (1975).
[50] D. Shackleton, J. Trochon, J. Frehaut *et al.*, "Measurement of the mean number of prompt neutrons and the mean energy of prompt gamma-rays emitted during resonance neutron-induced fission in $^{235}$U and $^{239}$Pu," PHYS. LETT. **B42**, 344–346 (1972).
[51] M. Sin, R. Capote, M. Herman, and A. Trkov, "Modelling Neutron-induced Reactions on $^{232-237}$U from 10 keV up to 30 MeV," NUCL. DATA SHEETS **139**, 138-170 (2017).
[52] A. Trkov, R. Capote *et al.*, "Evaluation of the neutron induced reactions on $^{235}$U from 2.25 keV up to 30 MeV," Presented at ND2016, Brugges, Belgium, EPJ WEB OF CONF. **146**, 02029 (2017).
[53] R. Capote, M. W. Herman, P. Obložinský *et al.*, "RIPL–Reference Input Parameter Library for calculation of nuclear reactions and nuclear data evaluations," NUCL. DATA SHEETS **110**, 3107–3214 (2009) (see http://www-nds.iaea.org/RIPL-3/).
[54] J. Raynal, "Optical model and coupled-channel calculations in nuclear physics", in: *Computing as a language of physics, ICTP International Seminar Course*, Trieste, 2-20 August 1971, Report **STI/PUB-306**, Int. Atomic Energy Agency, Vienna 1972, pp.281–322. ECIS code distributed by the NEA DATA Bank (OECD, Paris).
[55] E. Sh. Soukhovitskiĭ, R. Capote, J. M. Quesada, S. Chiba, "Dispersive coupled-channel analysis of nucleon scattering from $^{232}$Th up to 200 MeV," PHYS. REV. **C72**, 024604 (2005).
[56] E. Sh. Soukhovitskiĭ, R. Capote, J. M. Quesada, S. Chiba, D. S. Martyanov, "Nucleon scattering on actinides using a dispersive optical model with extended couplings," PHYS. REV. **C94**, 064605 (2016).
[57] J. M. Quesada, R. Capote, A. Molina, M. Lozano, "Dispersion relations in the nuclear optical model," COMP. PHYS. COMMUN. **153**, 97–105 (2003).
[58] J. M. Quesada, R. Capote, A. Molina, M. Lozano, J. Raynal, "Analytical expressions for the dispersive contributions to the nucleon-nucleus optical potential," PHYS. REV. **C67**, 067601 (2003).
[59] A. M. Lane, "New term in the nuclear optical potential: implications for $(p,n)$ mirror state reactions," PHYS. REV. LETT. **8**, 171–172 (1962).
[60] A. M. Lane, "Isobaric spin dependence of the optical potential and quasi-elastic $(p,n)$ reactions," NUCL. PHYS. **35**, 676–685 (1962).
[61] J. M. Quesada, R. Capote, E.Sh. Soukhovitskiĭ, S. Chiba, "Approximate Lane consistency of the dispersive coupled-channels potential for actinides," PHYS. REV. C **76**, 057602 (2007).
[62] R. Capote, E. Sh. Soukhovitskiĭ, J. M. Quesada, S. Chiba, "Is a global coupled-channel dispersive optical model potential for actinides feasible?," PHYS. REV. **C72**, 064610 (2005); RIPL 2408 potential.
[63] R. Capote, S. Chiba, E. Sh. Soukhovitskiĭ, J. M. Quesada, E. Bauge, "A global dispersive coupled-channel optical model potential for actinides," J. NUCL. SCI. TECH. **45**, 333–340 (2008); RIPL 2408 potential.
[64] F. S. Dietrich, I. J. Thompson, T. Kawano, "Target-state dependence of cross sections for reactions on statically deformed nuclei," PHYS. REV. **C85**, 044611 (2012).
[65] P. G. Young, M. B. Chadwick, R. E. MacFarlane *et al.*, "Evaluation of Neutron Reactions for ENDF/B-VII: $^{232-241}$U and $^{239}$Pu," NUCL. DATA SHEETS **108**, 2589–2654 (2007).
[66] W. Hauser, H. Feshbach, "The inelastic scattering of neutrons," PHYS. REV. **87**, 366–373 (1952).
[67] H. M. Hoffmann, J. Richert, J. W. Tepel, H. A. Weidenmüller, "Direct reactions and Hauser-Feshbach theory," ANN. PHYS. (N.Y.) **90**, 403–437 (1975).
[68] T. Kawano, R. Capote, S. Hilaire, P. Chau Huu-Tai, "Statistical Hauser-Feshbach theory with width-fluctuation correction including direct reaction channels for neutron-induced reactions at low energies," PHYS. REV. **C94**, 014612 (2016).
[69] R. Capote, A. Trkov, M. Sin, M. Herman, A. Daskalakis, Y. Danon, "Physics of Neutron Interactions with $^{238}$U: New Developments and Challenges," NUCL. DATA SHEETS **118**, 26–31 (2014).
[70] S. Björnholm, A. Bohr, B. R. Mottelson, "Role of symmetry of the nuclear shape in rotational contributions to nuclear level densities," in pp. 367–372, Ref. [71].
[71] *Third IAEA Symp. on Physics and Chemistry of Fission*, Rochester, New York, 13–17 August 1973, Report **STI/PUB/347, vol. I**, Int. Atomic Energy Agency, Vienna 1974.
[72] R. Capote, V. Osorio, R. López, E. Herrera, M. Piris, "Analysis of experimental data on neutron-induced reactions and development of code PCROSS for the calculation of differential pre-equilibrium emission spectra with modelling of the level density function," Final report on research contract 5472/RB, Report **IAEA(CUB)-004** Int. Atomic Energy Agency, Vienna 1991.
[73] S. Goriely, S. Hilaire, A. J. Koning, M. Sin, R. Capote, "Towards a prediction of fission cross sections on the basis of microscopic nuclear inputs," PHYS. REV. **C79**, 024612 (2009).
[74] S. Goriely, S. Hilaire, A. J. Koning, R. Capote, "Towards an improved evaluation of neutron-induced fission cross sections on actinides," PHYS. REV. **C83**, 034601 (2011).
[75] P. Romain, B. Morillon, H. Duarte, "Bruyères-le-Châtel Neutron Evaluations of Actinides with the TALYS Code: the Fission Channel," NUCL. DATA SHEETS **131**, 222–258 (2016).
[76] E. Bauge *et al.*, "Coherent investigation of nuclear data at CEA DAM: Theoretical models, experiments and evaluated data," EUR. PHYS. J. **A48**, 113–152 (2012).
[77] M. Sin, R. Capote, M. Herman, A. Trkov, "Extended optical model for fission," PHYS. REV. **C93**, 034605 (2016).
[78] T. Ichikawa, P. Möller, A. J. Sierk, "Character and prevalence of third minima in actinide fission barriers," PHYS. REV. **C87**, 054326 (2013).
[79] M. Sin, R. Capote, "Transmission through multi-humped fission barriers with absorption: A recursive approach," PHYS. REV. **C77**, 054601 (2008).

[80] V. N. Kononov, E. D. Poletayev, B. D. Yurlov, "Measurement of alpha, neutron fission and the $^{235}$U and $^{239}$Pu fission and capture cross sections for 10–80 keV neutrons," At. Energy **38**, 105–109 (1975); EXFOR 40412.

[81] R. G. Johnson, M. S. Dias, A. D. Carlson, O. A. Wasson, "The $^{235}$U standard neutron cross section. II. Measurements from 1.0 to 6.0 MeV using the dual thin scintillator," Private communication by A. D. Carlson; EXFOR 12924.

[82] A. D. Carlson, O. A. Wasson, P. W. Lisowski, J. L. Ullmann, N. W. Hill, "Measurements of the $^{235}$U($n$,f) cross section in the 3 to 30 MeV neutron energy region," in *Proc. Int. Conf. on Nuclear Data for Science and Technology*, Jülich, Fed. Rep. of Germany, 13–17 May 1991, S. M. Qaim, (Ed.), pp. 518–519, Springer (1991); EXFOR 14015.

[83] P. W. Lisowski, A. Gavron, W. E. Parker, S. J. Balestrini, A. D. Carlson, O. A. Wasson, N. W. Hill, "Fission cross sections ratios for $^{233}$U, $^{234}$U, $^{236}$U relative to $^{235}$U from 0.5 to 400 MeV," in *Proc. Int. Conf. on Nuclear Data for Science and Technology*, Jülich, Fed. Rep. of Germany, 13–17 May 1991, S. M. Qaim, (Ed.), pp. 732–733, Springer (1991); EXFOR 14011.

[84] T. Iwasaki, Y. Karino, S. Matsuyama, F. Manabe, M. Baba, K. Kanda, and N. Hirakawa, "Measurement of $^{235}$U fission cross section around 14 MeV," in *Proc. Int. Conf. on Nuclear Data for Science and Technology*, Mito, Japan, May 30–June 3 1988, S. Igarasi (Ed.), JAERI, pp.87–90; EXFOR 22091.

[85] A. D. Carlson, J. W. Behrens, R. G. Johnson, G. E. Cooper, "Absolute measurements of the $^{235}$U($n$,f) cross-section for neutron energies from 0.3 to 3 MeV," in *Proc. Adv. Group Meet. on Nuclear Standard Reference Data*, Geel, 12–16 Nov. 1984, Report **IAEA-TECDOC-335**, Int. Atomic Energy Agency, Vienna, pp.162–166 (1985). Available online at https://www-nds.iaea.org/publications/tecdocs/iaea-tecdoc-0335.pdf; EXFOR 10987.

[86] O. A. Wasson, A. D. Carlson, K. C. Duvall, "Measurement of the $^{235}$U neutron-induced fission cross section at 14.1 MeV," Nucl. Sci. Eng. **80**, 282–303 (1982); EXFOR 10971.

[87] M. Mahdavi, G. F. Knoll, K. Zasadny, J. C. Robertson, "Measurements of the 14-MeV fission cross-sections for $^{235}$U and $^{239}$Pu," in *Proc. Int. Conf. on Nuclear Data for Science and Technology*, Antwerp, Belgium, 6-10 Sept. 1982, K. H. Bockhoff (Ed.), Springer, pp.58–61 (1982); EXFOR 12826.

[88] Li Jing-Wen, Li An-Li, Rong Chao-Fan, Ye Zhong-Yuan, Wu Jing-Xia, Hao Xiu-Hong, "Absolute measurements of $^{235}$U and $^{239}$Pu fission cross section induced by 14.7 MeV neutrons," in *Proc. Int. Conf. on Nuclear Data for Science and Technology*, Antwerp, Belgium, 6-10 Sept. 1982, K. H. Bockhoff (Ed.), Springer, pp. 55–57 (1982); EXFOR 30634.

[89] T. A. Mostovaya, V. I. Mostovoy, S. A. Biryukov, A. A. Osochnikov, A. V. Tsvetkov, "Fission cross-sections measurement for $^{233}$U and $^{235}$U in the energy range 0.1–100 keV and cross-section ratio measurement $^{233}$U/$^{235}$U up to 2 MeV," in *Proc.* $5^{th}$ *All Union Conf. on Neutron Phys.* (Kiev, September 1980), **vol. 3**, p.30–32 (1980), USSR (in Russian); EXFOR 40616.

[90] W. P. Poenitz, "Relative and absolute measurements of the fast-neutron fission cross wection of $^{235}$U," Nucl. Sci. Eng. **53**, 370–392 (1974); EXFOR 10333.

[91] N. Otuka, E. Dupont, V. Semkova, B. Pritychenko *et al.*, "Towards a More Complete and Accurate Experimental Nuclear Reaction Data Library (EXFOR): Int. Collaboration Between Nuclear Reaction Data Centres (NRDC)," Nucl. Data Sheets **120**, 272–276 (2014). Data available online (*e.g.*, at http://www-nds.iaea.org/exfor/).

[92] R. Batchelor, K. Wyld, "Neutron scattering by $^{235}$U and $^{239}$Pu for incident neutrons of 2, 3 and 4 MeV," Report **55/69**, A.W.R.E. Aldermaston Reports, UK (1969); EXFOR 20036.

[93] D. M. Drake, "Inelastic neutron scattering and gamma production from fast-neutron bombardment of $^{235}$U," Nucl. Phys. **A133**, 108–112 (1969); EXFOR 10016.

[94] B. H. Armitage, A. T. G. Ferguson, J. H. Montague, N. Starfelt, "Inelastic scattering of fast neutrons by $^{235}$U," *Conf. on Nuclear data for reactors; vol.I* , 17–21 Oct. 1966, Paris, France, IAEA Report **STI/PUB-140**, Int. Atomic Energy Agency, Vienna, 383–392 (1967); EXFOR 21086. Available online at https://www-nds.iaea.org/publications/proceedings/66PARIS_1_1967.pdf.

[95] V. N. Andreev, "Inelastic scattering of neutrons of the fission spectrum and neutrons with an energy of 0.9 MeV on $^{235}$U and $^{239}$Pu," Neitronnaya Fizika, p.287 (Moskva, USSR, 1961); translated as Sov. Progr. in Neutr. Phys., p.211 (New York, USA, 1961).

[96] J. Frehaut, A. Bertin, R. Bois, "Measurement of the $^{235}$U($n$,2$n$) cross section between threshold and 13 MeV," Nucl. Sci. Eng. **74**, 29–33 (1980); EXFOR 21568.

[97] D. S. Mather, P. F. Bampton, R. E. Coles, G. James, P. J. Nind, "Measurement of ($n$,2$n$) cross sections for incident energies between 6 and 14 MeV," Report **AWRE-O-47/69**, A.W.R.E. Aldermaston Reports, UK (1969); EXFOR 20795.

[98] J. L. Kammerdiener, "Neutron spectra emitted by $^{239}$Pu, $^{238}$U, $^{235}$U, Pb, Nb, Ni, Al, and C irradiated by 14 MeV neutrons," Lawrence Rad. Laboratory (Berkeley and Livermore) Report **UCRL-51232**, University of California 1972.

[99] L. F. Hansen, C. Wong, T. T. Komoto, B. A. Pohl, E. Goldberg, R. J. Howerton, W. W. Webster, "Neutron and gamma spectra from $^{232}$Th, $^{235}$U, $^{238}$U and $^{239}$Pu after bombardment with 14 MeV neutrons," Nucl. Sci. Eng. **72**, 35–49 (1979).

[100] L. F. Hansen *et al.*, "Measurements and Calculations of the Neutron Emission Spectra from Materials used in Fusion-Fission Reactors," Nucl. Tech. **51**, 70–77 (1980).

[101] A. Wallner *et al.*, "Novel method to study neutron capture of $^{235}$U and $^{238}$U simultaneously at keV energies," Phys. Rev. Lett. **112**, 192501 (2014); EXFOR 23170.

[102] V. P. Vertebniy, N. L. Gnidak, A. V. Grebnev, A. L. Kirilyuk, E. A. Pavlenko, N. A. Trofimova, "Determination of total cross-section and scattering cross-section of $^{235}$U for neutron energies 2– and 24.5 keV," in *Proceed.* $5^{th}$ *All Union Conf. on Neutron Phys.* (Kiev, September 1980), **vol. 2**, p.254 (1980) (in Russian); EXFOR 40609.

[103] F. Corvi, L. Calabretta, M. Merla, M. S. Moore, T. van der Veen, "Measurement of the neutron induced fission and capture cross sections, and alpha of $^{235}$U in keV region," in *Prog. report from CEC-Countries and*

*CEC to NEANDC*, Report **NEANDC(E)-232, vol.3**, p.5 (1982); EXFOR 21177.

[104] L. W. Weston, G. De Saussure, R. Gwin, "Ratio of capture to fission in U235 at keV neutron energies," Nucl. Sci. Eng. **20**, 80 (1964); EXFOR 12407.

[105] G. De Saussure, L. W. Weston, R. Gwin, R. W. Ingle, J. H. Todd, R. W. Hockenbury, R. R. Fullwood, A. Lottin, "Measurement of the neutron capture and fission cross sections and of their ratio,alpha, for U-233, U-235, and Pu-239," Report **STI/PUB/140**, Proc. Nuclear Data For Reactors Conf., Paris 1966 (IAEA, Vienna 1967), vol.2, 233–250 (1966). Available online at https://www-nds.iaea.org/publications/proceedings/66PARIS_2_1967.pdf.

[106] J. C. Hopkins, B. C. Diven, "Neutron Capture to Fission Ratios in $^{233}$U, $^{235}$U, and $^{239}$Pu," Nucl. Sci. Eng. **12**, 169–177 (1962); EXFOR 12331.

[107] R. Gwin, E. G. Silver, R. W. Ingle, H. Weaver, "Measurement of the neutron capture and fission cross sections of $^{239}$Pu and $^{235}$U, 0.02 eV to 200 keV, the neutron capture cross sections of $^{197}$Au, 10 to 50 keV, and neutron fission cross sections of $^{233}$U, 5 to 200 keV," Nucl. Sci. Eng. **59**, 79–105 (1976).

[108] F. Corvi, "Status of neutron capture data of $^{233}$U, $^{235}$U, and $^{239}$Pu in the unresolved resonance region," in *Proc. NEANDC/NEACRP Specialist's Meeting on fast neutron capture cross sections*, April 20–23, 1982, Argonne National Laboratory Report **NEANDC(US)-214/L**, 314–335 (1982); EXFOR 21177.

[109] L. W. Weston, G. De Saussure, R. Gwin, "Neutron capture in 238-U and the ratio of capture to fission in 235-U," Technical Report **EANDC-33** (1963); EXFOR 12456.

[110] G. De Saussure, L. W. Weston, J. D. Kington, R. D. Smiddie, W. S. Lyon, "The measurement of alpha as a function of energy," Oak Ridge National Laboratory Report **No. 3360**, p.51 (1962).

[111] F. Corvi, P. Giacobbe, "Capture-To Fission Ratio of 235-U from the Measurement Of Low Energy Gamma-Rays," in *Proc. Conf. on Nucl. Cross Sections and Techn.*, Washington D.C., **National Bureau of Standards Special Publication 425**, p.599 (1975); EXFOR 22630.

[112] B. C. Diven, J. Terrell, A. Hemmendinger, "Capture-To-Fission Ratios For Fast Neutrons In $^{235}$U," Phys. Rev. **109**, 144 (1958); EXFOR 12416.

[113] J. M. Allmond, L. A. Bernstein, C. W. Beausang *et al.*, "Relative $^{235}$U($n$,$\gamma$) and ($n$,f) cross sections from $^{235}$U($d$,$p\gamma$) and ($d$,$p$f) reactions," Phys. Rev. **C79**, 054610 (2009); EXFOR 14230.

[114] G. R. Keepin, T. F. Wimett, R. K. Zeigler, "Delayed neutrons from fissionable isotopes of uranium, plutonium, and thorium," Phys. Rev. **107**, 1044 (1957).

[115] R. J. Tuttle, "Delayed-Neutron Data for Reactor-Physics Analysis," Nucl. Sci. Eng. **56**, 37–71, (1975).

[116] D. Neudecker, P. Talou, T. Kawano *et al.*, "Evaluations of energy spectra of neutrons emitted promptly in neutron-induced fission of $^{235}$U and $^{239}$Pu," Nucl. Data Sheets **148**, 293–311 (2018).

[117] M. Devlin *et al.*, "The Prompt Fission Neutron Spectrum of 235U(n,f) below 2.5 MeV for Incident Neutrons of 0.7 to 20 MeV," Nucl. Data Sheets **148**, 322–337 (2018).

[118] A. S. Vorobyev, O. A. Shcherbakov, "Integral Prompt Neutron Spectrum for Fission of $^{235}$U by Thermal Neutrons,"Report **INDC(CCP)-0455**, 21–41 (IAEA, Vienna 2014).

[119] N. Kornilov, F.-J. Hambsch, I. Fabry *et al.*, "The $^{235}$U(n,$f$) Prompt Fission Neutron Spectrum at 100 K Input Neutron Energy," Nucl. Sci. Eng. **165**, 117–127 (2010).

[120] V. N. Nefedov, B. I. Starostov, A. A. Boytsov, "Precision Measurements of $^{252}$Cf, $^{233}$U, $^{235}$U and $^{239}$Pu Prompt Fission Neutron Spectra (PFNS) in the Energy Range 0.04–5 MeV,"Report **INDC(CCP)-0457** (IAEA, Vienna 2014); translation into English from: Proc. All-Union Conf. on Neutron Phys. (Kiev 1983), **vol. 2**, 285–289 (1983).

[121] B. I. Starostov, V. N. Nefedov, A. A. Boytsov, "Prompt Neutrons Spectra from the Thermal Neutron Fission of $^{233}$U, $^{235}$U, $^{239}$Pu and Spontaneous Fission of $^{252}$Cf in the Secondary Neutron Energy Range 0.01–12 MeV,"Report **INDC(CCP)-293/L**, 19–32 (IAEA, Vienna 1989), translation into English from: Nucl. Constants, **3**, 16 (1985).

[122] B. I. Starostov, V. N. Nefedov, A. A. Boytsov, "Precision Measurements of $^{252}$Cf, $^{233}$U+n$_{th}$, $^{235}$U+n$_{th}$ and $^{239}$Pu+n$_{th}$ Prompt Fission Neutron Spectra (PFNS) in the Energy Range 2–11 MeV,"Report **INDC(CCP)-0458** (IAEA, Vienna 2014); translation into English from: Proc. of the All-Union Conf. on Neutron Phys. (Kiev, October 1983), **vol. 2**, 290–293 (1983).

[123] A. Lajtai, J. Kecskemeti, J. Safar, P. P. Dyachenko, V. M. Piksaikin, "Energy Spectrum Measurements of Neutrons for Energies 30 keV–4 MeV from Thermal Fission of Main Fuel Elements," NDST 2004, Santa Fe, NM, USA, AIP Conf. Proc. **769**, 613–616 (1985).

[124] Wang Yufeng, Bai Xixiang, Li Anli, Wang Xiazhong, Li Jingwen, Meng Jiangchen, Bao Zhongyu, "Experimental study of the prompt neutron spectrum of U-235 fission induced by thermal neutrons," Chin. J. Nucl. Phys. (Beijing) **11**, No.4, 47 (1989).

[125] A. A. Boytsov, A. F. Semenov, B. I. Starostov, "Relative Measurements of $^{233}$U+n$_{th}$, $^{235}$U+n$_{th}$ and $^{239}$Pu+n$_{th}$ Prompt Fission Neutron Spectra (PFNS) in the Energy Range 0.04 – 5 MeV," Proc. 6-th All-Union Conf. on Neutron Phys. (Kiev, October 1983), **vol. 2**, 294–297 (1983). Translated in Report **INDC(CCP)-0459** (IAEA, Vienna 2014).

[126] M. M. Islam and H.-H. Knitter, "The Energy Spectrum of Prompt Neutrons from the Fission of Uranium-235 by 0.40-MeV Neutrons," Nucl. Sci. Eng. **50**, 108–114 (1973).

[127] P. I. Johansson and B. Holmqvist, "An Experimental Study of the Prompt Fission Neutron Spectrum Induced by 0.5-MeV Neutrons Incident on Uranium-235," Nucl. Sci. Eng. **62**, 695–708 (1977).

[128] J. P. Lestone and E. F. Shores, "Uranium and Plutonium Average Prompt-fission Neutron Energy Spectra (PFNS) from the Analysis of NTS NUEX Data," Nucl. Data Sheets **119**, 213–216 (2014).

[129] J. P. Lestone and E. F. Shores, "Uranium and Plutonium Prompt-fission-neutron Spectra (PFNS) of NTS NUEX Data and the Corresponding Uncertainty Budget," Los Alamos National Laboratory Report LA-UR-14-24087 (2014).

[130] H.-H. Knitter, M. M. Islam and M. Coppola, "Investigation of Fast Neutron Interaction with $^{235}$U," Z. Phy. **257**, 108–123 (1972).

[131] G. S. Boĭkov, V. D. Dmitriev, G. A. Kudyaev *et al.*, "Spectrum of Neutrons Accompanying Fission of $^{232}$Th, $^{235}$U, and $^{238}$U by 2.9-MeV and 14.7-MeV Neutrons (Below and Above the Threshold of Emission Fission)," SOV. J. NUCL. PHYS. **53**, 392–405 (1991).
[132] T. N. Taddeucci, R. C. Haight, H. Y. Lee *et al.*, "Multiple-scattering Corrections to Measurements of the Prompt Fission Neutron Spectrum," NUCL. DATA SHEETS **123**, 135–139 (2015).
[133] D. Neudecker, T. N. Taddeucci, R. C. Haight *et al.*, "The Need for Precise and Well-documented Experimental Data on Prompt Fission Neutron Spectra from Neutron-induced Fission of $^{239}$Pu," NUCL. DATA SHEETS **131**, 289–318 (2016).
[134] M. E. Rising, P. Talou, T. Kawano *et al.*, "Evaluation and Uncertainty Quantification of Prompt Fission Neutron Spectra of U and Pu Isotopes," NUCL. SCI. ENG. **175**, 81–93 (2013).
[135] M. E. Rising, "Quantification and Propagation of Nuclear Data Uncertainties," Dissertation, The University of New Mexico, USA (2012).
[136] D. G. Madland and J. R. Nix, "New Calculation of Prompt Fission Neutron Spectra and Average Prompt Neutron Multiplicities," NUCL. SCI. ENG. **81**, 213–271 (1982).
[137] D. Neudecker, P. Talou, D. L. Smith *et al.*, "Evaluation of the $^{239}$Pu Prompt Fission Neutron Spectrum Induced by Neutrons of 500 keV and Associated Covariances," NUCL. INST. METH. PHYS. RES. A **791**, 80–92 (2015).
[138] T. Kawano, P. Talou, M. B. Chadwick *et al.*, "Monte Carlo Simulation for Particle and $\gamma$-Ray Emissions in Statistical Hauser-Feshbach Model," J. NUCL. SCI. TECHNOL. **47**, 462–469 (2010).
[139] D. A. Brown, M. B. Chadwick, R. Capote *et al.*, "ENDF/B-VIII.0: The $8^{th}$ Major Release of the Nuclear Reaction Data Library with CIELO-project Cross Sections, New Standards and Thermal Scattering Data," NUCL. DATA SHEETS **148**, 1–142 (2018).
[140] D. M. Drake, E. D. Arthur, M.G. Silbert, "Cross Sections for Gamma-Ray Production by 14-MeV Neutrons," NUCL. SCI. ENG. **65**, 49–64 (1978).
[141] S. Kopecky, I. Sirakov, H. I. Kim *et al.*, "Status of Evaluated Data Files for $^{238}$U in the Resonance Region," JRC Technical Report **EUR 27504 EN** (2015).
[142] H. Derrien, L. C. Leal, N. M. Larson, A. Courcelle, "Neutron Resonance Parameters of $^{238}U$ and the Calculated Cross Sections from the Reich-Moore Analysis of Experimental Data in the Neutron Energy Range from 0 to 20 keV," **ORNL/TM-2005/241**, Oak Ridge National Laboratory 2005.
[143] H. I. Kim, C. Paradela, I. Sirakov *et al.*, "Neutron capture cross section measurements for $^{238}$U in the resonance region at GELINA," EUR. PHYS. J. **A52**, 170 (2016).
[144] D. K. Olsen, G. de Saussure, R. B. Perez, E. G. Silver, F. C. Difilippo, R. W. Ingle, H. Weaver, "Precise Measurement and Analysis of Neutron Transmission Through Uranium-238," NUCL. SCI. ENG. **62**, 479–501 (1977).
[145] D. K. Olsen, G. de Saussure, R. B. Perez, F. C. Difilippo, R. W. Ingle, "Note on $^{238}$U + n Resolved Resonance Energies," NUCL. SCI. ENG. **66**, 141–144 (1978).
[146] F. C. Difilippo, R. B. Perez, G. de Saussure, D. K. Olsen, R. W. Ingle, "$^{238}$U neutron-induced fission cross section for incident neutron energies between 5 eV and 3.5 MeV," PHYS. REV. **C21**, 1400–1410 (1980).
[147] M. C. Moxon and J. B. Brisland, *GEEL REFIT, A least-squares fitting program for resonance analysis of neutron transmission and capture data computer code*, in **AEA-InTec-0630**, AEA Technology, October 1991.
[148] C. W. Reich, M. S. Moore, "Multilevel Formula for the Fission Process," PHYS. REV. **111**, 929–933 (1958).
[149] A. M. Lane, R. G. Thomas, "R–matrix theory of nuclear reactions ," REV. MOD. PHYS. **30**, 257–353 (1958).
[150] P. Schillebeeckx, B. Becker, Y. Danon *et al.*, "Determination of Resonance Parameters and their Covariances from Neutron Induced Reaction Cross Section Data," NUCL. DATA SHEETS **113**, 3054–3100 (2012).
[151] A. Trkov, G. L. Molnár, Zs. Révay, S. F. Mughabghab, R. B. Firestone, V. G. Pronyaev, A. L. Nichols, and M. C. Moxon, "Revisiting the $^{238}$U Thermal Capture Cross Section and Gamma-emission Probabilities from $^{239}$Np Decay," NUCL. SCI. ENG. **150**, 336–348 (2005).
[152] L. Koester, H. Rauch, E. Seymann, "Neutron Scattering Lenghts: A Survey of Experimental Data and Methods," AT. DATA & NUCL. DATA TABLES **49**, 65–120 (1991).
[153] B. Kos, I. Kodeli, P. Schillebeeckx, G. Žerovnik, to be published.
[154] ICSBEP 2016: Integral Handbook of Evaluated Criticality Safety Benchmark Experiments, Nuclear Energy Agency, OECD, Paris (2016). See http://www.oecd-nea.org/science/wpncs/icsbep/handbook.html.
[155] F. H. Fröhner, "Evaluation of the Unresolved Resonance Range of $^{238}$U," NUCL. SCI. ENG. **103**, 119–128 (1989).
[156] F. H. Fröhner, "Evaluation of the Unresolved Resonance Range of $^{238}$U + n, Part II: Differential Data Tests," NUCL. SCI. ENG. **111**, 404–414 (1992).
[157] I. Sirakov, R. Capote, H. I. Kim, S. Kopecky, B. Kos, C. Paradela, V.G. Pronyaev, P. Schillebeeckx, A. Trkov, "Evaluation of cross sections for neutron interactions with $^{238}$U in the energy region between 5 keV and 150 keV ," EUR. PHYS. J. **A53**, 199 (2017).
[158] W. P. Poenitz, "Data Interpretation, Objective, Evaluation Procedures and Mathematical Technique for the Evaluation of Energy-Dependent Ratio, Shape and Cross Section Data," in *Proc. Conf. on Nuclear Data Evaluation Methods and Procedures*, **BNL-NCS-51363**, p. 249 (1981).
[159] IAEA Standards Project Webpage, see https://www-nds.iaea.org/standards/codes.html.
[160] J. F. Whalen, A. B. Smith, "Uranium total cross section," Argonne National Laboratory Report **7710**, p.9 (1971); EXFOR 10009).
[161] V. N. Kononov, E. D. Poletaev, "Measurement of the total cross-section and resonance self-shielding capture cross-section for U-238 for 5–80 keV neutrons," Proc. of the $2^{nd}$ National Soviet Conf. on Neutron Phys. (Kiev, 28 May-1 June 1973), **vol. 2**, pp. 195–205 (1973), in Russian; EXFOR 41016).
[162] W. P. Poenitz, J. F. Whalen, A. B. Smith, "Total Neutron Cross Sections of Heavy Nuclei," NUCL. SCI. ENG. **78**, 333–341 (1981).
[163] W. P. Poenitz, J. F. Whalen, "Neutron total cross section measurements in the energy region from 47 keV to 20 MeV," Report **ANL/NDM-80**, Argonne National

Laboratory 1983.
[164] I. Tsubone, Y. Nakajima, Y. Furuta, "Neutron Total Cross Sections of $^{181}$Ta and $^{238}$U from 24.3 keV to 1 MeV and Average Resonance Parameters," NUCL. SCI. ENG. **88**, 579–591 (1984).
[165] H. Derrien, J. A. Harvey, K. H. Guber, L. C. Leal, N. M. Larson, "Average neutron total cross sections in the unresolved resonance energy range from ORELA high-resolution transmission measurements," **ORNL/TM-2003/291**, Oak Ridge National Laboratory 2004.
[166] J. A. Harvey, N. W. Hill, F. G. Perey, G. L. Tweed, L. C. Leal, "High-Resolution Neutron Transmission Measurements on $^{235}$U, $^{239}$Pu and $^{238}$U," Proc. Int. Conf. On Nuclear Data for Science and Technology, Mito, Japan 30 May–3 June 1988, pp. 115–118 (1988).
[167] J. L. Ullmann, T. Kawano, T. A. Bredeweg *et al.*, "Cross section and $\gamma$-ray spectra for $^{238}$U(n,$\gamma$) measured with the DANCE detector array at the Los Alamos Neutron Science Center," PHYS. REV. **C89**, 034603 (2014).
[168] F. Mingrone *et al.*(n_TOF collaboration), "Neutron capture cross section of $^{238}$U at the CERN n_TOF facility in the energy region from 1 eV to 700 keV," PHYS. REV. **C95**, 034604 (2017).
[169] T. Wright and the n_TOF collaboration, "Measurement up to 80 keV of the $^{238}$U(n,$\gamma$) Cross Section with the TAC at the CERN n_TOF Facility," submitted to PHYS. REV. **C.**
[170] M. C. Moxon, M. G. Sowerby, J. B. Brisland, "$^{238}$U Resolved Resonance Parameters," Proc. of Int. Conf. on Physics of Reactors, Operation, Design and Computation, PHYSOR'90 Marseille, 23 - 27 April 1990, pp. III 41 - 51.
[171] I. Sirakov, B. Becker, R. Capote, E. Dupont, S. Kopecky, C. Massimi, P. Schillebeeckx, "Results of total cross section measurements for $^{197}$Au in the neutron energy region from 4 to 108 keV at GELINA," EUR. PHYS. J. **A49**, 144 (2013).
[172] E. Sh. Sukhovitskii, S. Chiba, O. Iwamoto, K. Shibata, T. Fukahori, G. Mororovskij, "Programs OPTMAN and SHEMMAN Version 8 (2004)," **JAERI-Data/Code 2005-002**, Japan Atomic Energy Agency (2005).
[173] E. Sh. Soukhovitski, S. Chiba, R. Capote, J. M. Quesada, S. Kunieda, G. Mororovskij, "Supplement to OPTMAN Code, Manual Version 10 (2008)," **JAERI-Data/Code 2008-025**, Japan Atomic Energy Agency (2008).
[174] J. M. Quesada, R. Capote, E. Sh. Soukhovitskii, S. Chiba, "Rotational-vibrational Description of Nucleon Scattering on Actinide Nuclei Using a Dispersive Coupled-channel Optical Model," NUCL. DATA SHEETS **118**, 270–272 (2014).
[175] R. Capote, A. Trkov, M. Sin, M. W. Herman, E. Sh. Soukhovitskii, "Elastic and inelastic scattering of neutrons on $^{238}$U nucleus," EPJ WEB OF CONF. **69**, 00008 (2014).
[176] R. Capote, M. Sin, A. Trkov, M. W. Herman, D. Bernard, G. Noguere, A. Daskalakis, Y. Danon, "Evaluation of neutron induced reactions on U-238 nucleus," PROC. NEMEA-7 WORKSHOP **NEA/NSC/DOC(2014)13**, NEA, OECD (2014).
[177] R. E. Slovacek, D. S. Cramer, E. B. Bean, J. R. Valentine, R. W. Hockenbury, R. C. Block, "$^{238}$U(n,f) Measurements below 100 keV," NUCL. SCI. ENG. **62**, 455 (1977).
[178] P. A. Moldauer, "Direct reaction effects on compound cross sections" , PHYS. REV. **C12**, 744 (1975).
[179] C. A. Engelbrecht, H. A. Weidenmüller, "Hauser-Feshbach Theory and Ericson Fluctuations in the Presence of Direct Reactions," PHYS. REV. **C8**, 859 (1973).
[180] M. Dupuis, L. Bonneau, T. Kawano, "Microscopic preequilibrium calculations for neutron scattering on deformed nuclei," in *Proc. 2007 Int. Workshop on Compound-Nuclear Reactions and Related Topics (CNR–2007)*, Yosemite National Park, California, 2226 October 2007, edited by J. Escher, F. S. Dietrich, T. Kawano, and I. J. Thompson, AIP CONF. PROC. **1005**, 154 (2008).
[181] H. Wienke, R. Capote, M. W. Herman, M. Sin, "Deformation-dependent Tamura-Udagawa-Lenske multistep direct model," PHYS. REV. **C78**, 064611 (2008).
[182] M. Dupuis, T. Kawano, J.-P. Delaroche, E. Bauge, "Microscopic model approach to ($n$,x$n$) pre-equilibrium reactions for medium-energy neutrons," PHYS. REV. **C83**, 014602 (2011).
[183] M. Baba, H. Wakabayashi , N. Ito , K. Maeda, N. Hirakawa, "Measurement of Double-Differential Neutron Emission Spectra from Uranium-238," J. NUCL. SCI. TECH. **27**, 601-616 (1990).
[184] V. Ja. Baryba, B. V. Zuravlev, N. V. Kornilov, O. A. Salnikov, "Secondary neutron spectrum wich arise at u-238 bombardment by 14.3 MeV neutrons," Report **FEI-671** (FEI, Obninsk, Russia, 1976).
[185] B. V. Devkin, M. G. Kobozev, A. A. Lychagin, S. P. Simakov, V. A. Talalaev, "Differential cross sections of U(n,xn) reaction at 14.3 MeV neutron energy," VOP. AT. NAUKI I TEKHN., SER.YAD. KONST. **issue 2**, p.12 (1999), Russia. Translated in **INDC(CCP)-426**, p.17 (IAEA, Vienna 2001).
[186] D. O. Nellis, I. L. Morgan, "Gamma ray production cross sections for U235, U238, and Pu239," Report **ORO-2791-17**, Oak Ridge Operations Office, contract report 2791, p.17 (1966).
[187] J. M. Peterson, A. Bratenahl, J. P. Stoering, "Neutron total cross sections in the 17- to 29-Mev region," PHYS. REV. **120**, 521 (1960).
[188] C. A. Uttley, C. M. Newstead, K. M. Diment, "Neutron strength function measurements in the medium and heavy nuclei," *Nuclear Data For Reactors*, Conf., 17-21 October 1966, Paris. IAEA Report **STI/PUB/-140**, vol.1, 165–174 (IAEA, Vienna 1967). Available online at https://www-nds.iaea.org/publications/proceedings/66PARIS_1_1967.pdf.
[189] D. G. Foster, Jr., D. W. Glasgow, "Neutron Total Cross Sections, 2.5 - 15 MeV. I. Experimental," PHYS. REV. **C3**, 76–603 (1971).
[190] J. Cabe, M. Cance, "Measurements of the neutron total cross-sections of Be, B-11, C, Al, Si, S, Ti, V, Ni, U-235, U-238, and Pu-239 between 100 keV and 6 MeV," Report **CEA-R-4524**, CEA/DAM Ile-de-France, Bruyères-le-Châtel, Arpajon, France (1973); EXFOR 20480.
[191] L. Green, J. A. Mitchell, "Total cross section measurements with a $^{252}$Cf time-of-flight spectrometer," Report **WAPD-TM-1073**, Westinghouse Atomic Power Div. (Bettis), USA (1983).
[192] F. L. Green, K. A. Nadolny, P. Stoler, "Total neutron cross section of $^{235}$U," Progress report to the U.S. Nuclear Data Committee **USNDC-9**, p.170, USA (1973); EXFOR 10588.

[193] R. B. Schwartz, R. A. Schrack, H. T. Heaton, "Total Neutron Cross Sections of Uranium-235, Uranium-238, and Plutonium-239 from 0.5 to 15 MeV," NUCL. SCI. ENG. **54**, 322–326 (1974).
[194] R. Batchelor, W. B. Gilboy, J. H. Towle, "Neutron Interactions with $^{238}$U and $^{232}$Th in the Energy Region 1.6 MeV to 7 MeV," NUCL. PHYS. **65**, 236–256 (1965).
[195] M. Baba, K. Nomoto, K. Kanda, N. Hirakawa, J. Mitsui, T. Momota, "Total Cross Section of U-238 from 2 to 8 MeV," Progress Report **INDC(JPN)-17**, **EANDC(J)-30**, p.66 (JAERI, Tokai-mura, Ibaraki-ken, Japan, 1973). Numerical data from EXFOR 21092002.
[196] Yu. V. Grigoriev, V. N. Koshcheev, G. N. Manturov, I. A. Sirakov, V. V. Sinitsa, N. B. Yaneva, "Determination of the resonance structure parameters of the U-238 cross-section on the basis of the measurements of total and partial transmissions in the energy range 0.465 - 200 keV," Report **FEI-2072** (FEI, Obninsk, Russia, 1990).
[197] W. P. Abfalterer, F. B. Bateman, F. S. Dietrich, R. W. Finlay, R. C. Haight, G. L. Morgan, "Measurement of Neutron Total Cross Sections up to 560 MeV," PHYS. REV. **C63**, 044608 (2001).
[198] G. Haouat, J. Lachkar, Ch. Lagrange, J. Jary, J. Sigaud, Y. Patin, "Neutron scattering cross sections for $^{232}$Th, $^{233}$U, $^{235}$U, $^{238}$U, $^{239}$Pu, and $^{242}$Pu between 0.6 and 3.4 MeV," NUCL. SCI. ENG. **81**, 491–511 (1982); EXFOR 21782.
[199] R. C. Allen, R. B. Walton, R. B. Perkins, R. A. Olson, R. F. Taschek, "Interaction of 0.5– And 1.0–MeV neutrons with some heavy elements," PHYS. REV. **104**, 731–735 (1956); EXFOR 12207.
[200] D. S. Mather, L. F. Pain, "Measurement of $(n,2n)$ and $(n,3n)$ cross sections at 14 MeV incident energy," Report **AWRE-O-72/72**, A.W.R.E. Aldermaston Reports, UK (1972)
[201] L. R. Veeser, E. D. Arthur, "Measurement of $(n,3n)$ cross sections for $^{235}$U and $^{238}$U," in *Int. Conf. on neutron physics and nucl. data for reactors and other applied purposes*, Sept. 1978, Harwell, UK, p.1054 (1978); EXFOR 10795.
[202] E. M. Zsolnay, R. Capote, H. Nolthenius, A. Trkov, "Summary description of the new international reactor dosimetry and fusion file (IRDFF release 1.0)," Report **INDC(NDS)-0616** (IAEA, Vienna 2012). Available online at https://www-nds.iaea.org/IRDFF/.
[203] R. Capote, K. I. Zolotarev, V. G. Pronyaev, A. Trkov, "Updating and extending the IRDF-2002 dosimetry library," J. ASTM INT. **9**, JAI104119 (2012).
[204] J. D. Knight, R. K. Smith, B. Warren, "$^{238}$U(n,2n)$^{237}$U Cross Section From 6 To 10 MeV," PHYS. REV. **112**, 259 (1958).
[205] H. Karius, A. Ackermann, W. Scobel, "The Pre-Equilibrium Contribution to the (n,2n) Reactions of $^{232}$Th and $^{238}$U," J. PHYS. **G5**, 715–722 (1979).
[206] N. V. Kornilov, B. V. Zhuravlev, O. A. Salnikov, P. Raics, S. Nagy, S. Daroczy, K. Sailer, J. Csikai, "Measurement of cross sections for the $^{238}$U(n,2n) reaction from 6.5 to 14.8 MeV," Report **INDC(HUN)-17**, p.47 (IAEA, Vienna 1980).
[207] C. Konno, Y. Ikeda, K. Oishi, K. Kawade, H. Yamamoto, H. Maekawa "Activation Cross section measurements at neutron energy from 13.3 to 14.9 MeV," Report **JAERI-1329** (JAERI, Japan, 1993).
[208] X. Wang, S. Jiang, M. He, K. Dong, C. Xiao, "Accurate determination of cross sections for $^{238}$U(n,2n)$^{237}$U induced by neutrons around 14 MeV," NUCL. INST. METH. PHYS. RES. **A621**, 326–330 (2010).
[209] Krishichayan *et al.*, "Accurate $^{238}$U(n,2n)$^{237}$U reaction cross-section measurements from 6.5 to 14.8 MeV," PHYS. REV. **C96**, 044623 (2017).
[210] A. A. Filatenkov, "Neutron activation cross sections measured at KRI in neutron energy region 13.4 - 14.9 MeV," Report **INDC(CCP)-0460** (IAEA, Vienna 2016).
[211] X. Wang, S. Jiang, M. He, K. Dong, C. Xiao, Y. Hu, Q. You, H. Chen, L. Hou, W. Yu, X. Ruan, "Determination of cross sections for the $^{238}$U(n,3n)$^{236}$U reaction induced by 14-MeV neutrons with accelerator mass spectrometry," PHYS. REV. **C87**, 014612 (2013).
[212] A. Wallner *et al.*, Preliminary data, Private communicaton, 2014.
[213] A. M. Daskalakis, R. M. Bahran, E. J. Blain *et al.*, "Quasi-differential neutron scattering from $^{238}$U from 0.5 to 20 MeV," ANN. NUCL. ENERGY **73**, 455-464 (2014).
[214] R. D. Mosteller, S. C. Frankle, P. G. Young, "Data testing of ENDF/B-VI with MCNP: critical experiments, thermal-reactor lattices, and time-of-flight measurements," Report **LA-UR-96-2143**, Los Alamos National Laboratory 1996.
[215] C. Wong *et al.*, "Livermore pulsed sphere program: program summary through July 1971," Report **UCRL-51144**, Lawrence Livermore National Laboratory 1972.
[216] W. Webster, C. Wong, "Measurements of the neutron emission spectra from spheres of N, O, W, $^{235}$U, $^{238}$U and $^{239}$Pu pulsed by 14-MeV neutrons," Report **UCID-17332**, Lawrence Livermore National Laboratory 1976.
[217] E. F. Plechaty, R. J. Howerton, "Calculational models for LLL Pulsed Spheres (CSEWG Shielding Benchmark Collection No. STD 19)," Report **UCID-16372**, Lawrence Livermore National Laboratory 1973.
[218] A. A. Marchetti, G. W. Hedstrom, "New Monte Carlo Simulations of the LLNL Pulsed-Sphere Experiments," Report **UCRL-ID-131461**, Lawrence Livermore National Laboratory 1998.
[219] J. A. Bucholz, S. C. Frankle, "Improving the LLNL Pulsed Sphere Experiments Database and MCNP Models," Report **LA-UR-03-0609**, Los Alamos National Laboratory 2003.
[220] R. Procassini, M. S. McKinley, "Modern Calculations of Pulsed-Sphere Time-of-Flight Experiments Using Mercury Monte Carlo Transport Code," in *Joint Int. Conf. on Supercomputing in Nucl. Appl. and Monte Carlo 2010 (SNA + MC2010)*, Tokyo, Japan, October 17-21, 2010.
[221] E. Goldberg *et al.*, "Neutron and Gamma-Ray Spectra from a Variety of Materials Bombarded with 14-MeV Neutrons," NUCL. SCI. ENG., **105**, 319–340 (1990).
[222] T. Goričanec, A. Trkov, R. Capote Noy, "Analysis of the U-238 Livermore Pulsed Sphere Experiments Benchmark Evaluations," Report **INDC(NDS)-0742** (IAEA, Vienna 2017). Available online at http://www-nds.iaea.org/publications/indc/indc-nds-0742.pdf.